X-BAND HIGH POWER FERRITE PHASE SHIFTERS

A THESIS SUBMITTED TO
THE GRADUATE SCHOOL OF NATURAL AND APPLIED SCIENCES
OF
MIDDLE EAST TECHNICAL UNIVERSITY

BY

HAKKI İLHAN ALTAN

IN PARTIAL FULFILLMENT OF THE REQUIREMENTS
FOR
THE DEGREE OF MASTER OF SCIENCE
IN
ELECTRICAL AND ELECTRONICS ENGINEERING

SEPTEMBER 2010

Approval of the thesis:

X-BAND HIGH POWER FERRITE PHASE SHIFTERS

submitted by **HAKKI İLHAN ALTAN** in partial fulfillment of the requirements for the degree of **Master of Science in Electrical and Electronics Engineering Department, Middle East Technical University** by,

Prof. Dr. Canan Özgen   _____
Dean, Graduate School of **Natural and Applied Sciences**

Prof. Dr. İsmet Erkmen   _____
Head of Department, **Electrical and Electronics Engineering**

Assoc. Prof. Dr. Özlem Aydın Çivi   _____
Supervisor, **Electrical and Electronics Engineering Dept., METU**

Assoc. Prof. Dr. Şimşek Demir   _____
Co-Supervisor, **Electrical and Electronics Eng. Dept., METU**

Examining Committee Members:

Prof. Dr. Canan Toker   _____
Electrical and Electronics Engineering Dept., METU

Assoc. Prof. Dr. Özlem Aydın Çivi   _____
Electrical and Electronics Engineering Dept., METU

Assoc. Prof. Dr. Şimşek Demir   _____
Electrical and Electronics Engineering Dept., METU

Prof. Dr. Altunkan Hızal   _____
Electrical and Electronics Engineering Dept., METU

Eyüp Töngel, M.Sc.   _____
ASELSAN Inc.

Date: 01.09.2010

I hereby declare that all information in this document has been obtained and presented in accordance with academic rules and ethical conduct. I also declare that, as required by these rules and conduct, I have fully cited and referenced all material and results that are not original to this work.

Name, Last name : Hakkı İlhan Altan

Signature   :

iii

ABSTRACT

X-BAND HIGH POWER FERRITE PHASE SHIFTERS

Altan, Hakkı İlhan

M.S., Department of Electrical and Electronics Engineering

Supervisor: Assoc. Prof. Dr. Özlem Aydın Çivi

Co-Supervisor: Assoc. Prof. Dr. Şimşek Demir

September 2010, 130 pages

Ferrite phase shifters are key components of passive phased array antenna systems. In a modern radar system, microwave components in the transmit path should handle high microwave power levels. Also low loss operation in phase shifters is critical, since radar range depends on the microwave power transmitted from the antennas. In this respect, ferrite phase shifters provide required performance characteristics for phased array radar systems. In this thesis, Reggia-Spencer type and twin-toroid type ferrite phase shifters operating at X-Band are designed, simulated, fabricated and measured. Measurements of the fabricated ferrite phase shifters are compared with simulation results. Electromagnetic simulations are performed using CST.

Keywords: Ferrite Phase Shifter, X-Band, Reggia-Spencer, Twin-Toroid

ÖZ

X-BANT YÜKSEK GÜÇLÜ FERİT FAZ KAYDIRICILAR

Altan, Hakkı İlhan

Yüksek Lisans, Elektrik ve Elektronik Mühendisliği Bölümü

Tez Yöneticisi: Doç. Dr. Özlem Aydın Çivi

Yardımcı Tez Yöneticisi: Doç. Dr. Şimşek Demir

Eylül 2010, 130 sayfa

Ferit faz kaydırıcılar pasif faz dizili anten sistemlerinde kullanılan en önemli yapılardan bir tanesidir. Modern radar sistemlerinde gönderme hattında bulunan elemanların yüksek mikrodalga güç seviyelerine dayanabilmeleri gerekmektedir. Ayrıca radar mesafesi antenden gönderilen mikrodalga güce bağlı olduğundan faz kaydırıcıların düşük kayıplarla çalışmaları önemlidir. Bu konuda ferit faz kaydırıcılar faz dizili radar sistemleri için gerekli olan performans karakteristiklerini sağlamaktadır. Bu tezde, X-Bant'ta çalışan Reggia-Spencer tipi ve ikiz-toroid tipi ferit faz kaydırıcıların tasarımları, benzetimleri, üretimi ve ölçümleri anlatılmıştır. Gerçeklenen ferit faz kaydırıcılardan alınan ölçümler benzetim sonuçlarıyla kıyaslanmıştır. Elektromanyetik benzetimler CST kullanılarak yapılmıştır.

Anahtar Kelimeler: Ferit Faz Kaydırıcı, X-Bant, Reggia-Spencer, İkiz-Toroid

To my Wife

ACKNOWLEDGMENTS

TABLE OF CONTENTS

ix

LIST OF TABLES

LIST OF FIGURES

LIST OF ABBREVIATIONS

AM   : Amplitude Modulation

BW   : Bandwidth

CP   : Circular Polarization

CST   : Computer Simulation Technology

DC   : Direct Current

DPS   : Differential Phase Shift

EM   : Electromagnetic

FD   : Frequency Domain

FDTD   : Finite Difference Time Domain

FEM   : Finite Element Method

LP   : Linear Polarization

LPR   : Linear Polarizer

LSE   : Longitudinal Section Electric

LSM   : Longitudinal Section Magnetic

LTCC   : Low Temperature Co-fired Ceramic

MT   : Matching Transformer

NRQWP   : Nonreciprocal Quarter Wave Transformer

PM   : Phase Modulation

QWP   : Quarter Wave Polarizer

RF   : Radio Frequency

RMS   : Root Mean Square

TE   : Transverse Electric

TM   : Transverse Magnetic

TRL   : Thru-Reflect-Line

VEE   : Visual Engineering Environment

VNA   : Vector Network Analyzer

YIG   : Yttrium Iron Garnet

CHAPTER 1

INTRODUCTION

Phase shifters are microwave devices capable of altering the insertion phase of the electromagnetic signals. Although phased array radar antenna systems are the main application area of phase shifters, they are also used in microwave instrumentation and measurement systems, and industrial applications [1].

Modern phase array systems may require thousands of phase shifters which require controlling the phase accurately for low sidelobes and low steering errors. Depending on the system requirements, phase shifters can be subjected to power levels from mW to the MW range. Phase shifters can be categorized in three main categories in terms of the main material used to alter the insertion phase, namely semiconductor phase shifters, ferroelectric phase shifters and ferrite phase shifters.

Ferrite phase shifters are a special class of phase shifters capable of handling high RF power levels. Ferrite phase shifters can be operated from RF to millimeter-wave frequencies with low insertion losses. They have been used in phased array systems since 1950s especially in the applications where high power handling and high reliability is needed.

In this thesis design, simulation, fabrication and measurements of the reciprocal type Reggia-Spencer ferrite phase shifter and nonreciprocal type twin-toroid ferrite phase shifter are presented.

1.1 Literature Review of Ferrite Phase Shifters

Modern ferrite materials first appeared toward the end of World War II in the work of Snoek and co-workers [2-4]. This work focused on realizing high frequency transformer cores having high permeability without eddy current losses.

In 1948 the terms "ferrimagnetism" and "ferrite" first appeared in technical literature when Neel [5] explained magnetic properties of these magnetic materials. In 1949, Polder [6] made the description of ferrites in terms of tensor susceptibility and this model has been the basis for analyzing the response of ferrites to microwave excitation.

Prior to the advent of electronically variable phase shifters, mechanical phase shifters are used. Rotary vane phase changer first proposed by Fox in 1947 [7] and the helical line phase changer reported by Stark in 1957 [8] are examples of mechanical phase shifters.

Scharfman [9] described three variation of a longitudinally magnetized ferrite used as a phase shifter in waveguide. In 1956, Angleakos and Korman [10] found that radiation lobe could be shifted by the application of a DC field on ferrite below that required for ferromagnetic resonance.

Reggia and Spencer [11] first reported a practical ferrite phase shifter to be used in a phased array antenna in 1957. This reciprocal device is called the Reggia-Spencer phase shifter and must be driven continuously. A latching version was described later [12].

In 1958, Clavin [13] investigated ferrite slabs mounted against the sidewalls of rectangular waveguide. Truehaft and Silber [14] first proposed internal toroids for nonreciprocal waveguide phasers to eliminate external magnetic circuits. This approach provided latching operation and greatly reduced switching time and power. The twin-toroid phase shifter overcame higher order mode propagation problems in single-toroid structure by avoiding switching wires to couple high RF fields [15].

Also weight and dimensions of the phase shifter is greatly reduced by forming the waveguide structure with the metallization of the twin-toroid structure. Throughout the 1960s and 1970s, fast switching, digital, latching ferrite phase shifters had been one of the primary objects of ferrite device development [16].

In 1970s dual mode phase shifter reported by Boyd and Whicker [17, 18] replaced the Reggia-Spencer phase shifter as a reciprocal phase shifting unit. Because of its small physical size and low production cost, dual-mode phase shifters are used both in single and two axis scanning phased arrays in large quantities. Also dual-mode ferrite phase shifters provided lowest insertion losses at millimeter-wave frequencies [1]. In 1972, Hord, Rosenbaum and Benet [19] reported the Faraday rotation type ferrite phase shifter.

In 1972, Boyd and Klein [20] reported the rotary-field ferrite phase shifter having reciprocal and accurate phase shifting characteristics. Physical size of the structure restrained its use only in single-axis scanning systems. Low insertion loss and modulo 360° phase shifting characteristics are key performance parameters of rotary field ferrite phase shifters. The latching version of this type of ferrite phase shifter is described in 1995 [21].

Microstrip meander line phase shifters [22, 23] provided phase control in small dimensions as compared to waveguide type ferrite phase shifters. However power handling of planar ferrite devices is much smaller than that for waveguide devices. Recently main effort is made to obtain low loss and wideband planar microwave ferrite devices by combining high temperature superconducting ceramics with ferrite materials [24]. A differential phase shift in excess of 200° with an insertion loss generally below 2 dB from 6 to 12 GHz was reported by Dionne [25].

1.2 Outline of the Thesis

In Chapter 2, general properties of ferrite phase shifters are described. Classification of ferrite phase shifters in terms of electrical properties is presented and performance characteristics are given in detail. Several important types of ferrite phase shifters are explained.

In Chapter 3, design and fabrication processes of the reciprocal Reggia-Spencer ferrite phase shifter at X-Band is presented. Measurement results of the fabricated structures is given and compared with the EM Simulation results.

In Chapter 4, analytical and numerical analysis of twin-toroid ferrite phase shifter is discussed. EM simulations models for twin-slab geometry are developed by comparing the results with analytical solutions given in [26]. These models are extended for twin-toroid structure and results of the model are compared with measurement results of a practical twin-toroid phase shifter at X-Band [27].

In Chapter 5, design of an X-Band Twin-Toroid ferrite phase shifter is presented by using the simulation models developed in Chapter 4. Measurement results of the deigned twin-toroid ferrite phase shifter are presented and these results are compared with the EM simulation results. Some practical improvements in the design are investigated.

Finally, conclusions about the design and fabrication of Reggia-Spencer type and twin-toroid type ferrite phase shifters are summarized in Chapter 6.

In the Appendix A, important microwave and DC characteristics of ferrite materials are explained and their effect on phase shifter performance is discussed.

4

CHAPTER 2

FUNDAMENTALS OF FERRITE PHASE SHIFTERS

The basis of operation of ferrite phase shifters is the interaction between the electromagnetic waves and spinning electrons in a magnetized ferrite. In a magnetized ferrite, the magnetic moment of the spinning electron precesses about the applied DC magnetic field H_{DC}, and the precession frequency is proportional to the magnitude of H_{DC}. The permeability of the ferrite takes the form of a tensor, the elements of which are a function of H_{DC}. The propagation constant which is dependent on the permeability of the ferrite material changes as H_{DC} is changed. As a consequence of the change of propagation constant, different insertion phases are obtained by changing the magnitude and direction of H_{DC} [1].

In this Chapter, general characteristics of ferrite phase shifters are described and several important ferrite phase shifter types are explained in detail.

2.1 Basic Definitions

Phase shifter is a one or two port microwave device capable of altering the insertion phase of the signal passing through it. *Insertion phase* ϕ is the phase delay experienced by the signal between input and output ports of the device. In Figure 2.1 schematic representation of a two port phase shifter is given. ϕ_1 and ϕ_2 are the insertion phases for state 1 and state 2 respectively.

5
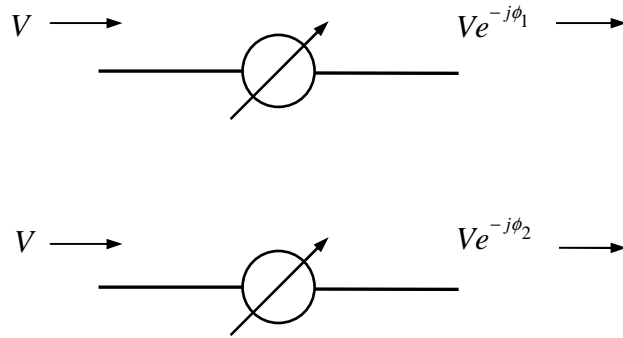
Figure 2.1 A two port phase shifter device showing two insertion phase states

Differential phase shift (DPS) is defined as the difference between insertion phases of two different phase states of the phase shifter and is given by

$$\Delta\phi = \phi_1 - \phi_2 \qquad\qquad (2.1)$$

Electrically longest or shortest state is chosen to be the *reference phase state* which corresponds to the zero DPS state.

Ideally, phase shifters change only the insertion phase of the signal and it is perfectly matched at its two ports. Then the scattering matrix for a two port phase shifter is represented as

$$[S_{ideal}] = \begin{bmatrix} 0 & e^{-j\phi} \\ e^{-j\phi} & 0 \end{bmatrix} \qquad\qquad (2.2)$$

It is seen in (2.2) that insertion phase of the device is the same for two directions of propagation. This device is called a *reciprocal phase shifter* (RPS).

In practice all phase shifters have some losses and they are not perfectly matched at its input and output ports. Then the scattering matrix for a non-ideal phase shifter is represented as

$$[S] = \begin{bmatrix} S_{11} & |S_{12}|e^{-j\phi} \\ |S_{21}|e^{-j\phi} & S_{22} \end{bmatrix}$$

(2.3)

Also insertion phase or insertion loss for two directions of propagation can be different for nonreciprocal phase shifters. Some types of ferrite phase shifters and active phase shifters are nonreciprocal. The scattering matrix for a non-ideal and *nonreciprocal phase shifter* (NRPS) is represented as

$$[S] = \begin{bmatrix} S_{11} & |S_{12}|e^{-j\phi_1} \\ |S_{21}|e^{-j\phi_2} & S_{22} \end{bmatrix}$$

(2.4)

2.2 Classification of Ferrite Phase Shifters

Many different types of ferrite phase shifters have been developed since the invent of the first practical ferrite phase shifter in 1957. In this section, classification of ferrite phase shifters in terms of the electrical characteristics is presented.

2.2.1 Classification in terms of Transmission Medium

Since ferrite phase shifters are used mainly in high power applications, the main transmission medium for ferrite phase shifters is waveguide and coaxial line. However, since these geometries are bulky their usage in airborne or space applications is very limited. As ceramic technology is advanced, ferrite phase shifters in planar geometries appeared. Microstrip line, stripline, coplanar waveguide

7

geometries are examples of the planar geometries used in ferrite phase shifters. Recently hybrid ferrite phase shifters are developed using Low Temperature Co-fired Ceramic (LTCC) technology [28].

2.2.2 Longitudinal versus Transverse Magnetization

Ferrite phase shifters can be categorized whether the magnetization direction is longitudinal or transverse to the direction of propagation. Ferrite phase shifters that are longitudinally magnetized alter the insertion phase of the signal by Faraday rotation phenomenon. Transversely magnetized ferrite phase shifters are generally nonreciprocal and phase shift is obtained by the interaction of circularly polarized RF magnetic field and DC biased ferrite medium.

2.2.3 Reciprocal versus Nonreciprocal Operation

Interaction between microwave signals and ferrite material is nonreciprocal. However reciprocal operation can be obtained for some ferrite phase shifter types by using nonreciprocal ferrite elements cascaded with the main phase shifting element. Reciprocal ferrite phase shifters are mainly used in monostatic radar systems where single antenna performs both transmit and receive operations. Nonreciprocal ferrite phase shifters are mainly used in bistatic radar systems. However they can be operated in monostatic radars at the expense of an increased minimum target detection range because of the required switching of ferrite phase shifters.

2.2.4 Latching versus Nonlatching Operation

As explained in Chapter 2, ferrite materials exhibit hysteresis properties which provide them to hold magnetic flux even when the magnetic bias is removed. Latching ferrite phase shifters operate according to this principle and do not require continuous holding current. This greatly reduces the DC power consumption since current is needed only when switching from different phase states. The ferrite material used in latching ferrite phase shifters should have square hysteresis characteristics to utilize the latching property efficiently. Also for latching operation air gaps on the path of DC magnetic flux should be minimized. Figure 2.2 shows the

effect of air gap on hysteresis characteristics for the toroid given in inset of the figure. For simplicity hysteresis curve is assumed to be perfectly square, i .e. remanent magnetization level equals saturation magnetization level, for the case with no air gap. As air gap length l_g is increased the required DC magnetic field to take the rod to saturation increases and remanent flux density in the latched state decreases.
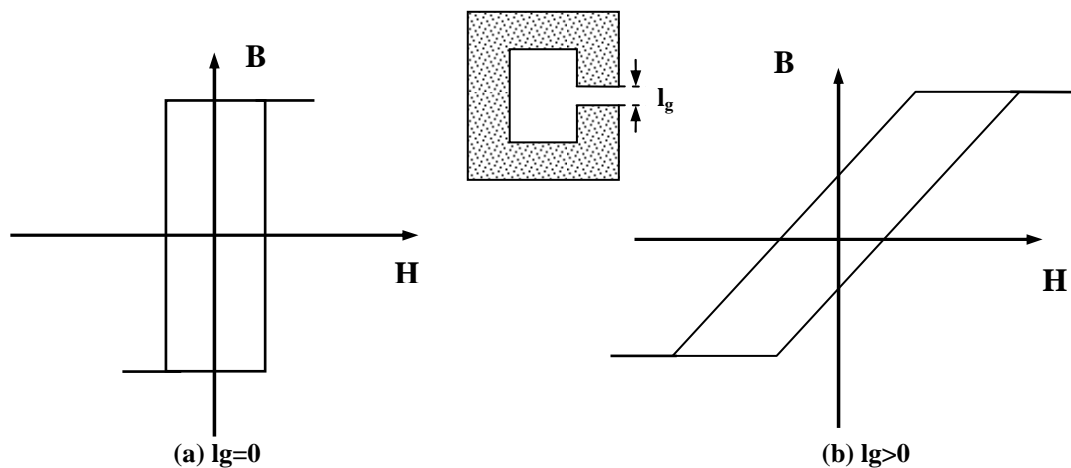
Figure 2.2 Effect of air gap on hysteresis characteristics

2.2.5 Digital versus Analog Operation

Analog phase shifters provide continuous variation of insertion phase whereas digital phase shifters allow variation in discrete steps. A digital phase shifter consists of cascaded phase bits with phase shifts incremented in binary steps. For most of the ferrite phase shifters DPS is linearly proportional to the length of the ferrite element used. For digital operation ferrite elements with lengths being multiples of each other are used. Lengths are arranged to obtain maximum of 360° DPS. Each ferrite element is operated either in negative remanent magnetization point or positive remanent magnetization point. For analog operation a long ferrite element capable of providing 360° DPS is used. Intermediate values of DPS are obtained by operating the device on minor hysteresis loops between negative remanent magnetization and positive remanent magnetization points. Digital ferrite phase shifters require

9

independent driver circuitry for each phase bit. This increases the driver complexity and switching power. However switching is faster in digital type ferrite phase shifters, since each bit is switched at the same time. The concept of digital and analog phase shifters is given in Figure 2.3.
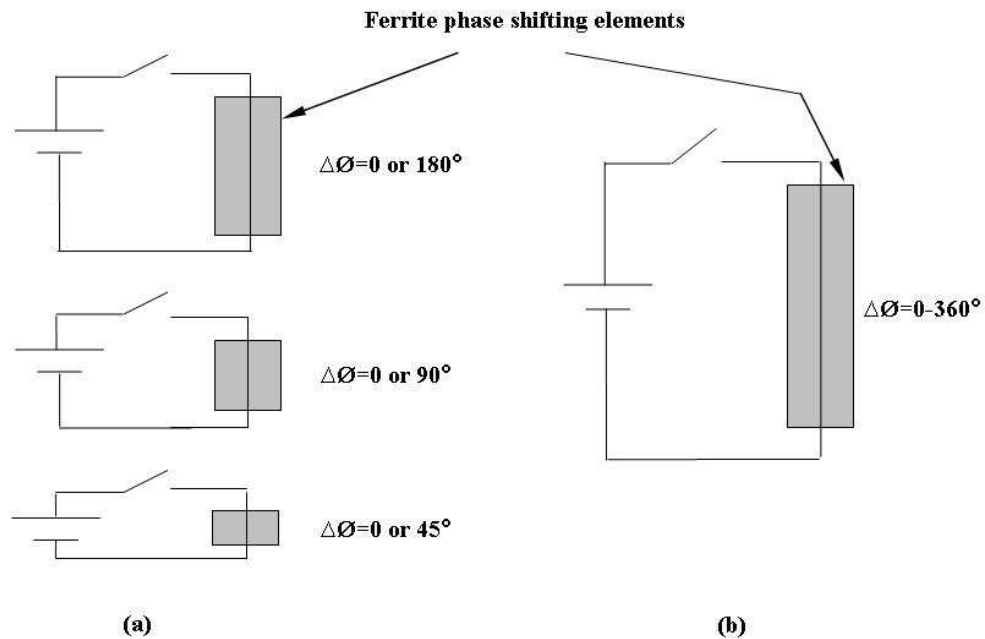
Figure 2.3 Digital (a) and analog (b) operation

Note that today's modern radar systems require digital control systems for high accuracy and fast operation. For this reason digital phase shifting operation shouldn't be confused with digitally controlled analog phase shifting. An analog type phase shifter can be controlled digitally with a digital driver circuitry.

2.3 Performance Characteristics of Ferrite Phase Shifters

When designing a ferrite phase shifter some trade-offs should be made to satisfy the requirements of the system where it is used. In this section some performance characteristics of ferrite phase shifters are described and their effect on the system performance is explained.

2.3.1 Insertion Loss

Insertion loss of a ferrite phase shifter should be as low as possible. 0.7-1.2dB average insertion loss is typical for ferrite phase shifters at X-band in waveguide geometry. Ferrite phase shifters are high power devices and they are most frequently used in passive phase array radar systems where the radar range depends on the phase shifter loss. Insertion loss in the phase shifter is converted to heat which in return deteriorate the phase shifting performance of the phase shifter or even may destroy it in high average power systems.

Peak power requirement of the ferrite phase shifter is another factor determining the insertion loss of a ferrite phase shifter. As explained in the Appendix A, while addition of some rare-earth metals in ferrite composition increases peak power handling capability, it also increases the average insertion loss. Because of this reason, ferrite materials used in low and high power applications should be chosen differently for low loss operation.

Insertion loss modulation which may result from the phase state changes (PM-AM modulation) should be low for high performance phased array antenna systems.

2.3.2 Phase Accuracy

Phase errors of a ferrite phase shifter should be as low as possible to reduce steering errors and side-lobe levels of a radar system. Phase resolution of a ferrite phase shifter is defined as:

$$Phase\ Resolution = 360\ /\ 2^{n} \qquad\qquad \textbf{(2.5)}$$

where n is the number of ferrite elements used in a digital type ferrite phase shifter or the number of control bits used in a digitally controlled analog type ferrite phase shifter.

In practice there are phase errors resulting from the non-ideal performance of the driver circuitry, frequency and temperature changes.

In terminology, effect of frequency on DPS characteristics is described by phase flatness. As shown in Appendix A elements of the tensor permeability depend on frequency, thus DPS characteristics of the ferrite phase shifter will depend on frequency. In some ferrite phase shifter types, frequency dependence can be eliminated to some extent with some design techniques. If instantaneous bandwidth of a system is small, frequency dependence can be compensated by driver circuitry by dividing the operation bandwidth to subsections.

Generally as operating temperature increases phase shifting capacity of ferrite phase shifters decreases. Temperature sensitivity depends on the ferrite material used and 0.5-3°/°C temperature sensitivity is typical for ferrite phase shifters [1]. In analog type ferrite phase shifters temperature compensation can be done with a ferrite element capable of providing more than 360° of DPS at room temperature. Temperature compensation is critical in the case where different phase shifters operate at different RF power levels, thus at different temperatures, because of the amplitude tapering in a phased array system.

Apart from these sources, *memory effect* can cause repeatability errors resulting from the hysteresis characteristics of ferrite materials. In order to increase the phase shifting repeatability, ferrite memory is deleted by switching the phase shifter to a reference phase state before switching to the desired phase state. Generally the reference phase state is either the negative or positive remanent magnetization point in the hysteresis loop.

Phase error for a phase shifter is defined for a specified operating frequency, temperature and phase setting as:

$$\Delta\phi_{error} = Commanded\ Phase - (Measured\ Phase - 0°\ Phase\ Reference) \qquad \textbf{(2.6)}$$

Phase error for a ferrite phase shifter is typically specified by a peak value and an RMS value at a specified temperature and phase state over the operating frequency range. It is important that average phase error for all phase states is subtracted from peak phase errors in the calculation of RMS phase error. The calculation of RMS phase error at a specified temperature and frequency is as follows:

$$\Delta\phi_{RMS\_error} = \sqrt{\frac{(\Delta\phi_{error\_1} - \Delta\phi_{avg})^2 + (\Delta\phi_{error\_2} - \Delta\phi_{avg})^2 + ... + (\Delta\phi_{error\_n} - \Delta\phi_{avg})^2}{n}} \quad \textbf{(2.7)}$$

where $\Delta\phi_{error\_1}$, …, $\Delta\phi_{error\_n}$ are peak phase errors for n phase states defined in (2.6) and $\Delta\phi_{avg}$ is the average phase error for all phase states at a specified temperature and frequency.

The maximum permissible phase error for a phase shifter depends on the system in which it is used. For systems having large number of radiating elements, phase accuracy is not as critical as for small systems with less radiating elements. The RMS phase error permissible for a ferrite phase shifter is typically up to about 6° [1].

2.3.3 Switching Time

Switching time for a phase shifter should be as low as possible for fast operation. In nonreciprocal ferrite phase shifters, switching time determines the minimum detectable radar range. Switching time of ferrite phase shifters depend on the type of phase shifter and typically in the range 1us to about 150us. Switching time can be reduced by increasing the magnitude of the voltage pulses generated in the driver circuit.

2.3.4 Power Handling Capability

Ferrite phase shifters should handle required power depending on the radar range and data rate of the system. As explained in the Appendix A.5, peak power handling of a ferrite phase shifter is limited by the increase of insertion loss at a critical RF power level. The critical power level depends on the ferrite material and ferrite phase shifter geometry. As frequency of operation increases, peak power handling of ferrite material decreases. Average power handling level of ferrite phase shifters depend on the increase of temperature in ferrite material because of the RF heating resulting from losses. If temperature increases above the temperature limit in which the driver circuit is calibrated, phase errors increase and 360° of DPS may not be accomplished. Also too much temperature increase in the structure may cause physical damage to the elements which are bonded together with adhesives. By forced air cooling or liquid cooling techniques, average power handling level can be increased.

2.3.5 Physical Size and Weight

Maximum physical size and weight of the ferrite phase shifter is determined by the system requirements. For mobile, airborne or space applications weight should be minimized, whereas for ground based applications, the weight requirement can be relaxed. The interelement spacing in an array is generally $\lambda/2$. Hence for a two-axis scanning system phase shifter module should fit within cross-sectional area of $\lambda/2$ x $\lambda/2$.

2.3.6 Figure of Merit

The figure of merit of a ferrite phase shifter is defined as the maximum DPS per dB of insertion loss [1]. 300-700 degree/dB is typical for ferrite phase shifters. Also ferrite phase shifters can be characterized by the value of maximum DPS per unit length in cm or inches.

2.4 Ferrite Phase Shifter Topologies

In this Section, electrical characteristics and operation principles of several important types of ferrite phase shifters is presented.

2.4.1 Reggia-Spencer Ferrite Phase Shifter

Reggia-Spencer phase shifter is a reciprocal ferrite phase shifter having both latching and non-latching versions. Operation BW of Reggia-Spencer ferrite phase shifter is limited by both resonances in transmission characteristics and high slope of the DPS. Insertion loss is typically <1dB in 5% BW.

Reggia-Spencer ferrite phase shifter consists of a longitudinally magnetized ferrite rod at the center of a rectangular waveguide excited in TE_{10} mode. Impedance matching is obtained by tapering ferrite rod from both sides as in Figure 2.4 or by putting dielectric transformers at the ends. Longitudinal magnetic field is biased by the DC current passing through the solenoid wound around the waveguide. Since a closed magnetic circuit is not present, cylindrical rod can not hold magnetization after removing the current. Because of this, Reggia-Spencer phase shifter is a nonlatching type ferrite phase shifter and requires continuous DC current to hold the phase stable. If reference state is chosen to be the state with no current, the value of DPS increases as the magnitude of the current is increased.

The theory of operation of Reggia-Spencer phase shifter is investigated by many authors [29-34]. Theory of suppressed rotation [33] states that the main mechanism in phase shifting is the magnetic field controlled cross-coupling between TE_{10} mode and a higher order mode which is actually a hybrid mode and is below cut-off. Frequency dependent coupling causes DPS to be highly sensitive to frequency. Above the cut-off frequency of higher order mode, Faraday rotation is seen. Since electromagnetic waves with rotated polarization cannot propagate in rectangular waveguide, periodic resonances occur above cut-off. Operation BW of the Reggia-Spencer phase shifter is limited by these resonances which cause deep insertion loss spikes.

15
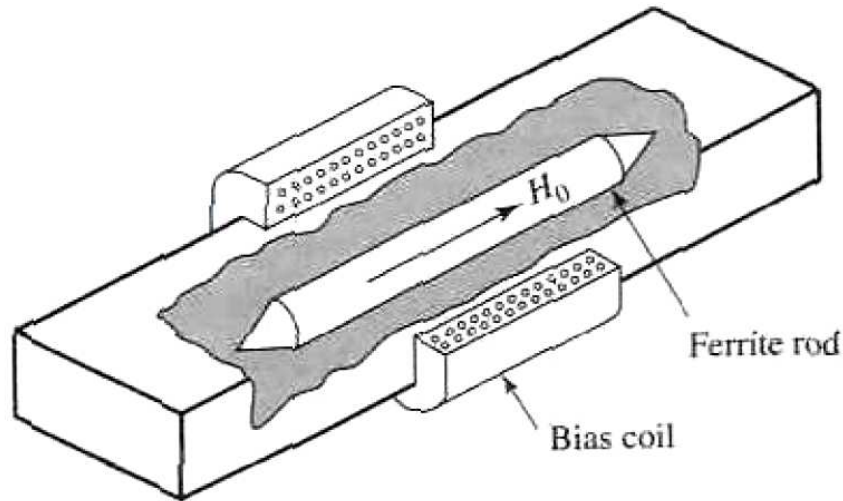
Figure 2.4 The structure of Reggia-Spencer ferrite phase shifter [35]

2.4.2 Twin-Toroid Ferrite Phase Shifter

Twin-toroid phase shifter is a waveguide type nonreciprocal ferrite phase shifter having high figure of merit (>400°/dB) and switching speed (<5us). BW of the twin-toroid phase shifter can be broaden up to 30% by using multi-section dielectric impedance matching elements and flat differential phase shift can be obtained in the BW. Twin-toroid phase shifter is a latching phase shifter where DC magnetic bias is needed only when switching between phase states. Between the state transitions, phase shifter acts as a passive device. Because of this total DC power consumption of the twin-toroid phase shifter is very low and depends on switching frequency. By carefully choosing the ferrite material type and geometry, phase shifters handling very high average and peak power levels can be designed since intrinsic geometry of the structure allows the heat generated by microwave loss to be transferred out from the ferrite material easily. Twin-toroid phase shifter can be used in two-axis scanning, airborne and space applications because of its small dimensions and weight [1].

The main phase shifting element of twin-toroid phase shifter consists of two identical ferrite toroids that are bonded together with a high permittivity dielectric material between them as shown in Figure 2.5. This ferrite-dielectric composite structure is

16

mounted in rectangular waveguide whose height and width is reduced to suppress higher order modes. Air gaps between the ferrite structure and waveguide can be minimized by metallization of the composite structure. Dielectric transformers and waveguide step transitions are used to match the wave impedance between the ferrite filled and reduced dimension waveguide to the standard rectangular waveguide as in Figure 2.6. The current passed through wires placed inside the toroidal holes provides the transverse magnetization in the toroids.
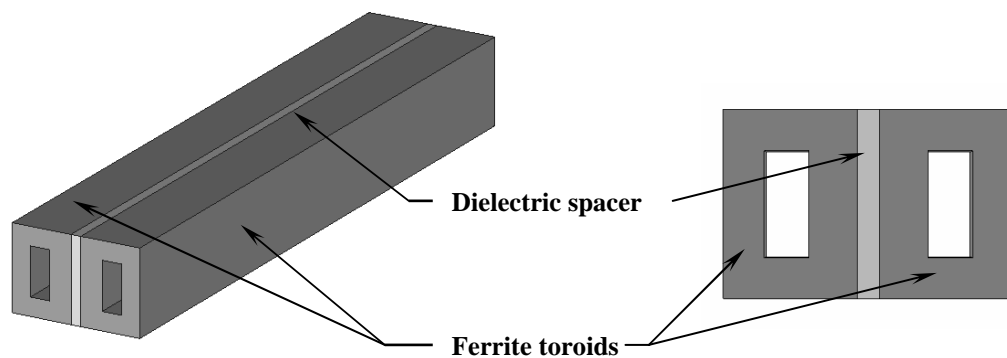
Figure 2.5 The phase shifting element of twin-toroid ferrite phase shifter consisting of ferrite-dielectric composite structure

Maximum differential phase shift is obtained at the positive remanent magnetization point assuming that the negative remanent magnetization point is chosen as the reference state. In the analog operation, intermediate values of differential phase shift can be obtained by applying short voltage pulses to the switching wire to operate at the remanent magnetization points on minor hysteresis loops as shown in Figure 2.7. Theory of operation of twin-toroid ferrite phase shifter is explained in detail in Chapter 4.
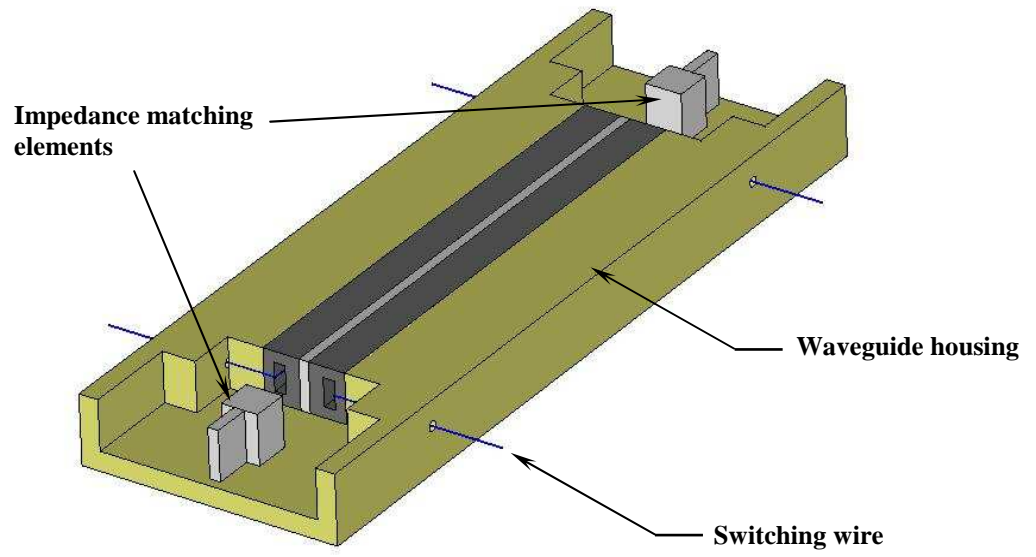
Figure 2.6 Twin-toroid structure in waveguide housing without cover
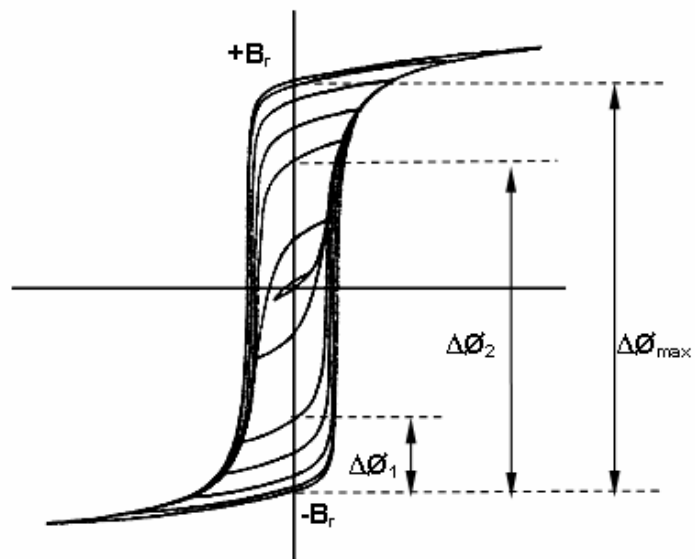
Figure 2.7 Different phase states shown on the hysteresis loop

18

2.4.3 Faraday Rotation Ferrite Phase Shifter

The Faraday rotation phase shifter uses the interaction between a circularly polarized wave and a longitudinally magnetized ferrite in a symmetrical waveguide which is circular or square in geometry [1].

By changing the magnitude of the longitudinal magnetic field magnitude, circularly polarized microwave field is rotated and hence phase shift is obtained. Since the rotation of the microwave field is in different senses for different directions of polarization, DPS is nonreciprocal. However by incorporating nonreciprocal circular polarizers at both ends, reciprocal DPS characteristic is obtained. Figure 2.8 shows the main elements of the Faraday-rotation ferrite phase shifter. The main phase shifting element is the variable Faraday rotator (FR). The nonreciprocal polarizer consists of a 45° Faraday rotator cascaded with a quarter wave plate (QWP). Quarter wave plate transforms a linearly polarized (LP) wave to a circularly polarized (CP) wave and vice versa. Linear polarizers (LPR) at the ends absorb any modes having E Field direction parallel to the resistive sheet.
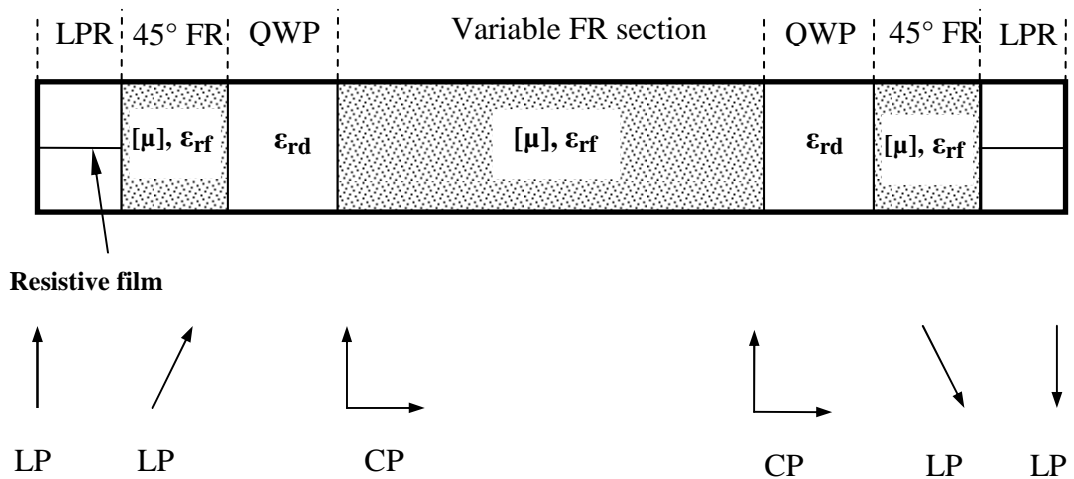
Figure 2.8 Polarization distribution in the Faraday rotation ferrite phase shifter [1]

19

2.4.4 Single-Toroid Ferrite Phase Shifter

Single-toroid phase shifter is a nonreciprocal, transversely magnetized ferrite phase shifter having high Figure of Merit (>500°/dB) and high power handling capability.

The structure of single-toroid phase sifter is shown in Figure 2.9. The main element of single-toroid phase shifter is a rectangular ferrite toroid with a high permittivity dielectric material placed in the toroidal hole. High permittivity material concentrates the field around the ferrite material to increase DPS per unit length. This whole structure is placed in a waveguide channel whose width is reduced to obtain flat DPS within the BW. The height of the channel is also reduced to suppress higher order longitudinal section electric (LSE) and longitudinal section magnetic (LSM) modes. Dielectric transformers are used at the ends of the ferrite toroid to match the impedance between reduced width and height waveguide to the standard waveguide.

Ferrite toroid

Dielectric insert

Dielectric matching transformer
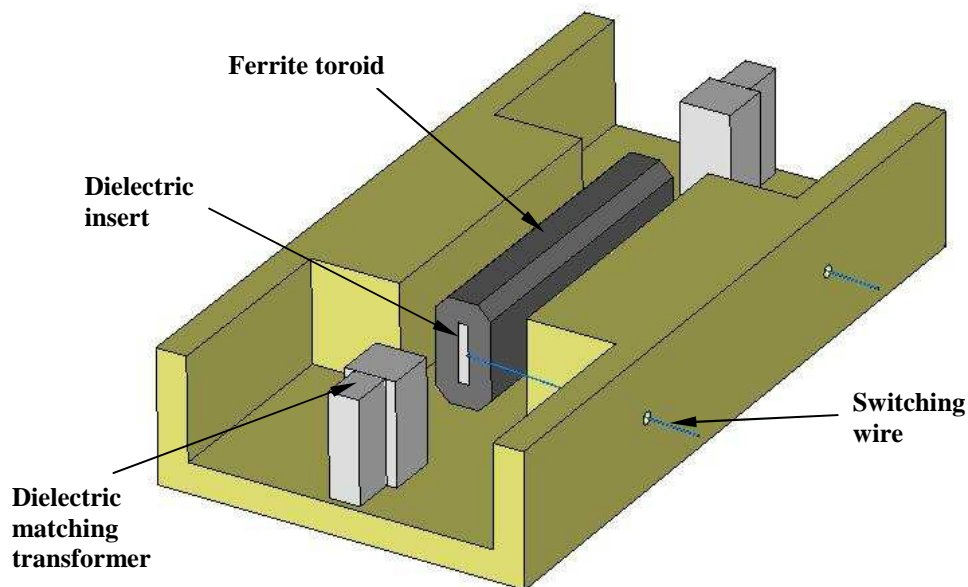
Switching wire

Figure 2.9 Single-toroid structure in waveguide housing without cover

Switching wire is mounted in the toroidal hole and bidirectional current is passed through it to obtain the necessary switching operations (RESET-SET scheme). The magnetizing wire is shielded along its length with a spiral-wrapped fine wire to suppress the coaxial mode supported by the wire [36].
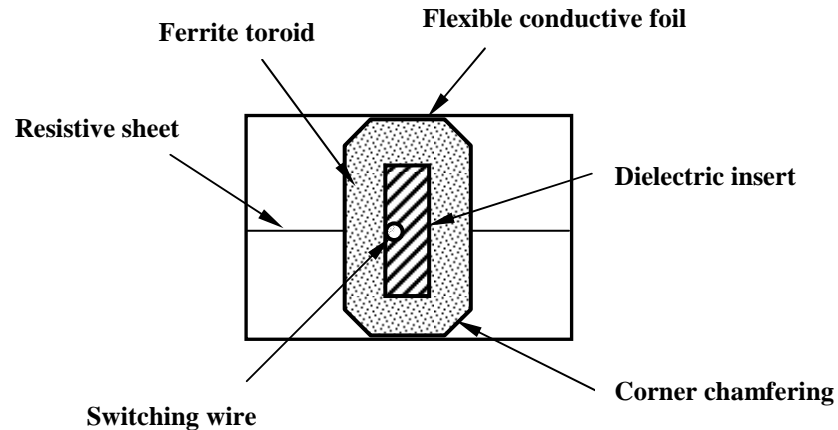
Figure 2.10 Cross-sectional view of single-toroid ferrite phase shifter

In Figure 2.10 some design improvements of the single-toroid structure is shown in the cross-sectional view. Resistive sheet are placed on a dielectric support and helps to suppress LSE and LSM higher order modes [37]. Chamfering of the toroid corners improves the figure of merit up to 10% [38]. Also flexible conductive foil is placed between ferrite toroid and waveguide walls. This layer decreases the mechanical stress on the toroid and reduces the effect of magnetostriction on phase shifting performance.

2.4.5 Dual-Mode Ferrite Phase Shifter

Dual mode phase shifter is a variant of the Faraday rotation phase shifter which has reciprocal phase shifting characteristics due to the cascaded nonreciprocal quarter-wave polarizers (NRQWP) at the ends of the variable Faraday rotator section. The nonreciprocal operation of the polarizers is schematically shown in Figure 2.11. Magnetization of NRQWP is provided with four-pole magnets. Dielectric matching

transformers (MT) are used to match the impedance between the rectangular waveguide and ferrite filled circular waveguide and placed at the ends of the ferrite structure as shown in Figure 2.12.
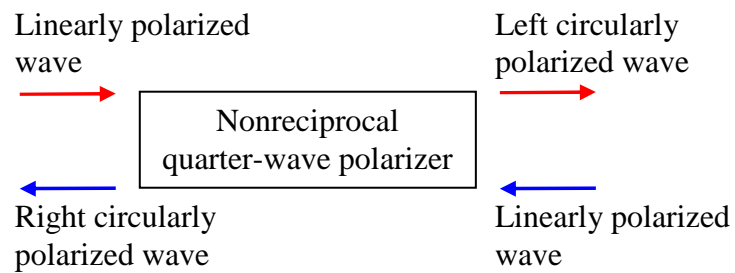
Figure 2.11 Operation of nonreciprocal quarter-wave polarizers
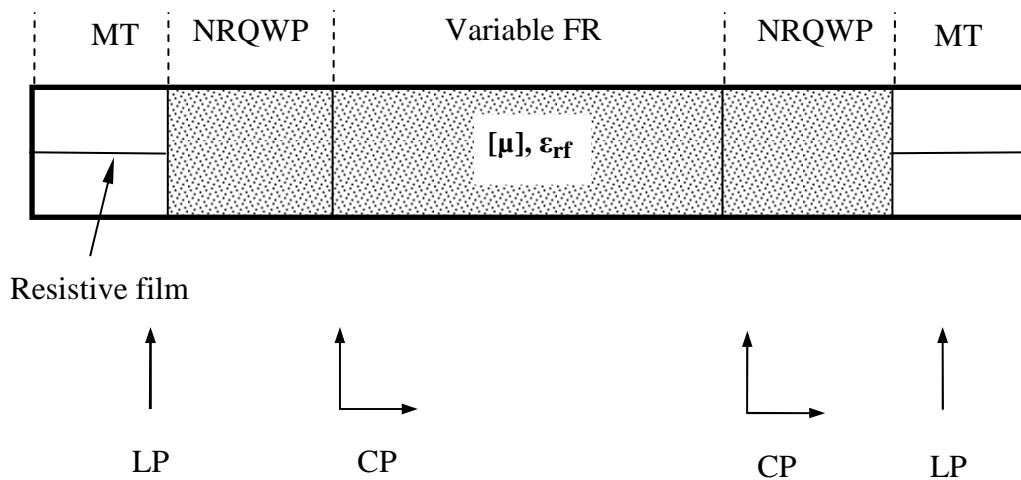
Figure 2.12 Cross sectional view of Dual-Mode phase shifter and polarization distrubution

2.4.6 Rotary-Field Ferrite Phase Shifter

Rotary field ferrite phase shifter is a reciprocal, transversely magnetized device having accurate phase shifting characteristics and high power handling capability.

Rotary-field ferrite phase shifter alters the insertion phase of the circularly polarized microwave field by rotating a quadrupole transverse DC magnetic field in a circular waveguide filled with ferrite called half wave plate. The main mode propagating in the ferrite half-wave plate is the TE_{11} mode. Quadrupole transverse DC magnetic field is produced by two windings called "*sine*" and "*cosine*". As name implies, in the sine winding the magnitude of the current is a function of sine function, whereas in the cosine winding the magnitude of the current is a function of cosine function. The configuration of the rotary-field ferrite phase shifter is given in Figure 2.13. Quarter-wave plate at the end of the ferrite rod transforms the linear polarization to the circular polarization and vice versa. Resistive sheet is placed in the dielectric matching section to absorb the microwave fields having E field parallel to it. The whole structure is metalized to form the circular waveguide structure and mounted in the magnetic yoke as shown.

Magnetic yoke act as a medium to produce closed magnetic circuit and it is made from a ferrimagnetic or ferromagnetic material depending on whether the device is latching or nonlatching respectively. Sine and cosine windings are wound in the slots of the magnetic yoke such as the stator of a motor.
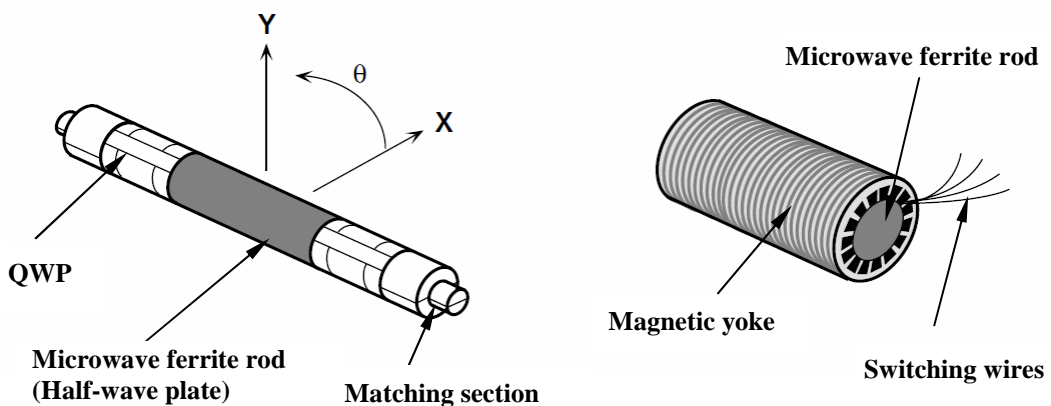
Figure 2.13 Main elements of the rotary-field ferrite phase shifter

Ideally sine winding is arranged to produce a radial magnetic flux B_{sine} which has dependence

$$B_{\sin e} = B_{s0} \sin 2\theta$$

(2.8)

Cosine winding produce magnetic flux B_{cosine} which has dependence

$$B_{\cos ine} = B_{c0} \cos 2\theta$$

(2.9)

where B_{s0} and B_{c0} vary as $B_0 \sin \phi$ and $B_0 \cos \phi$ respectively with ϕ defined as an electrical angle and θ is the orientation angle around the circumference of the rod shown in Figure 2.13. Total magnetic flux generated can be written as a superposition of magnetic flux generated by these two windings individually as

$$B = B_0 (\sin \phi \sin 2\theta + \cos \phi \cos 2\theta)$$
$$B = B_0 \cos(2\theta - \phi)$$

(2.10)

Thus a change $\delta \phi$ degrees in the electrical angle parameter cause a mechanical rotation of the ferrite half-wave plate quadrupole transverse magnetic field by $\delta \phi / 2$ degrees. The microwave insertion phase of the signal passing through the half wave plate changes by $\delta \phi$ degrees since it changes by twice the rotation angle of the half-wave plate [39].
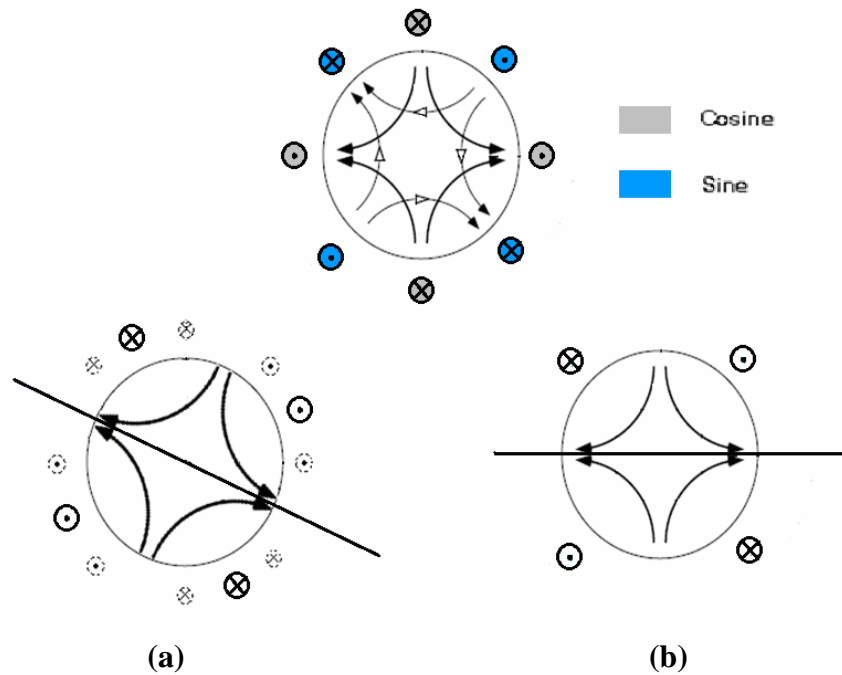
Figure 2.14 Interlaced magnetic flux in the microwave ferrite and superposition of the fluxes for two cases (a) $\phi = 45°$ (b) $\phi = 90°$

In Figure 2.14 magnetic flux generated by sine and cosine windings are shown. As it is observed the fields have a 45° displacement from each other and are orthogonal. Superposition of the fields is given for two cases: (a) $\phi = 45°$ and (b) $\phi = 90°$.

The practical operating frequency of the rotary-field phase shifters is approximately 2-20GHz [1]. Since the electrical length of the ferrite half wave plate needs to be 180° only, lower insertion loss (maximum 1 dB) can be obtained than other ferrite phase shifter types. Since the magnitude of the total magnetic flux is same for all phase states, insertion loss modulation is very low for rotary-field phase shifters. [39].

Lower RMS phase errors are possible as the number of slots in the yoke is increased. For the latching version phase accuracy is worse than nonlatching version since the ferrite material is brittle, it is practically not possible to increase the number of slots in the ferrite yoke [39]. Large size of the ferrite yoke limits the rotary-field phase shifters to be used only in single axis scanning phased array antenna systems.

2.4.7 Meander-Line Ferrite Phase Shifter

Meander-line ferrite phase shifter is an analog and latching ferrite phase shifter in microstrip or stripline geometry. It has both reciprocal and nonreciprocal versions.

The structure of the nonreciprocal meander-line phase shifter in microstrip geometry is given in Figure 2.15. Ferrite is magnetized by passing current through the holes drilled in the ferrite substrate. The direction of magnetization at the center of the meander line part is shown in Figure 2.16. Meander line parameters are arranged to produce circularly polarized RF magnetic fields below the center line AA′. At sections away from the center line AA′, polarization changes to elliptical and then linear at the ends [1]. Thus only about 65% of the meander line turns produce nonreciprocal DPS, whereas the entire 100% contributes to insertion loss [40].
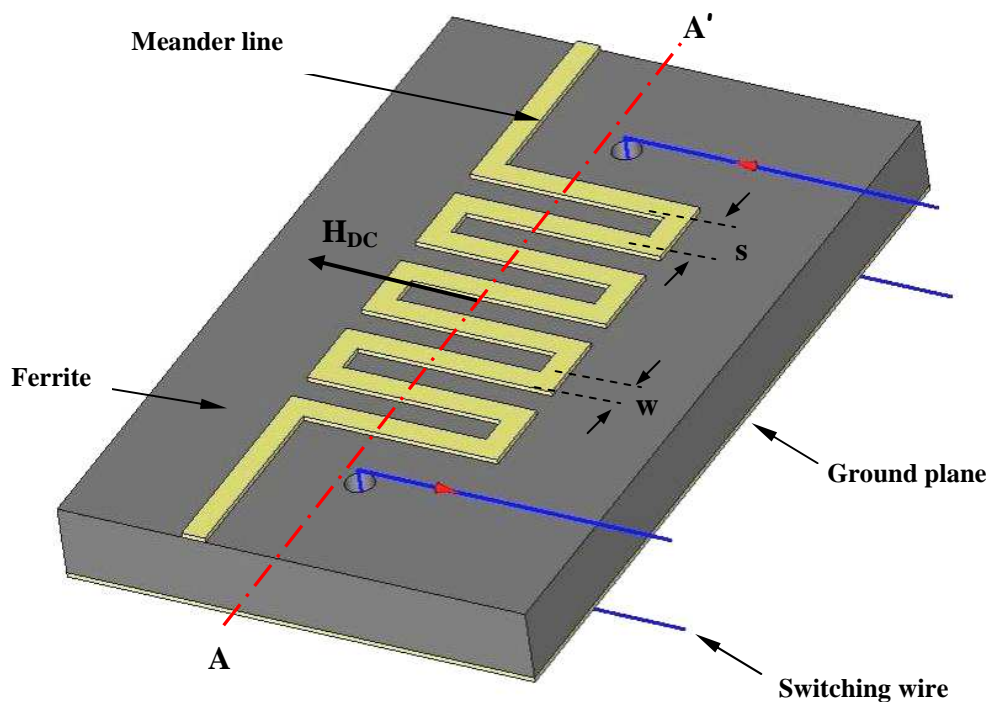
Figure 2.15 Meander line ferrite phase shifter in microstrip geometry
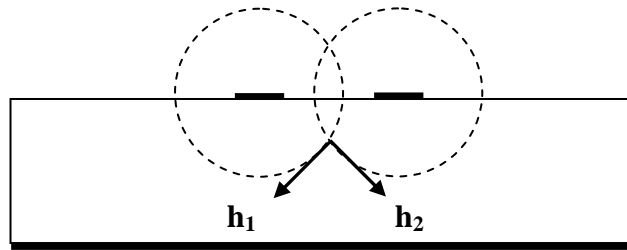
Figure 2.16 Circularly polarized RF magnetic fields generated by meander lines on AA′ plane

CHAPTER 3

ANALYSIS AND DESIGN OF REGGIA-SPENCER FERRITE PHASE SHIFTER

In this Chapter, design of an X-band Reggia-Spencer phase shifter is explained using analytical expressions given in the literature and structure is optimized with numerical analysis done with CST Microwave Studio®. Three different structures are fabricated and it is seen that measurement results agree well with the analytical and numerical solutions.

3.1 Design Considerations

Design procedure can be categorized in three steps.

- Initial determination of ferrite material parameters
- Determination of ferrite geometry
- Choosing ferrite material

First two steps are coupled problems and should be solved together to meet the specifications given in Table 3.1.

Table 3.1 Phase shifter specifications

Operation bandwidth	10% at X-Band
Insertion Loss	<1dB
Return Loss	>10dB
Phase Coverage	0-360°

In [41], design of Reggia-Spencer phase shifter is explained in detail by analytically solving the problem of electromagnetic wave propagation in rectangular waveguide partially filled with ferrite material. In this Chapter, the exact geometry is solved numerically in the given frequency band of operation.

3.1.1 Determining Ferrite Material Parameters and Geometry

In Figure 3.1 several examined configurations for Reggia-Spencer phase shifter are given. Teflon or polyfoam support is used to hold the ferrite in its place in rectangular waveguide for configurations (a) and (b). However the drawback of these structures is the difficulty of operation in high average power levels because of the heat removal problem. Cooling with low loss dielectric liquid increases average power handling of these configurations [42].

(a) Rod configuration

(b) Bar configuration

(c) Full-height bar configuration

(d) Bar configuration with E-plane dielectric slabs

Microwave ferrite material

(e) Bar configuration with H-plane dielectric slabs

Boron Nitride or Beryllium Oxide
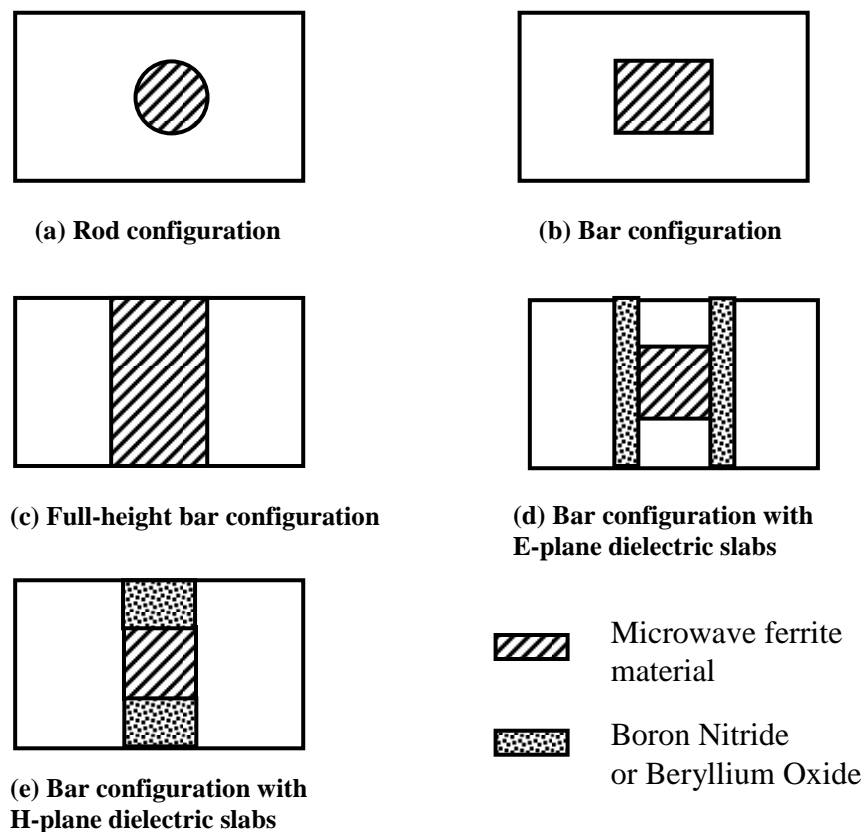
Figure 3.1 Reggia-Spencer Phase Shifter Configurations

29

For configuration (c) lower DPS per unit length is obtained as compared to partial height configurations [43]. In configurations (d) and (e) ferrite material is placed between dielectric slabs having high thermal conductivities to easily remove the heat generated in the ferrite structure by RF heating. Operation in 100 Watt of average microwave power level resulted in 12°C temperature rise between waveguide wall and center of the ferrite material causing only 3% decrease in DPS in configuration (d) [44]

In this study, configuration (a) is designed and fabricated. For this configuration optimum parameters for ferrite material and rod dimensions are given in Table 3.2.

Table 3.2 Optimum design parameters for rod configuration [1]

Parameter	Optimum Value	Calculated Value
Saturation Magnetization, $4\pi M_s$ (Gauss)	$\dfrac{\gamma 4\pi M_s}{\omega_0} \cong 0.5$	$4\pi M_s \cong 1700$
Diameter of ferrite rod, D (mm)	$\dfrac{\lambda_0}{1,706\sqrt{\varepsilon_r}} \le D \le \dfrac{\lambda_0}{1,308\sqrt{\varepsilon_r}}$	$4.7 \le D \le 6.2$
Length of ferrite rod (mm)	$l = \dfrac{\Delta\phi_{max}}{\Delta\beta}$	$l = 120$

where ω_0 is the center frequency of the phase shifter, λ_0 is the free-space wavelength at the center frequency, ε_r is the dielectric constant of the ferrite material which is around 15, $\Delta\phi_{max}$ is the maximum required differential phase shift which is 360° and $\Delta\beta$ is differential phase shift per unit length which is expressed as:

$$\Delta\beta = \frac{\pi\sqrt{\varepsilon_r}}{\lambda_0} \frac{\omega_m \omega_i}{\left(\omega_i^2 - \omega^2\right)} \tag{3.1}$$

where

$$\omega_i = \omega_0 + \frac{\omega_m}{2} \tag{3.2}$$

$$\omega_0 = \gamma H_0 \tag{3.3}$$

$$\omega_m = \gamma 4\pi M_s \tag{3.4}$$

From (3.1) it is seen that differential phase shift is proportional with $4\pi M_s$ of the ferrite material. However magnetic losses of the ferrite increase as $4\pi M_s$ increases because of the low field loss phenomenon and peak power handling capacity of the ferrite material decreases with $4\pi M_s$ as explained in Appendix A. On the other hand, choosing a ferrite material with low $4\pi M_s$ would result in a small amount of DPS per unit length. Ferrite material length would have to be made longer to achieve 360° of DPS. As a consequence dielectric and conductive losses increase. At that optimum $4\pi M_s$ value the figure of merit ($\Delta\Phi$/dB) is maximized and adequate power handling is achieved. [1]

Below the lower limit of the rod diameter, phase shift is negligible whereas above the upper limit Faraday rotation starts to develop causing periodic resonances. [1]

Practically rod length is tuned after experimentation with the structure. Since (3.1) does not take into account of the rod diameter effect, $\Delta\beta$ may turn out to be much higher than expected if rod diameter is close to the upper rod diameter limit. [1]

3.2 Numerical Analysis

3.2.1 Analysis of DPS

Simulation model consisting of the ferrite rod, vacuum, waveguide ports and dielectric parts at front and back surfaces of the ferrite rod is shown in Figure 3.2. Finite element method (FEM) based frequency domain (FD) solver of CST is used in EM simulations. Outer surfaces of the vacuum are defined as electric boundary condition which represents the waveguide walls. Cylindrical dielectric parts having same permittivity with ferrite material are needed in order to excite modes at the waveguide ports correctly.
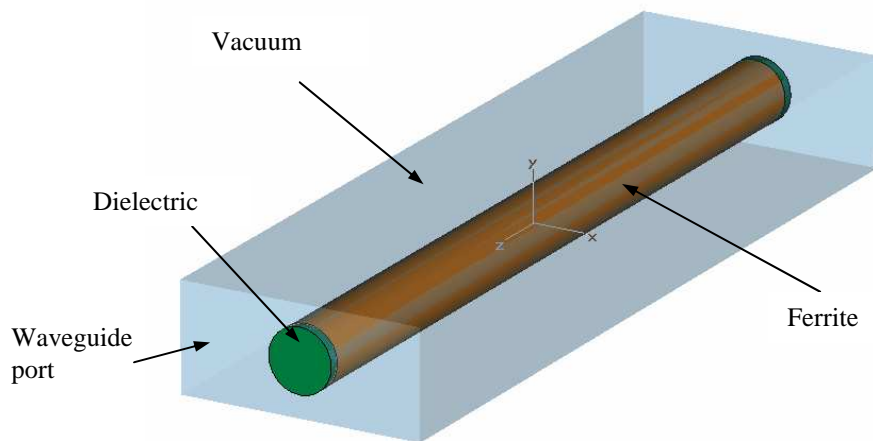
Figure 3.2 Simulation model for Reggia-Spencer phase shifter
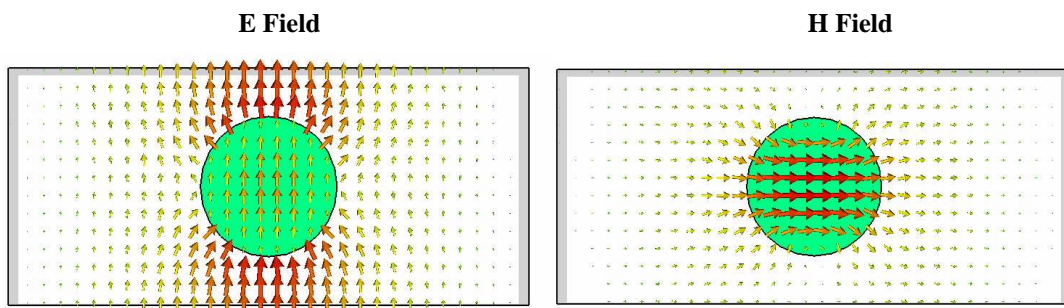
Figure 3.3 TE$_{10}$-like mode at the waveguide ports

Figure 3.3 shows the excited TE_{10}-like mode at the waveguide ports. Note the distortion of the fields at the boundary of the dielectric material because of the high dielectric constant.

Figure 3.4 shows the effect of $4\pi M_s$ and ferrite diameter change on maximum DPS per unit length for the structure given in the inset of figure. It can be observed that DPS increases as $4\pi M_s$ is increased. Also below rod diameters of 5 mm, phase shifting is negligible. Above rod diameters of 6 mm insertion loss spikes are seen below the center frequency which shows the development of Faraday rotation.
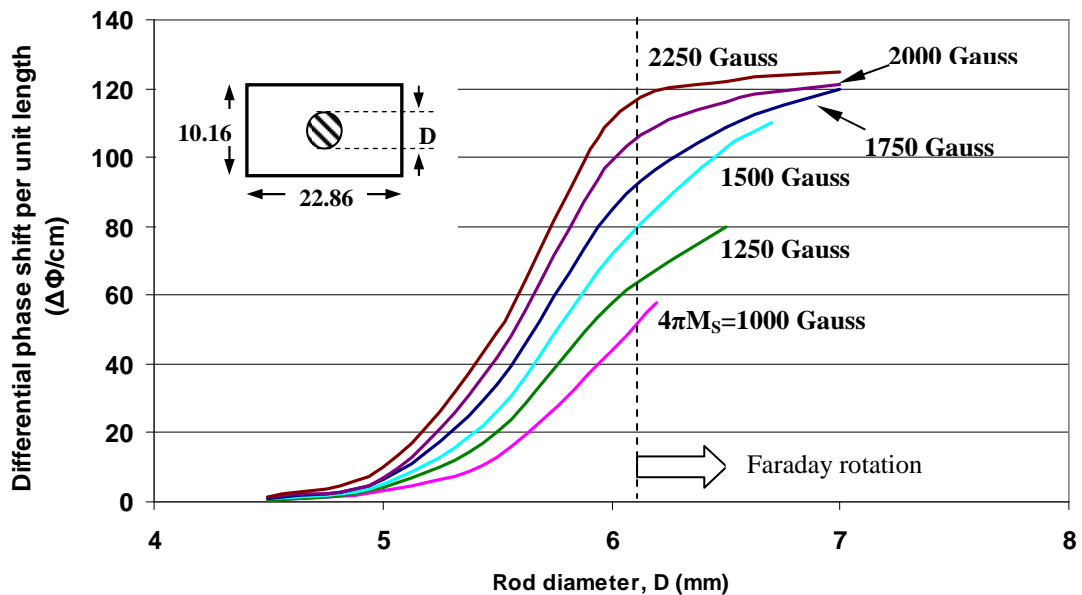
Figure 3.4 Rod diameter dependence of differential phase shift with $4\pi M_s$ as parameter

In Figure 3.5 EM simulation results of frequency dependence of DPS for Reggia-Spencer phase shifter is given within a 10% bandwidth for several rod diameters. There is a strong dependence of DPS on frequency since the coupling between the main mode and the cross-polarized evanescent mode increases with frequency.

33
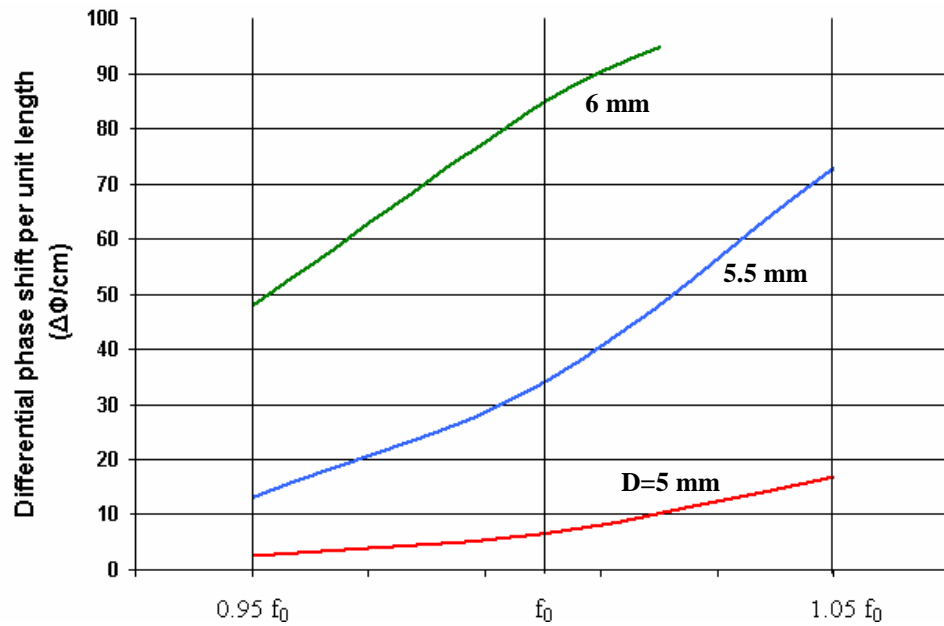
Figure 3.5 Frequency dependence of DPS with rod diameter as parameter ($4\pi M_s$=1750 G)

3.2.2 Effect of Faraday Rotation on Transmission Characteristics

As marked in Figure 3.6 Faraday rotation causes insertion loss spikes at the cut-off frequency of cross-polorized mode. Decrease of ferrite rod diameter moves the onset of Faraday rotation and thus insertion loss spikes higher in frequency.
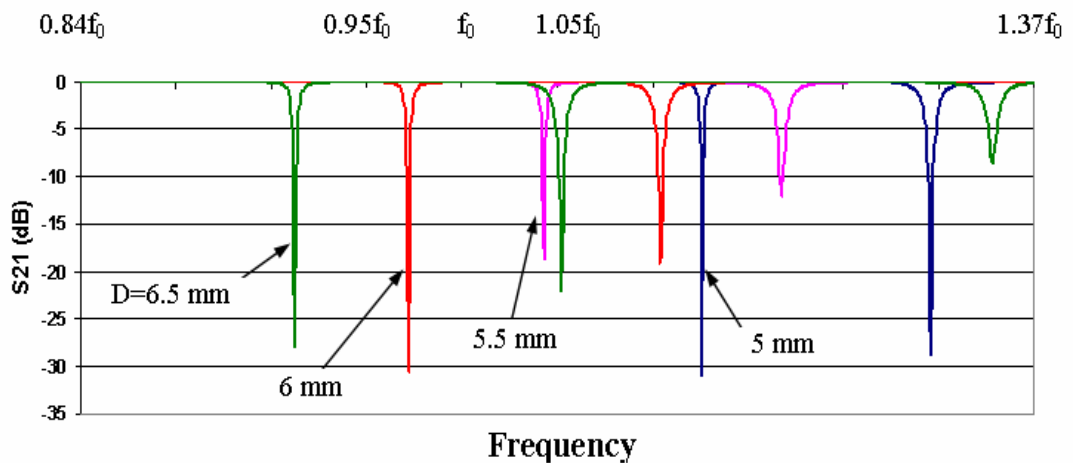
Figure 3.6 Insertion loss spikes caused by the Faraday rotation effect

When choosing the rod diameter both phase shifting performance and transmission characteristics should be taken into account. Since maximum differential phase shift occurs at onset of Faraday rotation, rod diameter should be chosen such that Faraday rotation occurs just above the highest operation frequency.

3.2.3 Impedance Matching

Impedance matching of the ferrite filled waveguide to the standard X-Band waveguide (WR-90) can be done by putting tapered dielectric transformers at the ends of the ferrite rod or by tapering the ferrite rod itself as shown in Figure 3.7.

Figure 3.7 Cross section of the tapered ferrite rod showing tapering length and tip radius
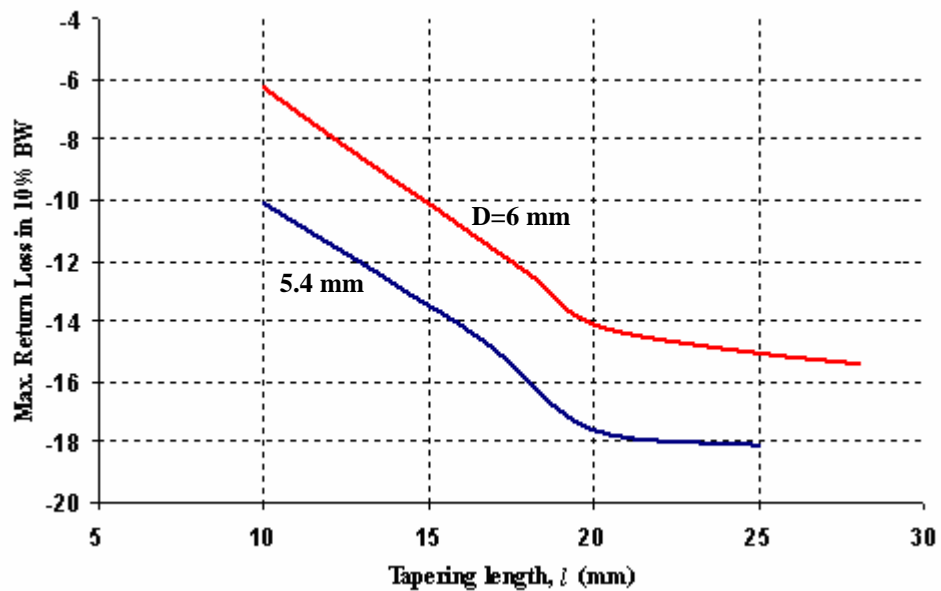
Figure 3.8 Input and output matching versus tapering length (Ø=0.5mm)

In Figure 3.8 electromagnetic simulation results of the maximum return loss values within a 10% bandwidth are given for two different ferrite rods having rod diameters of 5.4 mm and 6 mm. It can be observed that as tapering length is increased a linear improvement of matching is obtained up to tapering length of 20mm. Also for smaller rod diameters better impedance matching can be obtained which is because of the smaller dielectric filling ratio.

3.3 Practical Considerations and Measurement Results

Ferrite rods having diameter of 7.5 mm and length of 75mm have been purchased from the microwave ferrite manufacturer Advance Ferrite Technology (AFT) Microwave Gmbh. Ferrite material is a Calcium-Vanadium doped YIG with grade CV-18 where important microwave characteristics are given in Table 3.3. A photograph of the purchased ferrite rod before and after tapering process is shown in Figure 3.9. A photograph of the fabricated Reggia-Spencer ferrite phase shifter structure is shown in Figure 3.10. Standard X-Band waveguide (WR-90) is used as the waveguide housing of the phase shifter and switching coil of 1000 turns is wound around the waveguide. Wall thickness of the waveguide is reduced up to 0.1 mm in order to decrease switching time and switching energy. Waveguide wall is wrapped with a soft tape so that sharp waveguide sides do not cut the switching wires. Ferrite rod is held in position by a polyfoam support at both ends and position of the rod is tuned with plastic screws by measuring the transmission characteristics.

Table 3.3 CV-19 material parameters [45]

Saturation Magnetization	Remanent Magnetization	Resonance linewidth	Spinwave linewidth	Curie Temperature	Coercive Force
$4\pi M_S$ (Gauss)	$4\pi M_r$ (Gauss)	ΔH (Oe)	ΔH_k (Oe)	T_c (°C)	H_c (Oe)
1800	1210	12	2	230	0.4

Figure 3.9 Photograph of the ferrite rod, before and after tapering process

82 mm

Switching coil

Tuning screws
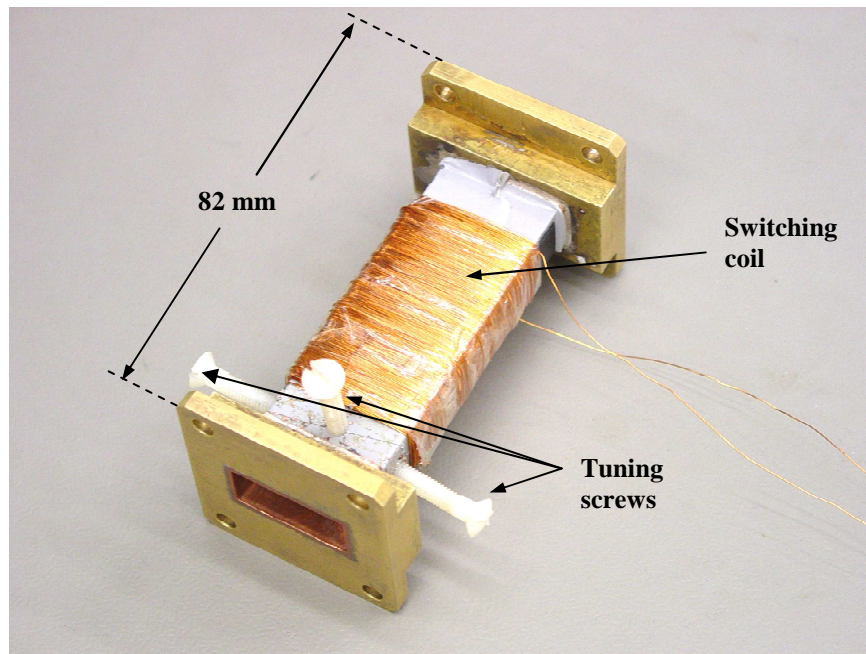
Figure 3.10 Photograph of the fabricated Reggia-Spencer ferrite phase shifter

Three structures are fabricated by changing the ferrite rod diameter. In the first trial, original rod diameter (D=7.5mm) is used. In the second trial, rod diameter is reduced to 5.5mm and in the third trial rod diameter is reduced to 6mm. In all cases impedance matching is obtained by 15mm tapering length and 0.8mm tip radius at both ends.

Measurements are taken with a Vector Network Analyzer (VNA) and continuous current is supplied with a DC power supply. A photograph of the measurement setup is given in Figure 3.11. For the DPS measurements at different temperatures an adjustable hot/cold plate device is used.
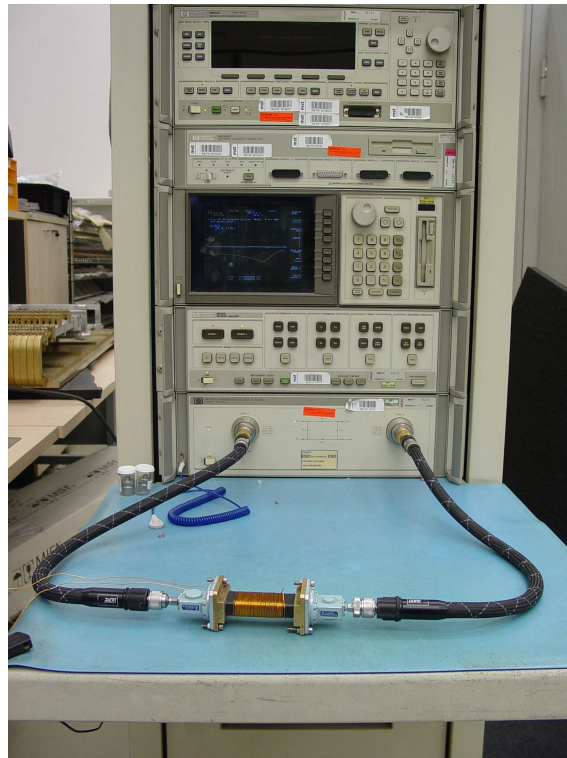
Figure 3.11 A photograph of the measurement setup for Reggia-Spencer ferrite phase shifter

3.3.1 First Trial

Insertion loss and return loss of the Reggia-Spencer phase shifter with ferrite rod diameter of 7.5 mm is given in Figure 3.12. A good impedance matching could not be obtained and deep resonances are observed in transmission characteristics originating from Faraday rotation. Because of the poor transmission characteristics DPS performance is not investigated for this structure.
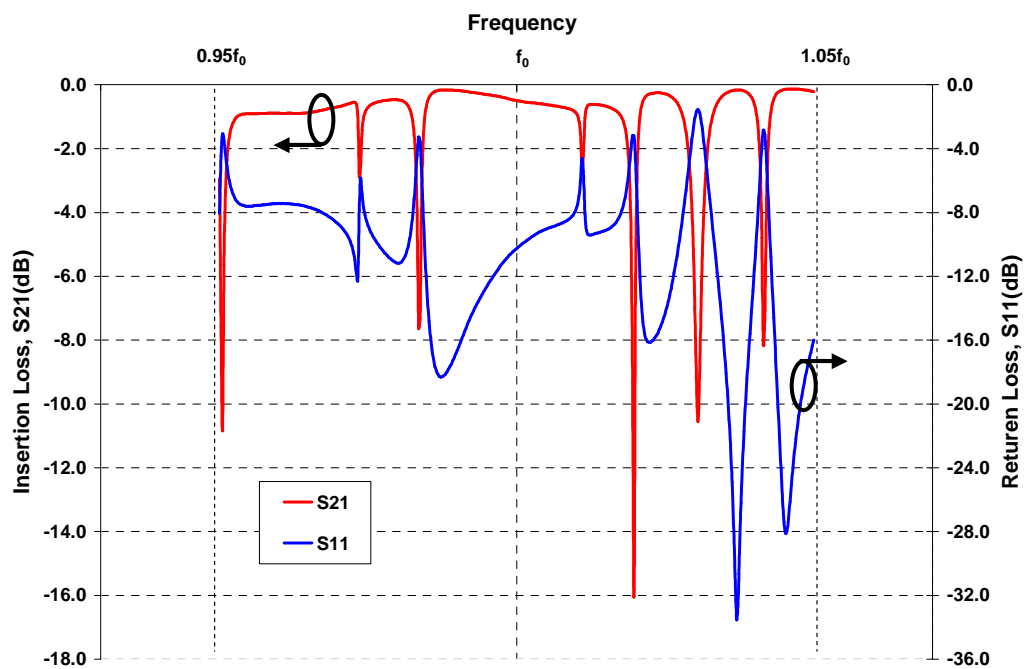
Figure 3.12 Measurement results of insertion loss and return loss characteristics for first trial (D=7.5mm)

3.3.2 Second Trial

Measured transmission characteristics for the second trial (D=5.5 mm) are given in Figure 3.13. Better impedance match is obtained and much less resonances is seen. At $f=1.02f_0$, insertion loss notch with magnitude -1.5dB is observed. By tuning the position of ferrite rod with the plastic screws the place and magnitude of the notch is seen to be adjustable. Insertion loss has an average value of -0.2dB with ±0.12dB modulation on it in 10% BW. Peak value of the return loss is -13dB.
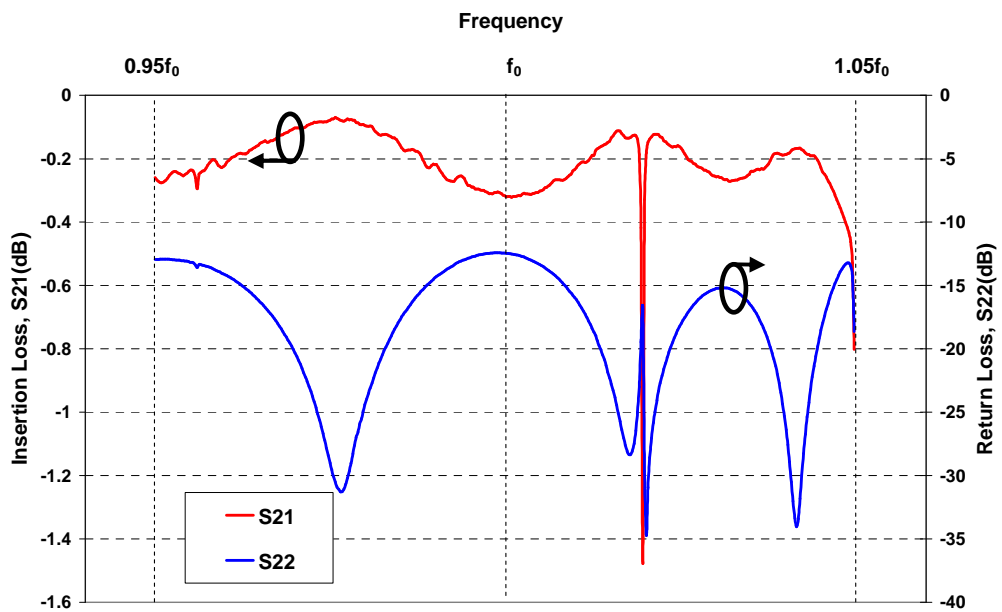
Figure 3.13 Measurement results of insertion loss and return loss characteristics for the second trial (D=5.5mm)

DPS versus switching current characteristics is given in Figure 3.14. Note that reference phase state is taken to be the state with no magnetization, i.e. no current applied, at each frequency point. High frequency dependence of DPS is observed which is expected from the EM simulation results given in Figure 3.5. Above 200mA DPS increases very slowly showing the saturation of the ferrite material.
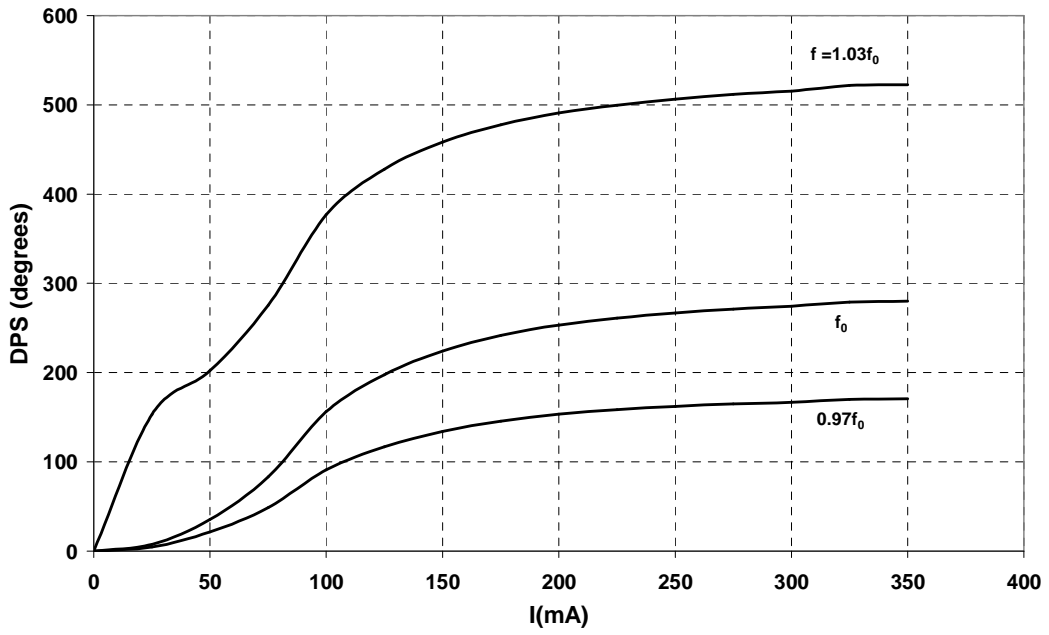
Figure 3.14 Measurement results of DPS for the second trial at room temperature (D=5.5mm)

The requirement of 360° DPS could not be satisfied for frequencies below $1.02f_0$. To satisfy this requirement in 10% BW, length of the ferrite rod should be around 25 cm which is unreasonable since losses increase too much.

3.3.3 Third Trial

Measured transmission characteristics for the third trial (D=6 mm) are given in Figure 3.15. Two large insertion loss spikes are seen in the BW, one at $f=1.005f_0$ with 2dB loss and the other at $f=1.04f_0$ with 8.1dB loss. Insertion loss has an average value of 0.4dB with ±0.3 dB modulation on it in 10% BW. Peak value of the return loss is -8dB.
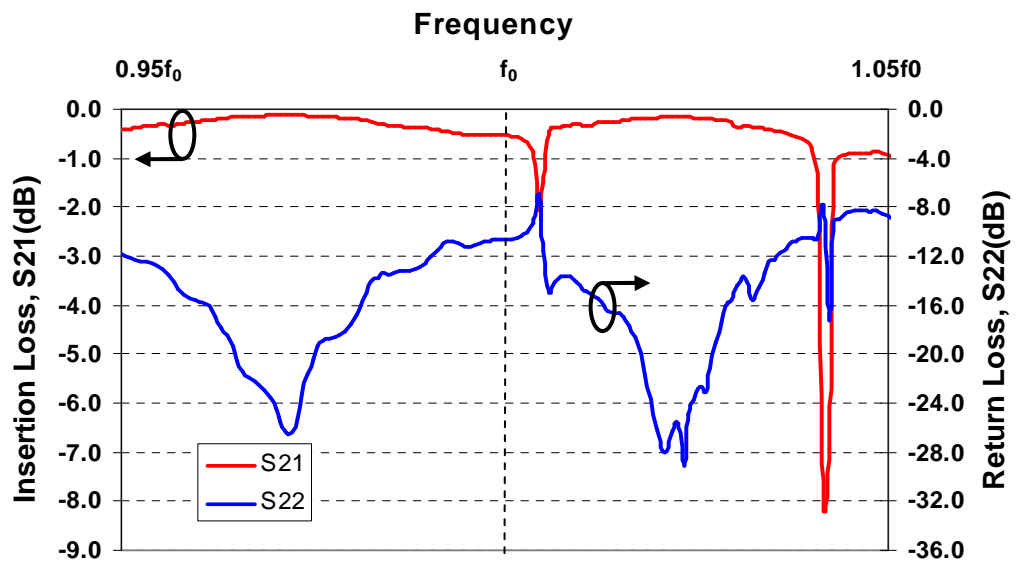
Figure 3.15 Measurement results of insertion loss and return loss characteristics for the third trial (D=6mm)
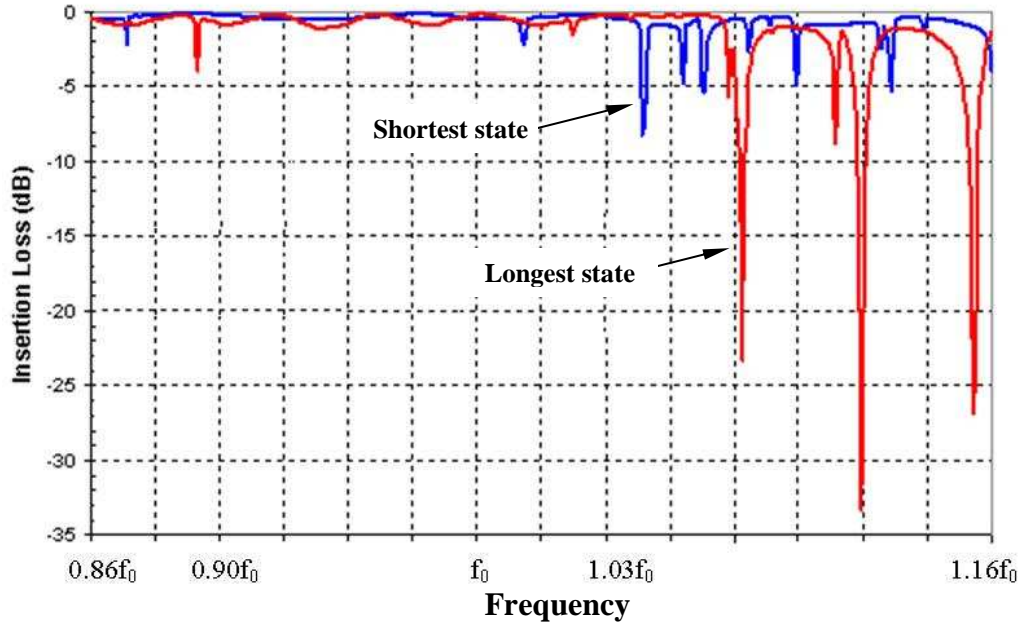
Figure 3.16 Insertion loss of shortest state and longest state (D=6mm)

In Figure 3.16 wideband measurement results of insertion loss for the shortest state (I=0 mA) and longest state (I=400 mA) is given. Deep resonances originating from Faraday rotation are observed above $1.03f_0$. After tuning amplitude of the resonances are reduced to -2.5dB in $0.9f_0$-$1.03f_0$ BW for all magnetization levels.
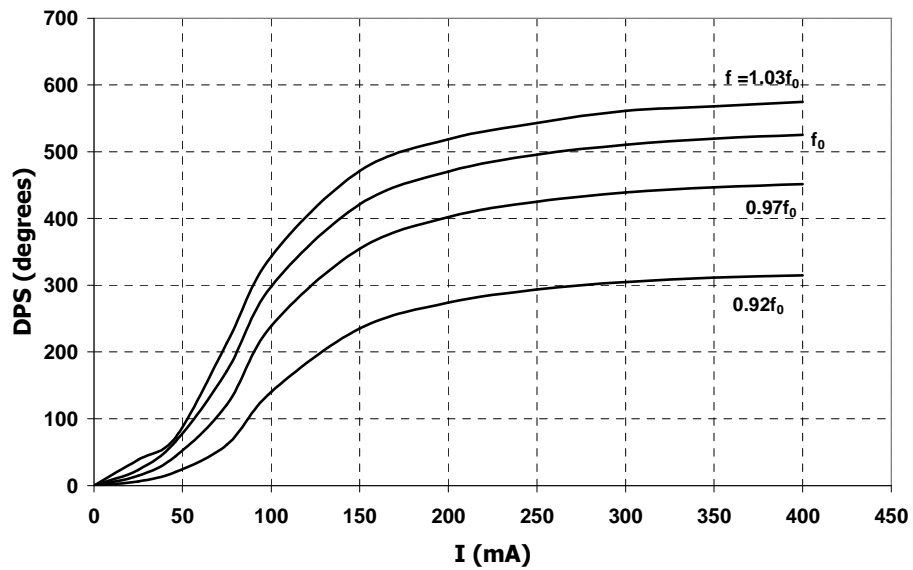
Figure 3.17 Measurement results of DPS for the third trial at room temperature (D=6 mm)

43

Measurement results of DPS for the third trial given in Figure 3.17. As compared to second trial DPS is much less dependent on frequency and requirement of 360° of DPS in 10% BW is satisfied.

The comparison of measurement results of maximum DPS, i.e. the insertion phase difference between the shortest state (I=0 mA) and the longest state (I=400 mA) and EM simulation results are given in Figure 3.18. There is an approximately 90° phase difference between the actual simulation model (tapered) and measurement result. This difference is thought to be resulting from the errors of the EM simulation at the cut-off frequency of the waveguide. The structure without tapering (Figure 3.2) has 200° more DPS than the structure with tapering at f=f_0 and there is much similarity with the measurement results at the frequencies where Faraday rotation exists.
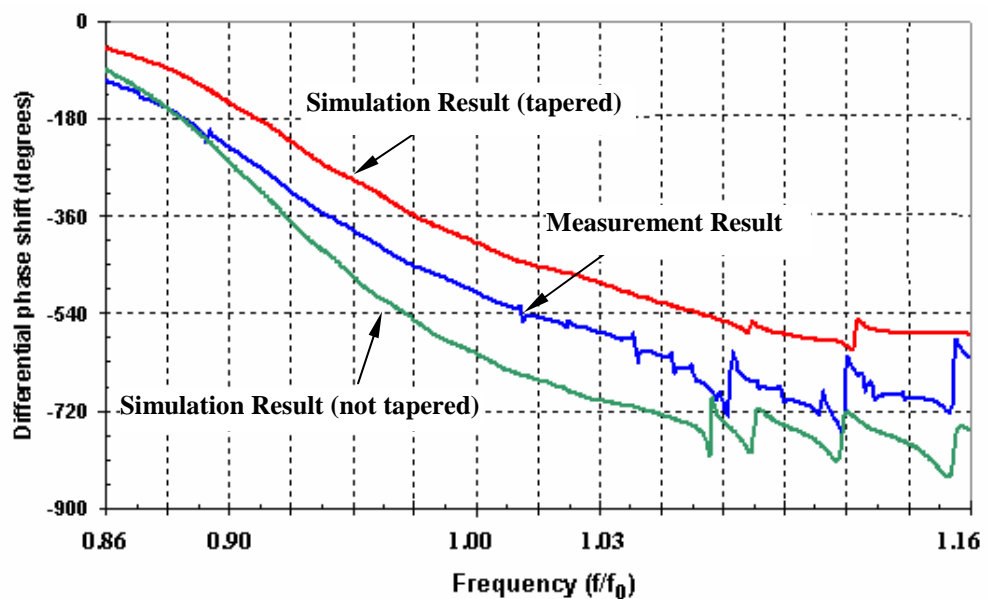
Figure 3.18 Differential phase shift between the longest state and shortest state (D=6mm)

In Figure 3.19 measurement results of maximum DPS between temperature range of 0-100°C is given. DPS decreases with increasing temperature because of the reduction of magnetic activity in the ferrite material. In Appendix A.2.2 effect of temperature on ferrite materials is explained in detail.

44
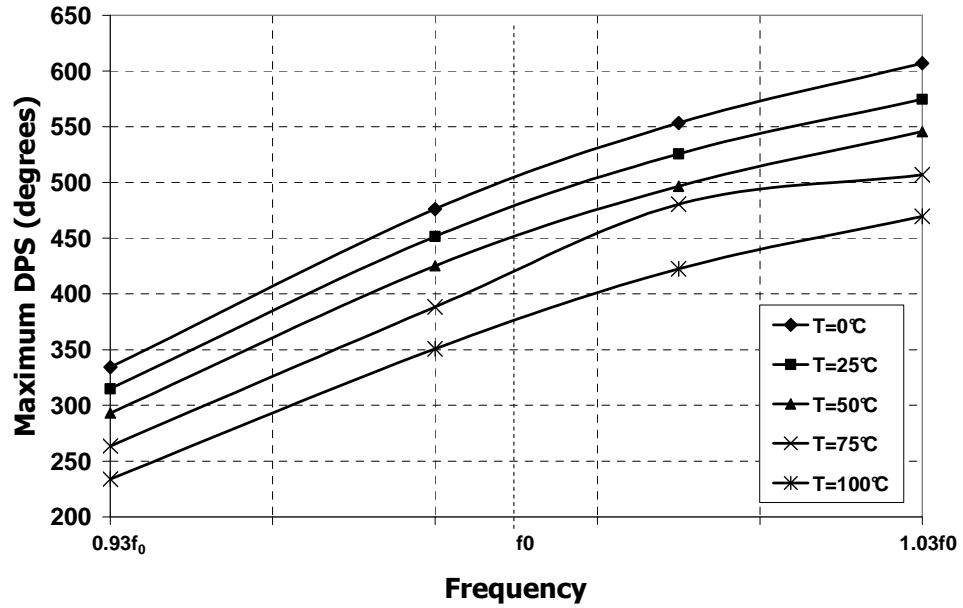
Figure 3.19 Variation of DPS with temperature (D=6mm)

3.4 Conclusion

Measurement results for the three structures having different ferrite rod diameters showed the difficulty of operation in 10% BW without resonances in transmission characteristics. This is because of the necessity of operation at the onset of Faraday rotation in order to obtain sufficient amount of DPS. If frequency dependent DPS is not a concern it is showed that resonance-free operation within a 5% BW is possible.

Maximum DPS is obtained with 400mA continuous holding current. However maximum current can be reduced to 250mA with only 5% decrease of DPS. Power dissipation at the maximum phase state is calculated as 0.188W with the total coil resistance of 15Ω. Average switching time between the phase states is measured as 4ms.

It is estimated that maximum peak power handling is 500 W and average power handling is 20 W for the fabricated prototype. Higher average power handling can be obtained with different configurations explained in Section 3.1.1. Temperature sensitivity of the designed prototype is found as 1.4

45

CHAPTER 4

ANALYTICAL AND NUMERICAL ANALYSIS OF TWIN-TOROID FERRITE PHASE SHIFTER

In Section 2.4.2 general characteristics of twin-toroid ferrite phase shifter is explained. Twin-toroid structure found widespread usage in radar applications since 1960s. However only approximate theories [26, 37, 46-48] used in determining the performance of the phase shifter because of the complicated boundary value problems of waveguides partially loaded with inhomogenously biased ferrites. Numerical methods, especially FEM and Finite Difference Time Domain (FDTD) method, provide an accurate characterization of toroidal ferrite phase shifters as for other ferrite devices such as circulators and isolators.

In this Chapter, the principle of operation of the twin-toroid ferrite phase shifter is explained and some important performance characteristics are examined using analytical expressions and numerical methods. In CST®, EM simulation models are developed estimating differential phase shift (DPS) and insertion loss characteristics accurately. Using a dielectric model, the propagation characteristics of higher order modes are investigated and methods to suppress these modes are explained.

4.1 Twin-Slab Approximation

In twin-toroid structure, microwave energy is mainly concentrated in the region around the high dielectric constant material at the center of the waveguide. In Figure 4.1 EM power and H field distribution in the twin-toroid structure on x-y plane is given for the wave propagating in +z direction.
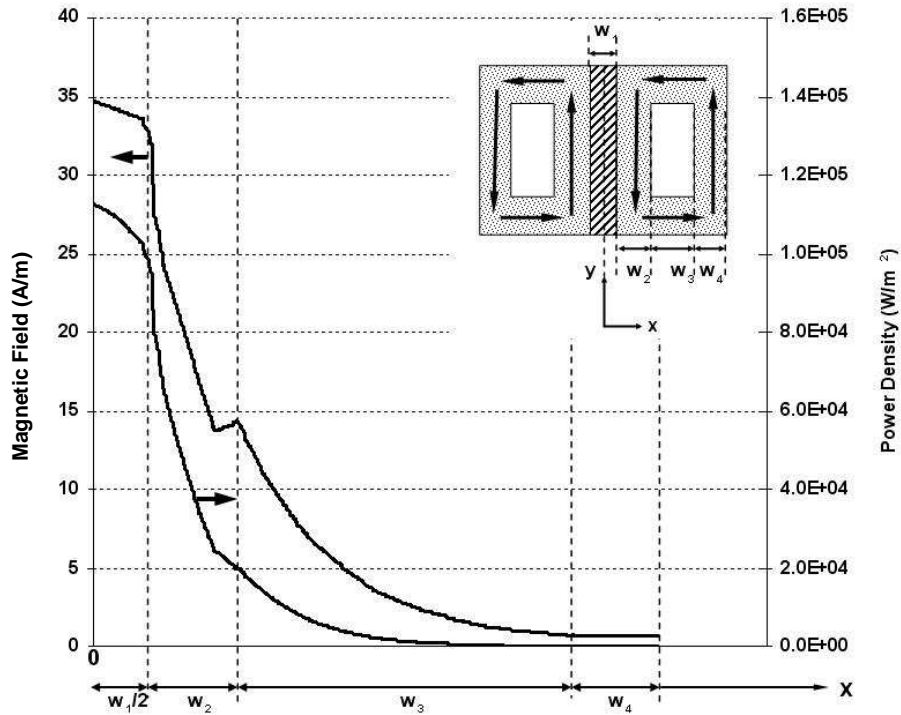
Figure 4.1 EM power density and H field distribution in x-y plane for x>0

Since the microwave magnetic field magnitude in the vertical ferrite regions near narrow waveguide wall is very small, their effect on differential phase shift can be neglected. The top and bottom walls of the toroids are magnetized in ±x directions which are parallel to the plane of circularly polarized H field (ordinary wave). Because of this, interaction of microwave fields with the ferrite material is small. Also the effect of top and bottom walls cancels each other since they are oppositely magnetized. The vertical ferrite regions next to the center dielectric slab have the dominant effect in generating the differential phase shift. The principle of operation of the twin-toroid phase shifter can then be approximated by the twin-slab approximation [26, 46] shown in Figure 4.2.

47
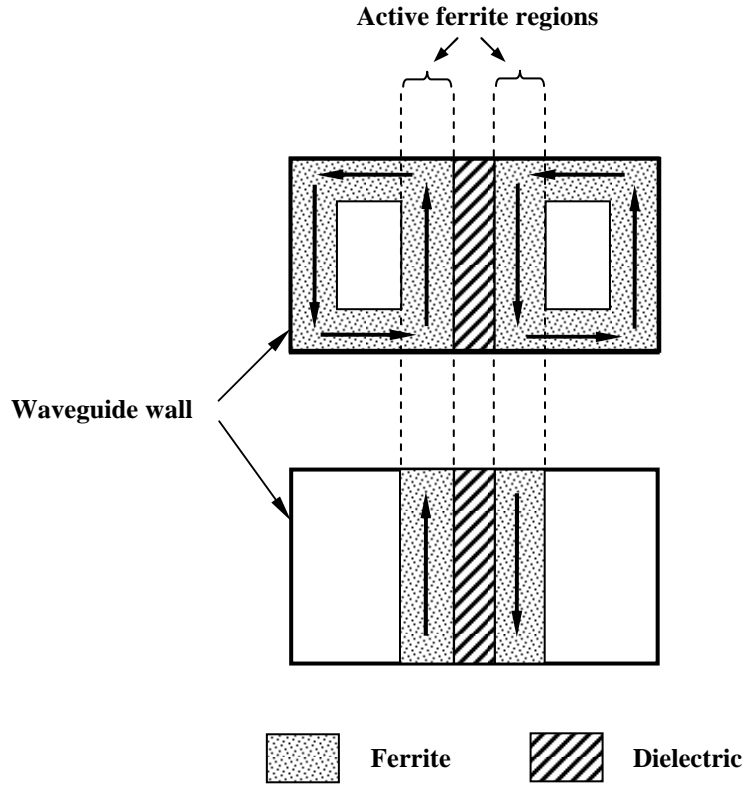
Figure 4.2 Reduction of the twin-toroid structure to the twin-slab geometry

4.1.1 Principle of Operation

In Figure 4.3, H Field polarization representation of the TE_{10} mode wave traveling in $+z$ direction in an empty rectangular waveguide is shown. On x-z plane, polarization of the H Field is linear (LP) at $x=0, \pm a/2$ and circular (CP) at $x=\pm x_1$. Between linearly and circularly polarized coordinates H field is elliptically polarized (EP). For $x<0$, the vector rotation of H field with time is clockwise whereas for $x>0$ it is anti-clockwise as shown for circularly polarized cases at $x=-x_1$ and $x=x_1$.

When ferrite slabs which are magnetized in –y and +y directions are placed at at $x=-x_1$ and $x=x_1$ respectively, magnetization causes the electrons to precess clockwise in the ferrite slab at $x=-x_1$ and anti-clockwise in the ferrite slab at $x=x_1$ as shown Figure 4.4.
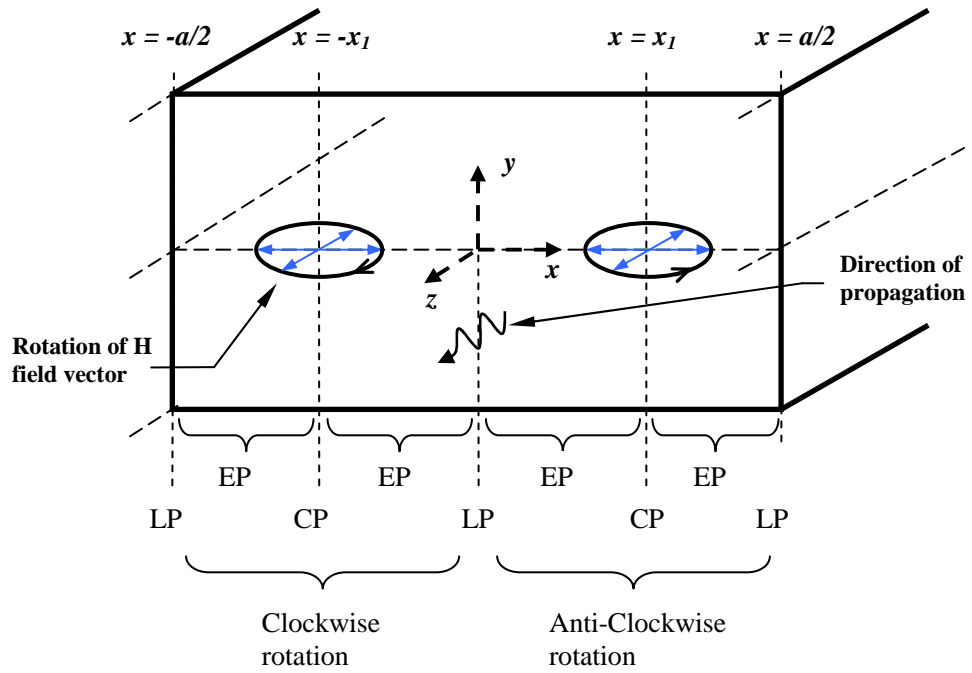
Figure 4.3 Polarization distribution of H field of TE10 Mode in an empty rectangular waveguide at xz plane
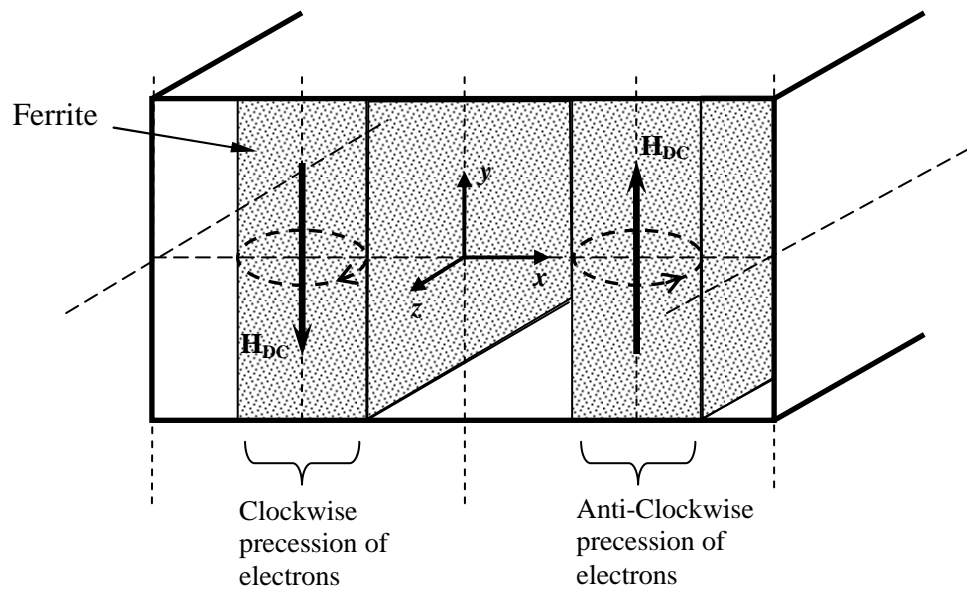
Figure 4.4 Precession senses of electrons in the ferrite slabs magnetized in ±y direction

When the precession of electron spin is in the same sense as the vector rotation of the H field, there is strong interaction between electromagnetic field and ferrite medium and resultant effective permeability of the ferrite is less than unity. If the precession of electrons is in the opposite sense with respect to the rotation of H field vector, then there is minimum interaction between ferrite medium and electromagnetic field and the resultant effective permeability is greater than unity [1].

Figure 4.5 and Figure 4.6 shows the strong interaction and weak interaction between electromagnetic wave and ferrite slabs respectively. For a given magnetization direction, the permeability and thus the propagation constant of a wave is different for two directions of propagation giving the twin-slab geometry non-reciprocal characteristics.
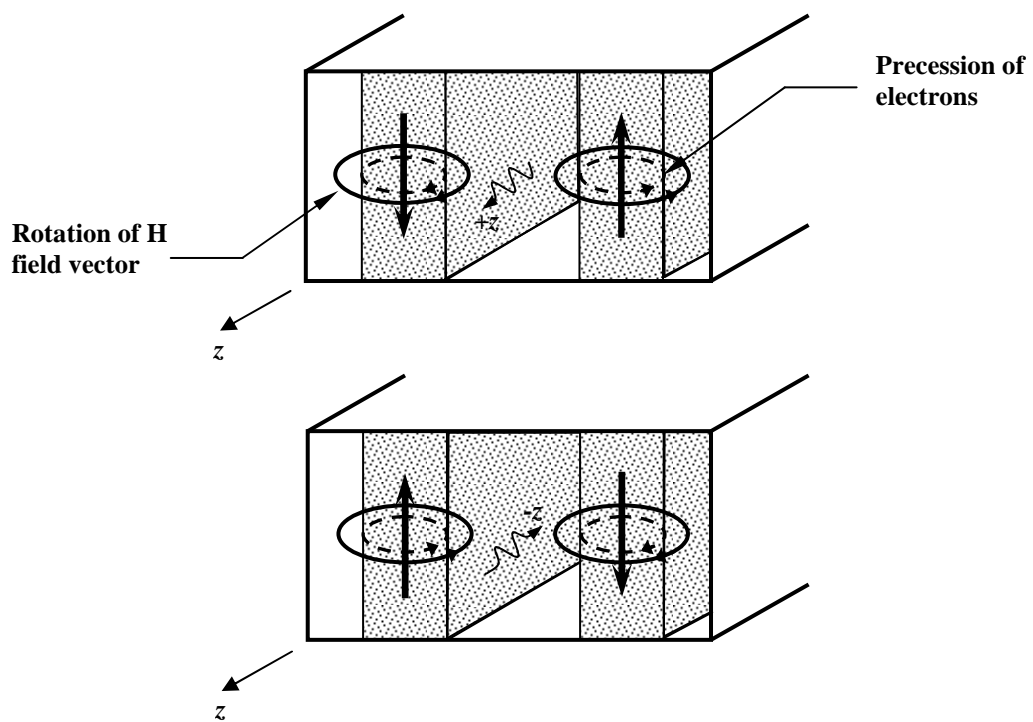
Figure 4.5 Strong interactions between electromagnetic field and ferrite slabs
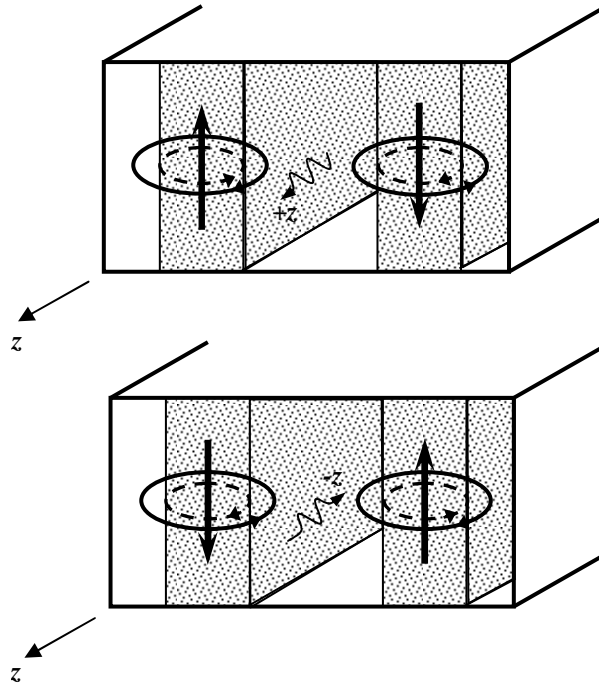
Figure 4.6 Weak interactions between electromagnetic field and ferrite slabs

For a given direction of propagation, if magnetization direction is reversed because of the change of interaction between ferrite material and electromagnetic wave, a different propagation constant and consequently differential phase shift is obtained.

Figure 4.7 shows EM simulation results of the microwave H field distribution for two directions of propagation for 1 Watt of incident power. + components of the H field correspond to the wave propagating in +z direction and - components of the H field correspond to the wave propagating in -z direction. As a high permittivity dielectric material is placed between the ferrite slabs, magnetic field is displaced such that both x and y components of the H field concentration in the ferrite material increase. Since interaction of H field with ferrite material increases, more DPS is obtained.
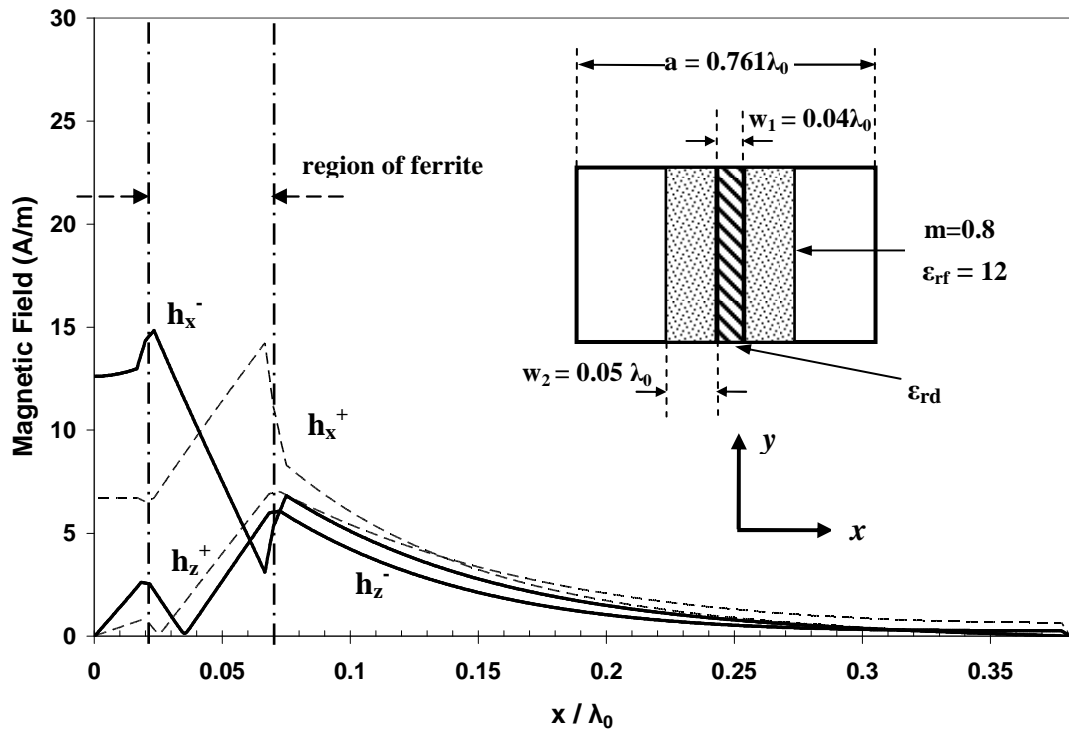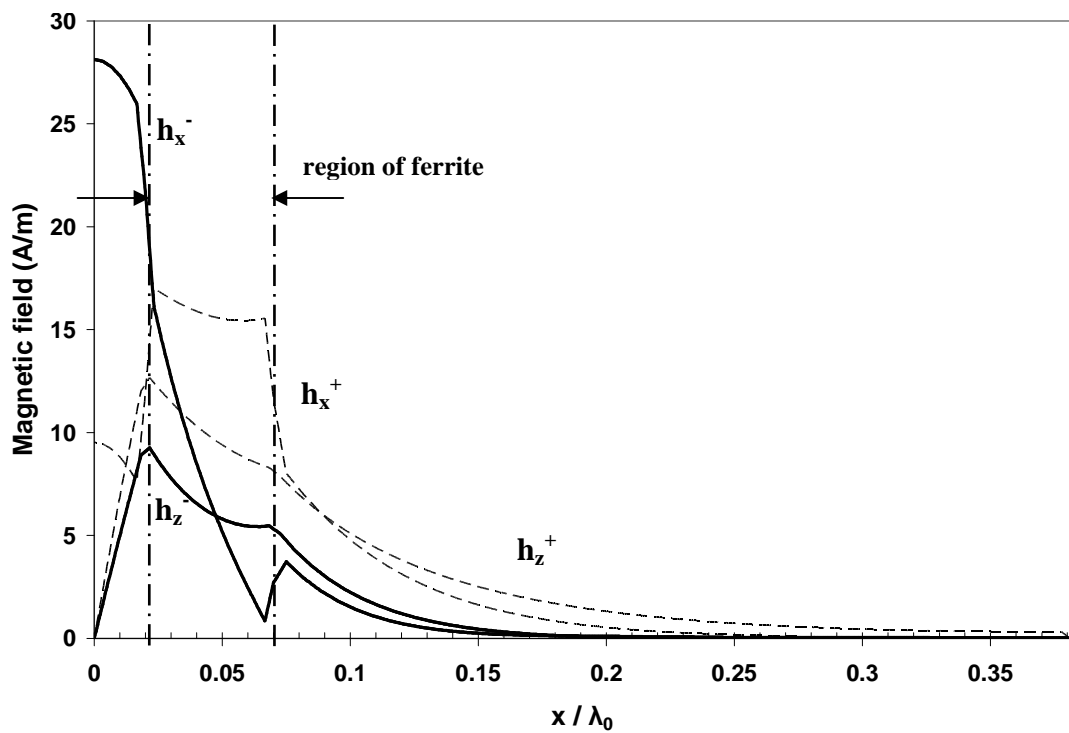
Figure 4.7 H field distribution for twin-slab geometry for x>0. (a) $\varepsilon_{rd} = 1$ **and (b)** $\varepsilon_{rd} = 40$
Ferrite material: m = $\gamma 4\pi Mr/w_0 = 0.8$

4.1.2 Numerical and Analytical Solutions of Differential Phase Shift

In this section, analytical results given in [26] and results obtained by EM simulations using CST are given and compared. In Figure 4.8, effect of remanent magnetization on the differential phase shift characteristics for the twin-slab geometry is given. The dimensions of the calculated structure are shown in inset of Figure 4.8. Note the almost linear increase of differential phase shift with normalized remanent magnetization $m = \gamma 4\pi M_r / w_0$ and with permittivity of dielectric material between ferrite slabs. Large values of differential phase shift is obtained as m approaches unity, however as will be discussed later impedance matching problems and increase of magnetic losses limit the value of m.
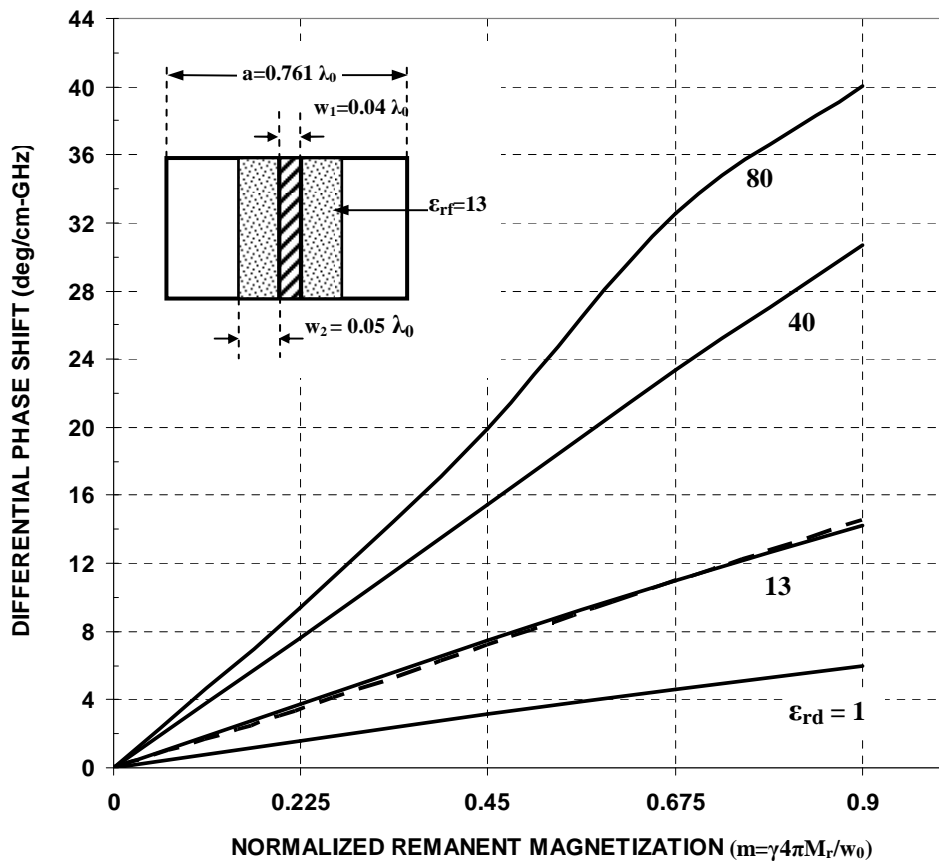
Figure 4.8 EM Simulation (solid lines) and analytical results (dashed line) of differential phase shift versus normalized remanent magnetization with central dielectric permittivity value as parameter

53

In Figure 4.9 analytical calculations and EM simulation results of DPS are plotted as a function of dielectric slab thickness for various dielectric materials. Note that the results for high dielectric constant materials show pronounced maxima as a function of w_1. Further increase of w_1 decreases the DPS because of the decrease of magnetic field intensity in the ferrite material.
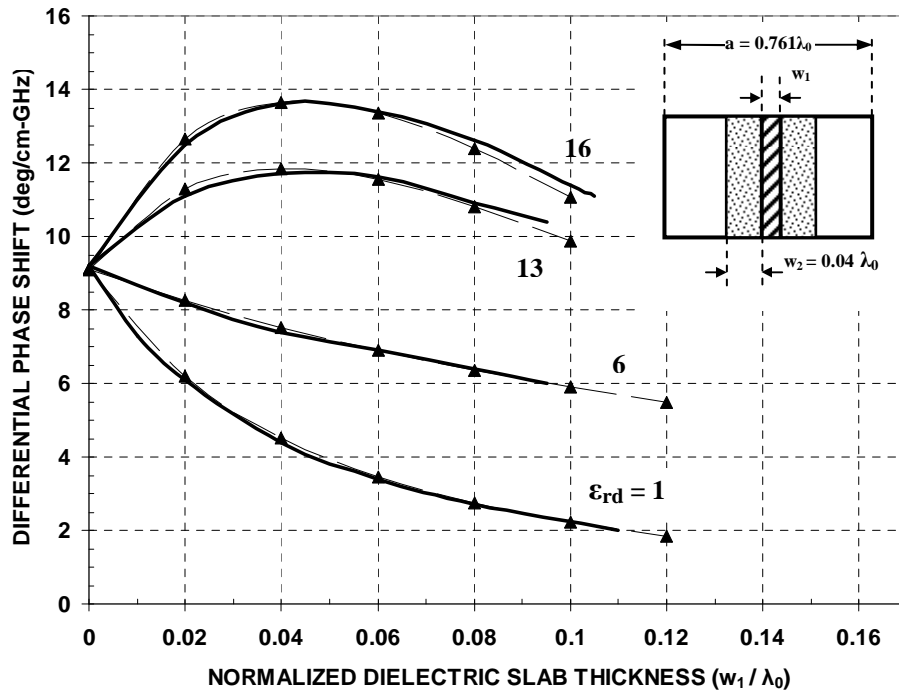
Figure 4.9 Analytical results(solid line) and EM simulation results(dashed line) of $\Delta\Phi$ versus w_1/λ_0 with ε_{rd} as parameter

In Figure 4.10 DPS characteristics versus frequency is given for several waveguide widths. As waveguide width is reduced the energy density in ferrite material increases causing the DPS to increase. For waveguide widths between 0.35-0.4 λ_0 flat differential phase shift is obtained for above 40% bandwidth. Since the frequency of operation of the device is above magnetic resonance, the magnetic activity of the ferrite decreases with increasing frequency. On the other hand, as frequency increases plane of circularly polarized H field move towards the high field region which increases the ferrite-microwave interaction. These two counteracting effects provide the DPS to be flat across a wide operating bandwidth.
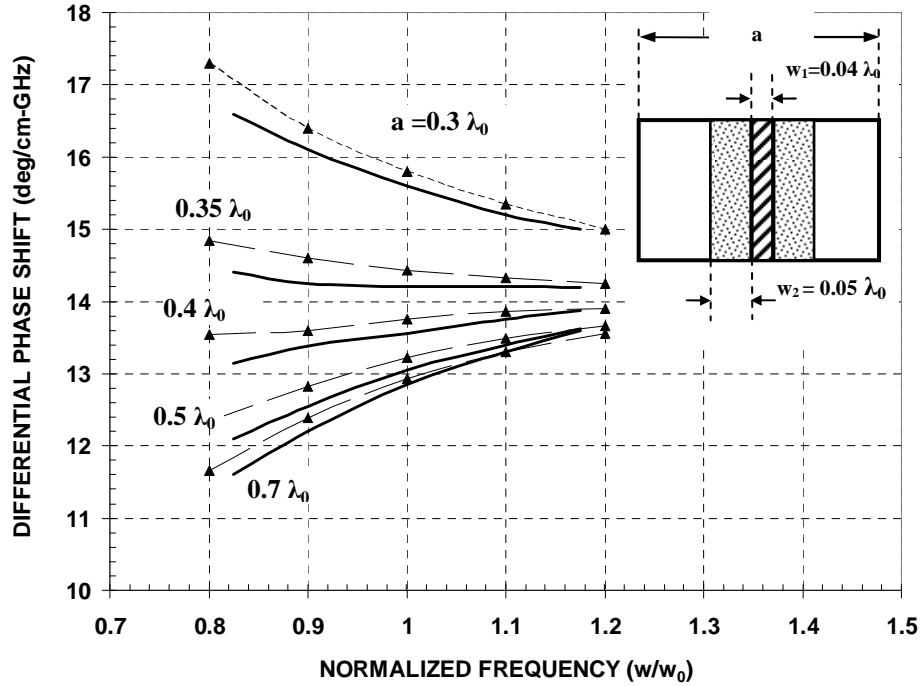
Figure 4.10 Analytical results(solid line) and EM simulation results(dashed line) of $\Delta\Phi$ versus w/w_0 with waveguide width a as parameter

4.1.3 Numerical and Analytical Solutions of Insertion Loss

Dielectric and magnetic losses are independent loss mechanisms occurring in ferrite materials. While dielectric loss tangents of garnet type ferrites are smaller than 0.0002, it could approach 0.0015 for spinel ferrites [45, 49, 59]. In twin-slab structure the loss contribution of the dielectric material between the ferrite slabs is high, since as shown in Figure 4.1 power is mainly concentrated in that region. Mismatch losses caused by reflections, conductive losses on waveguide walls, dielectric losses of impedance matching sections and dielectric losses of non-conductive epoxy used for bonding the ferrites and dielectric slab also contribute to the total loss of the structure.

Magnetic losses of ferrites depend on material parameters ($4\pi M_s$, ΔH, ΔH_k), magnetic state, operating frequency, power and temperature of the material. The magnetic loss for a partially magnetized state such as that would exist in a latching ferrite phase shifter or below resonance circulator can be characterized by a single loss parameter

μ" the imaginary part of the diagonal component of the permeability tensor for a demagnetized ferrite. For $\gamma 4\pi M_s/w < 0.7$ μ'' follows a simple power law relationship:

$$\mu'' = A\left(\frac{\gamma 4\pi M_s}{w}\right)^N$$

(4.1)

where A and N are determined for several garnets and MnMg, Ni and Li spinels. At larger values of $\gamma 4\pi M_s/w$, μ'' grows rapidly as low-field losses (Polder-Smit losses) set in [50, 62].

In Figure 4.11 schematic representation of magnetic losses shows the increase of magnetic losses below saturation of the ferrite for $\gamma 4\pi M_s/w > 0.7$. High absorptive properties at resonance regions are used in devices such as isolators.
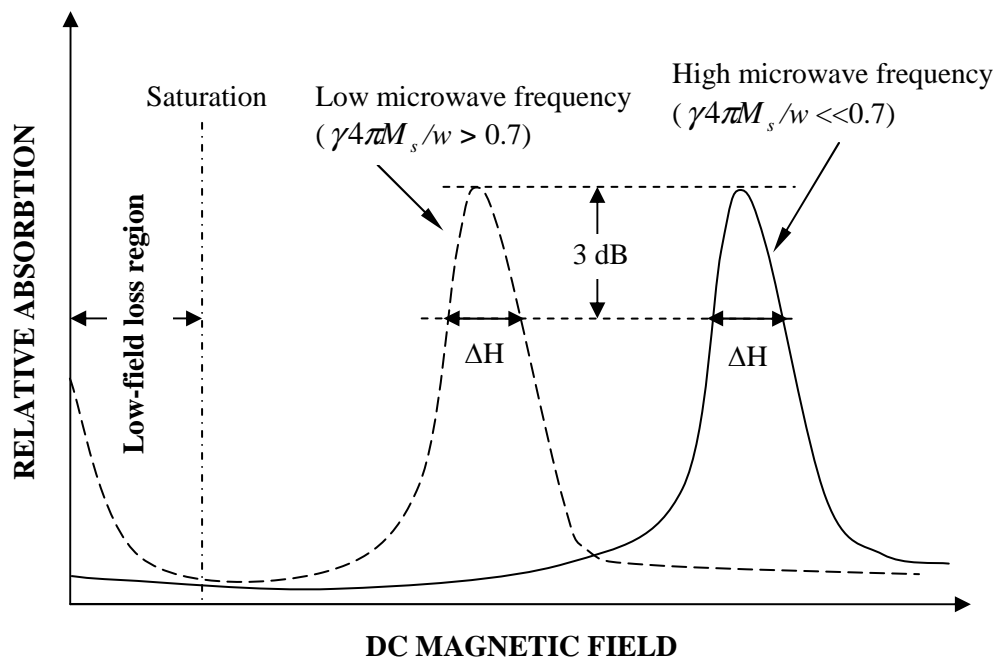
Figure 4.11 Schematic representation of absorbtion as a function of DC magnetic field for a typical ferrite showing resonance and low-field loss mechanisms

In Figure 4.12 measured values of μ'' [59] are given to compare the magnetic losses of several ferrite materials. Low-field losses cause a sharp increase of μ'' for $\gamma 4\pi M_s/w > 0.7$.
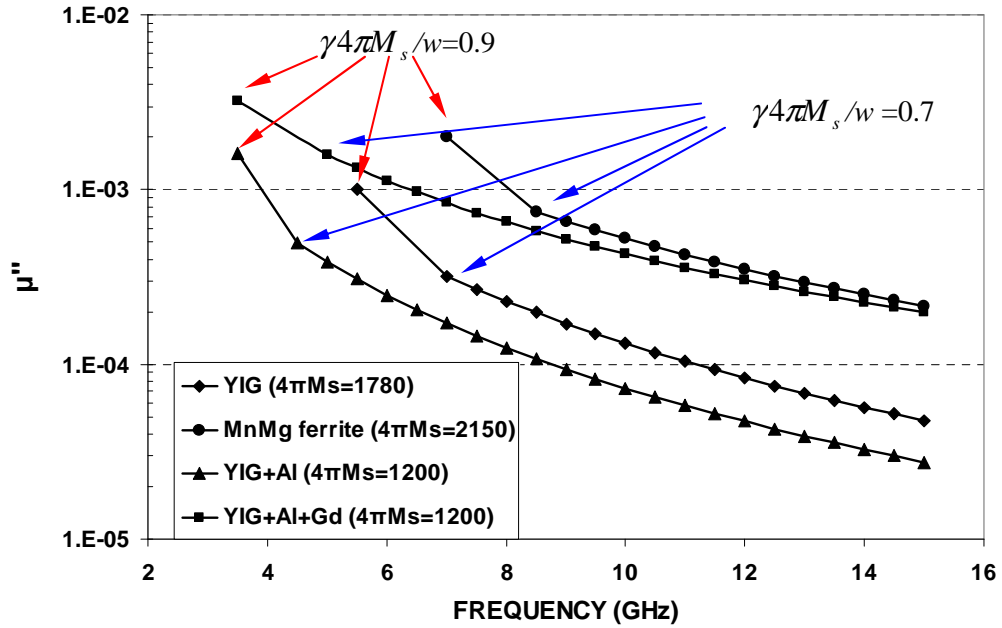
Figure 4.12 μ'' as a function of frequency for different ferrite materials

In EM simulations, magnetic losses arise from low-field loss phenomenon is modeled by changing the resonance linewidth of the ferrite material for each frequency point. In Figure 4.13 and Figure 4.14 EM simulation results of insertion loss for the twin-slab structure having 360° differential phase shift is given. Ferrite materials used are MnMg ferrite and YIG+Al+Gd garnet respectively and normalized dimensions of the structures are the same. The parameter $\gamma 4\pi M_s/w$ is changed by sweeping the frequency. The wall resistance is taken to be 0.07 ohm per square and dielectric loss tangent of the dielectric slab between the ferrite slabs is 0.001 by also taking into account of the loss of the non-conductive epoxy [26]. For ferrite materials dielectric loss tangent is taken as 0.0005. Mismatch losses are subtracted when calculating each loss component separately.

Dielectric and conductor losses for YIG+Al+Gd garnet and MnMg ferrite are about to be the same. Howaver magnetic loss for YIG+Al+Gd garnet is higher than that for MnMg ferrite as would be expected from Figure 4.12. While Gd substitution into the YIG family increases peak power handling capacity and temperature stability, it increases the magnetic losses.
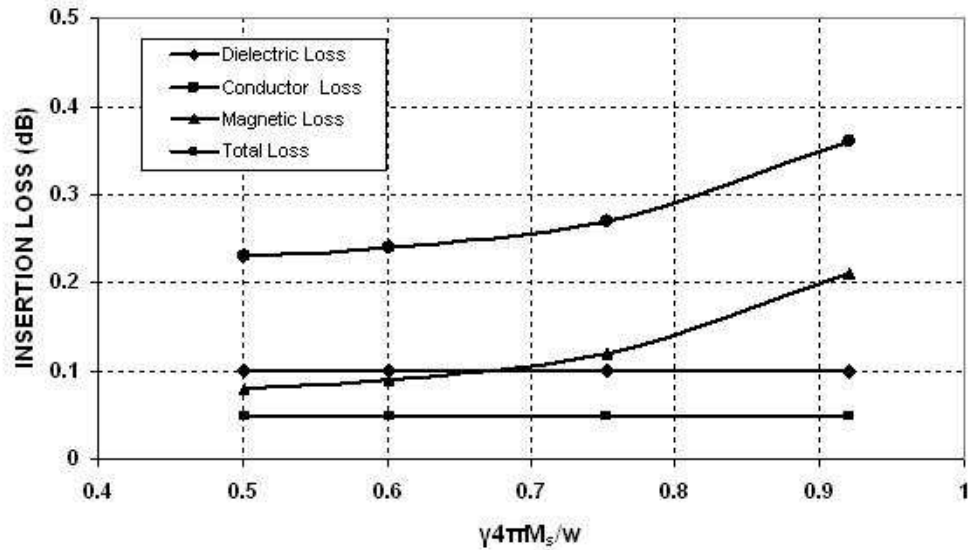
Figure 4.13 Insertion loss of the twin-slab structure with MnMg ferrite
$(w1=0.04\,\lambda_0\,,\,w2=0.05\,\lambda_0\,,\,a=0.761\,\lambda_0\,,\,\varepsilon_{rd}=13,\,\varepsilon_{rf}=12,\,4\pi Ms=2150)$
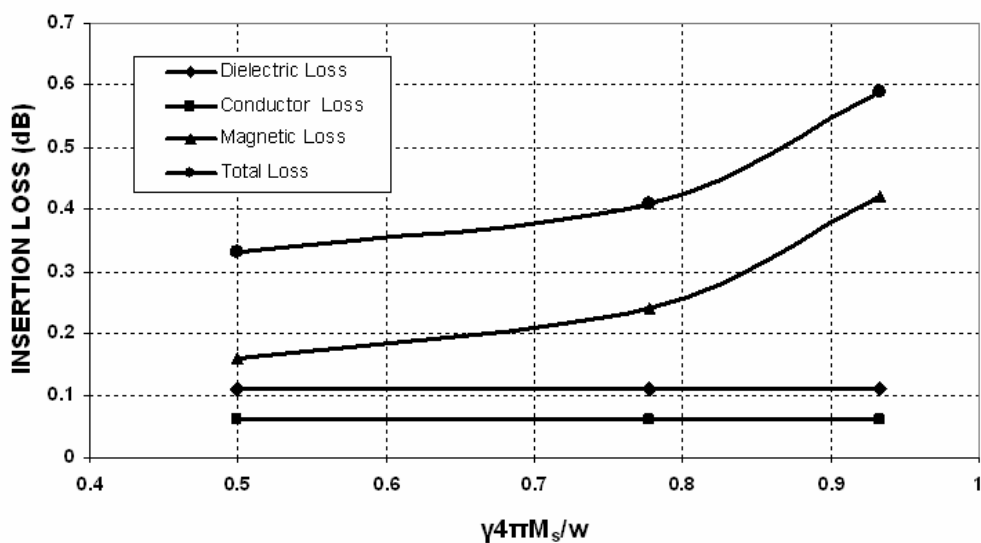
Figure 4.14 Insertion loss of the twin-slab structure with YIG+Al+Gd garnet
$(w1=0.04\,\lambda_0\,,\,w2=0.05\,\lambda_0\,,\,a=0.761\,\lambda_0\,,\,\varepsilon_{rd}=13,\,\varepsilon_{rf}=15,\,4\pi Ms=1200)$

4.2 Numerical Analysis of the Exact Twin-Toroid Geometry

Twin-slab approximation provided several important results in the development of the twin-toroid phase shifter. However as will be explained later in this section, it has some deficiencies in determining the differential phase shift characteristics and mode calculations of twin-toroid geometry. In this section, several models for twin-toroid phase shifter are developed and they are examined in terms of their accuracy on determining the differential phase shift by comparing with measurement results given in [27]. Higher order modes propagating in twin-toroid phase shifter and insertion loss characteristics are determined by EM simulations.

4.2.1 Magnetostatic Simulations of Magnetic Flux

In twin-slab approximation, magnetic flux density is assumed to be homogeneous and unidirectional in vertical ferrite slabs. However in toroidal structures magnetic flux direction is not uniform especially at the corners of the toroids [51, 52]. In Figure 4.15, B-H characteristics used in EM simulations are given. Magnetostatic simulation result of the magnetic flux distribution in twin-toroid structure is given in Figure 4.16.
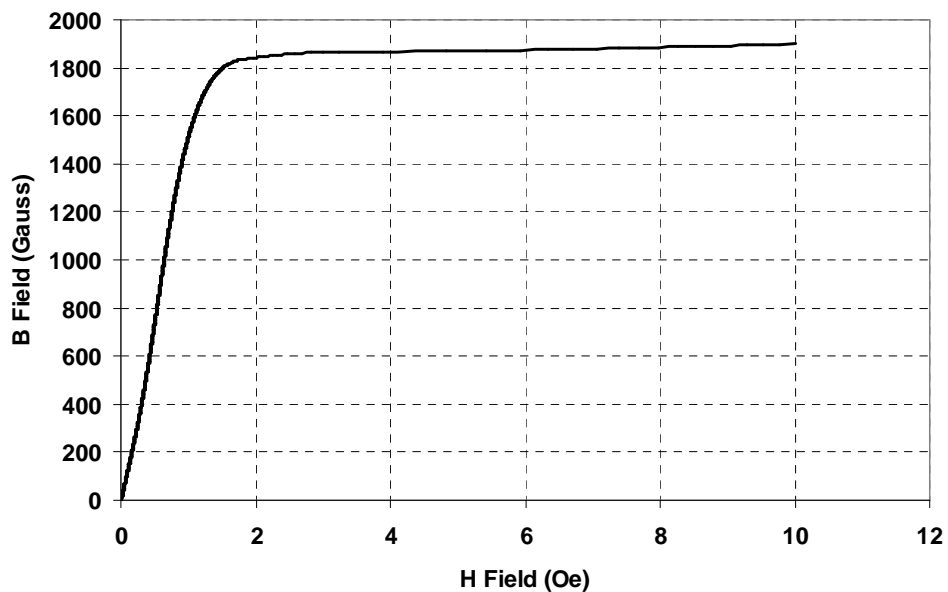
Figure 4.15 Nonlinear B-H data used in magnetostatic calculations
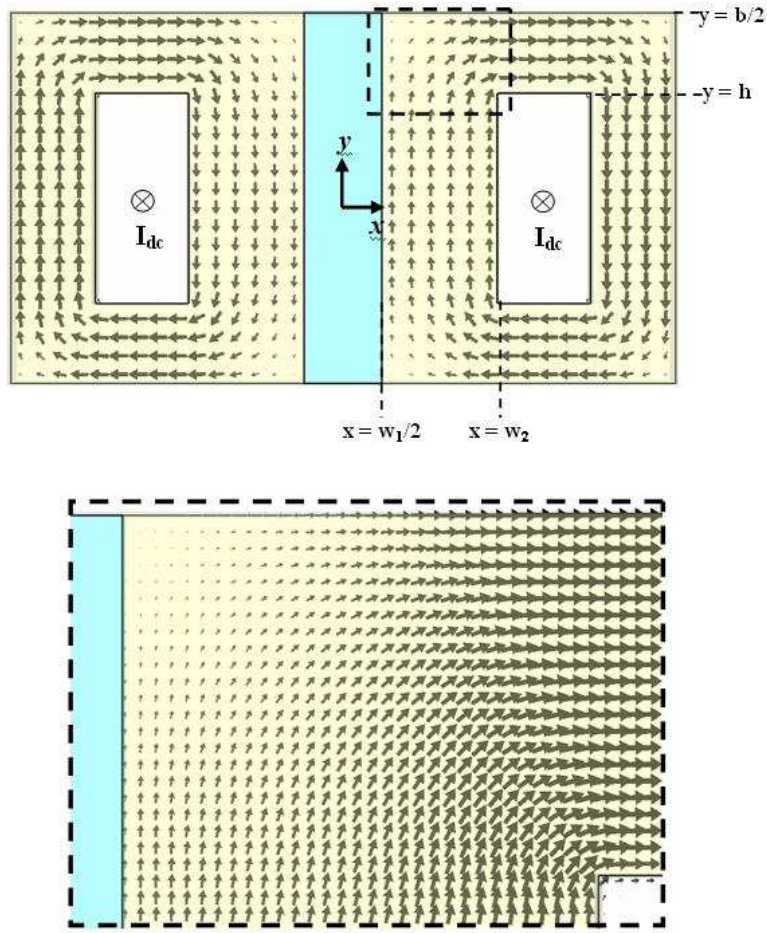
Figure 4.16 Magnetic flux distribution in twin-toroid structure also showing the corner fields in detail (I_{dc}=5A)

Magnetic flux density at the corner of the toroid can be expressed analytically [51] in terms of the notation of Figure 4.14 as

$$\overset{\rho}{B}(x,y) = \frac{B_0}{\sqrt{\sin^2 \phi + \sin^2 \psi}}(\sin \phi \cos \psi \hat{a}_x + \cos \phi \sin \psi \hat{a}_y) \tag{4.2}$$

$$\psi = \frac{\pi}{2}\frac{x - w_1/2}{w_2 - w_1/2}, \ \phi = \frac{\pi}{2}\frac{y-h}{b/2-h}$$

for $w_1/2 < x < w_2$ and $h < y < b/2$

Since modeling of this equation in EM solver is not possible, some simplifications should be made to include the effect of corners on differential phase shift. In Figure 4.17 developed models used in EM simulations are given.
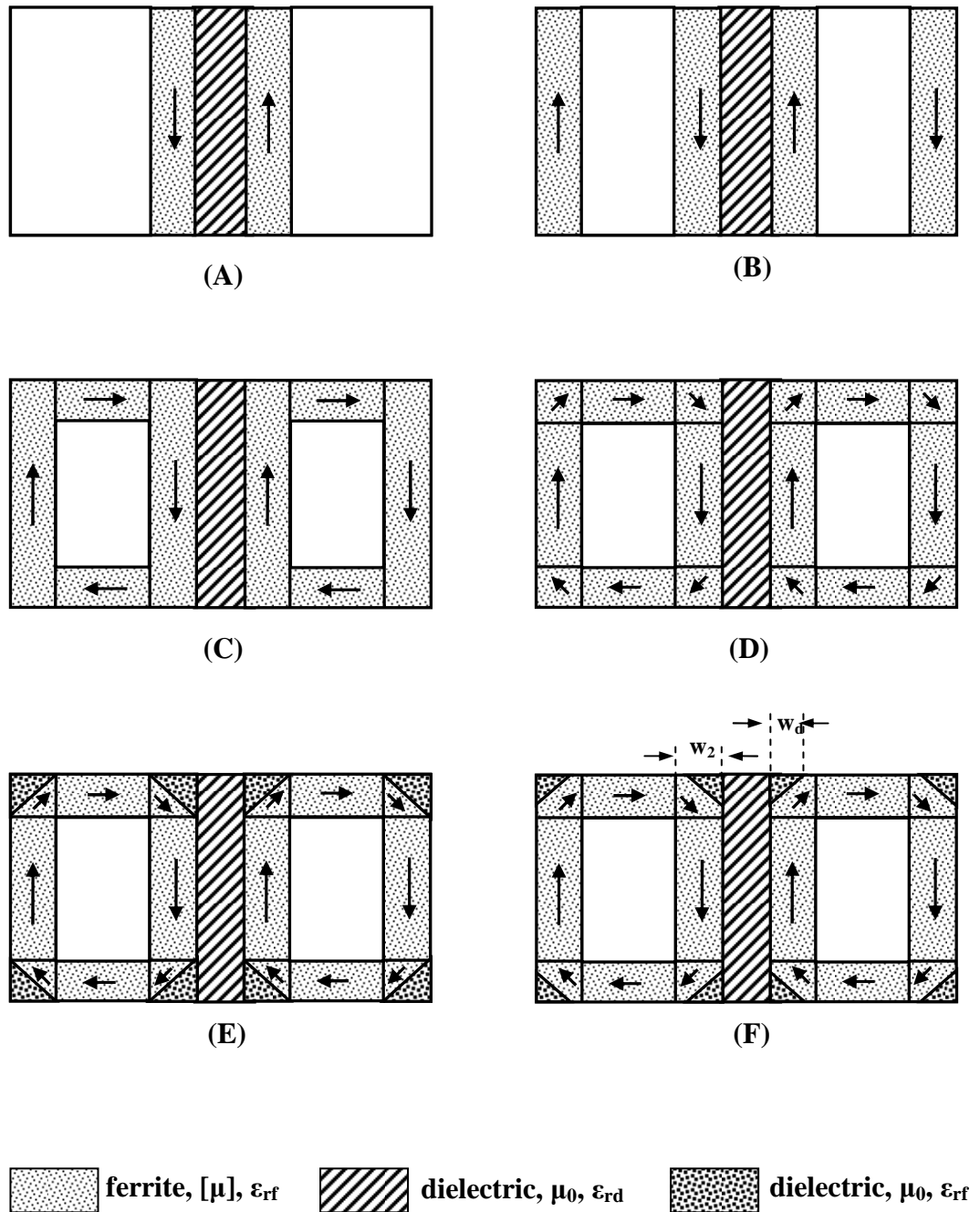
Figure 4.17 Different simulation models used for twin-toroid ferrite phase shifter

4.2.2 Simulation of Differential Phase Shift

For the twin-toroid geometry with cross-sectional view given in Figure 4.18, measurement results [27] and EM simulation results of the models defined in Section 4.2.1 are plotted in Figure 4.19, Figure 4.20, and Figure 4.21 for YIG material, MnMg spinel ferrite and Li spinel ferrite respectively.

w_1	1.4 mm
w_2	1.0 mm
w_3	4.0 mm
w_4	1.0 mm
h	2.0 mm
b	4.0 mm
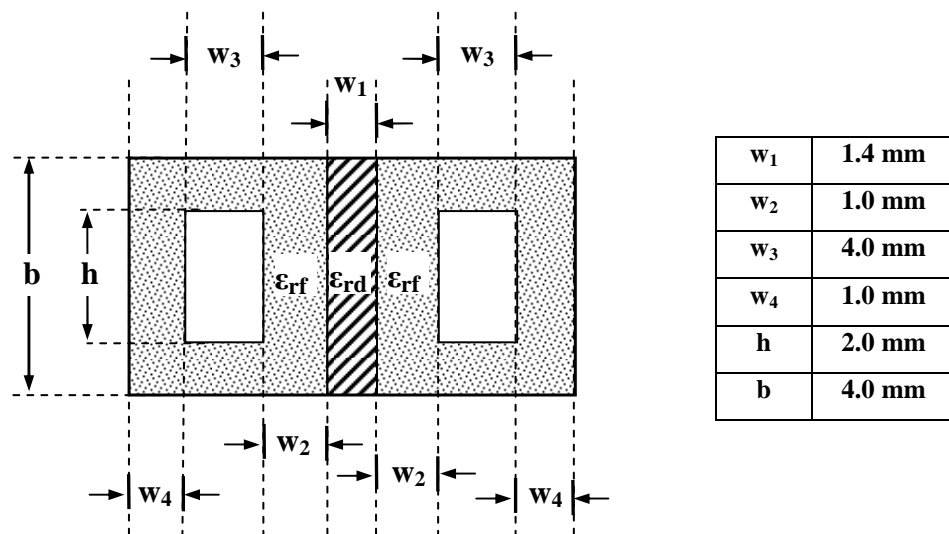
Figure 4.18 Cross-sectional dimensions of the twin-toroid structure used in EM Simulations
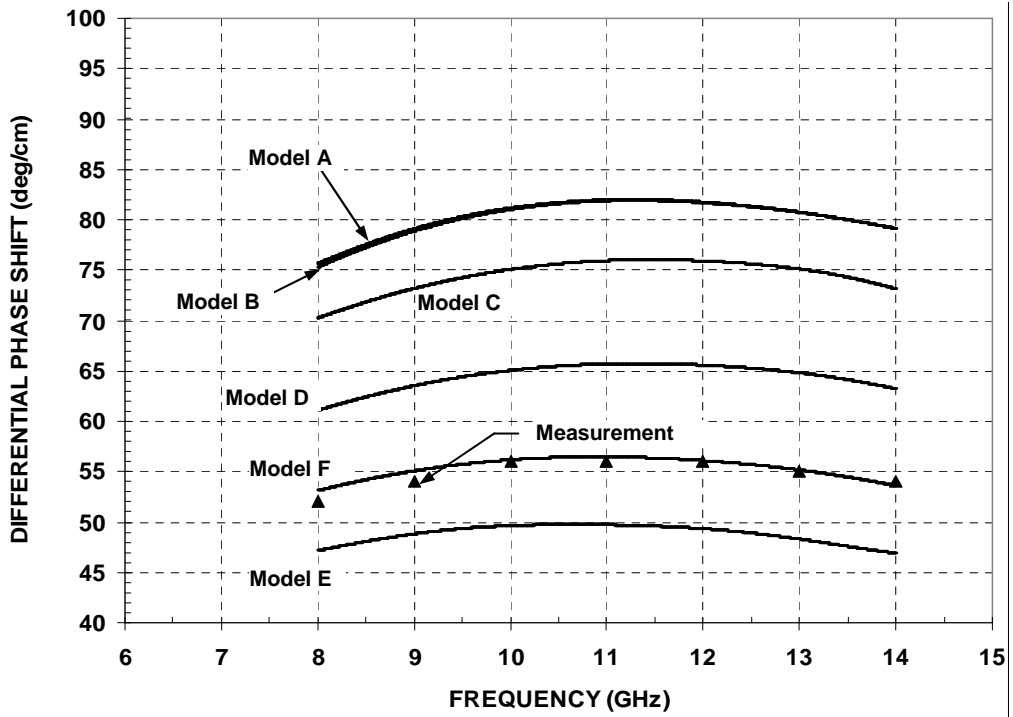
Figure 4.19 EM simulation results (solid lines) and measurement results (triangles) for YIG
(Ferrite material: $4\pi M_R$=1294 Gauss, ε_{rf}=14.74   Dielectric material: ε_{rd}=24.96)
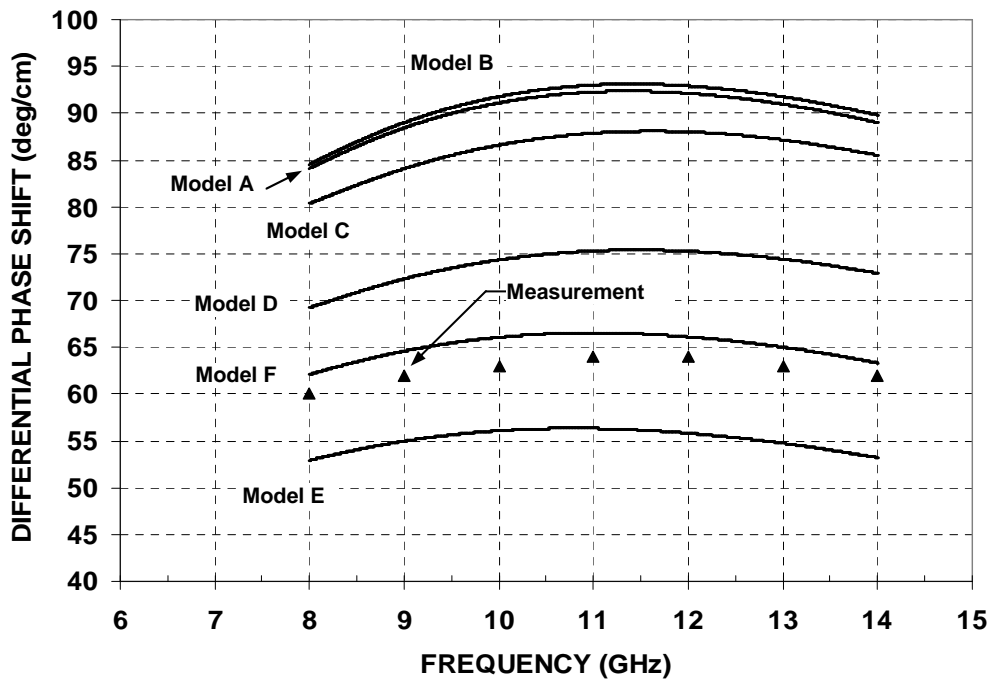
Figure 4.20 EM simulation results (solid lines) and measurement results (triangles) for MnMg ferrite
(Ferrite material: $4\pi M_R$=1420 Gauss, ε_{rf}=12.1   Dielectric material: ε_{rd}=25.64)

63
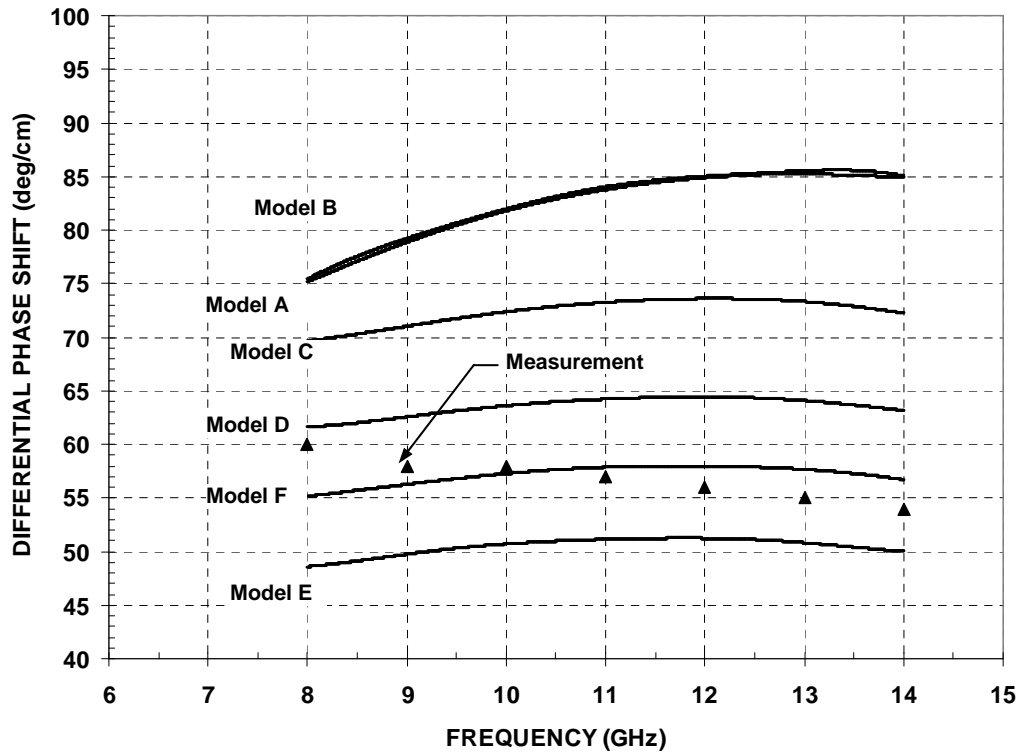
Figure 4.21 EM simulation results (solid lines) and measurement results (triangles) for Li ferrite
(Ferrite material: $4\pi M_R$=1730 Gauss, ε_{rf}=15.4   Dielectric material: ε_{rd}=16.05)

The results of Figure 4.19-21 indicate that the corner magnetization has considerable effect on DPS. The small difference between the results of Model A and Model B shows the small effect of vertical ferrite regions near the narrow waveguide walls on DPS. When horizontal ferrite sections are included (Model C) differential phase shift decreased over 10%. The main reason of that is the displacement of microwave H field from the vertical ferrite region near the dielectric slab. In Model D introduction of diagonal corner magnetization decreased differential phase shift over 10% with respect to Model D. Replacement of half of the toroid corners adjacent to the waveguide walls with dielectric material having permittivity same as that of ferrite material (Model E) caused a big decrease (>20%) of differential phase shift. The difference between the simulation results of Model F (w_d/w_2=0.7) and measurement results is below 9% for three different types of materials. With regard to these results, MODEL F provides the most accurate DPS solution and will be used in the design of twin-toroid ferrite phase shifter.

64

4.2.3 Simulation of Higher Order Modes

The propagation in waveguides which are inhomogeneously filled with dielectric slabs, occurs in LSE_{mn} (longitudinal section electric) and LSM_{mn} (longitudinal section magnetic) modes. For n=0 (no y-dependence) these modes become identical with the conventional TE_{m0} and TM_{m0} modes.

The propagating dominant mode in twin-toroid phase shifter is the LSE_{10} or TE_{10} mode. Differential phase shift flatness in the frequency band of operation can be adjusted by reducing the width of the waveguide section where the toroids are mounted. Also high dielectric constant materials are used to increase the differential phase shift per unit length. However both of these requirements may permit propagation of higher order LSE_{mn} and LSM_{mn} modes in the structure.

In practical ferrite phase shifter applications, those higher order modes may cause sharp spikes in transmission and reflection characteristics if there exist asymmetry in the cross-sectional geometry of the twin-toroid structure or imperfections and air gaps in the impedance matching elements [37, 53]. The upper frequency limit of the twin-toroid phase shifter is then limited by the cut-off frequency of the first higher order mode. The field lines of the first two higher order modes (LSE_{11}, LSM_{11}) propagating in dielectric slab loaded rectangular waveguide are shown in Figure 4.22.

In Figure 4.23 EM simulation results of the propagation constants for the first three higher order modes are given for the dielectric model of the structure given in Figure 4.18. LSE_{11} and TE_{20} modes start to propagate around 10 GHz and LSM_{11} mode around 11.9 GHz.
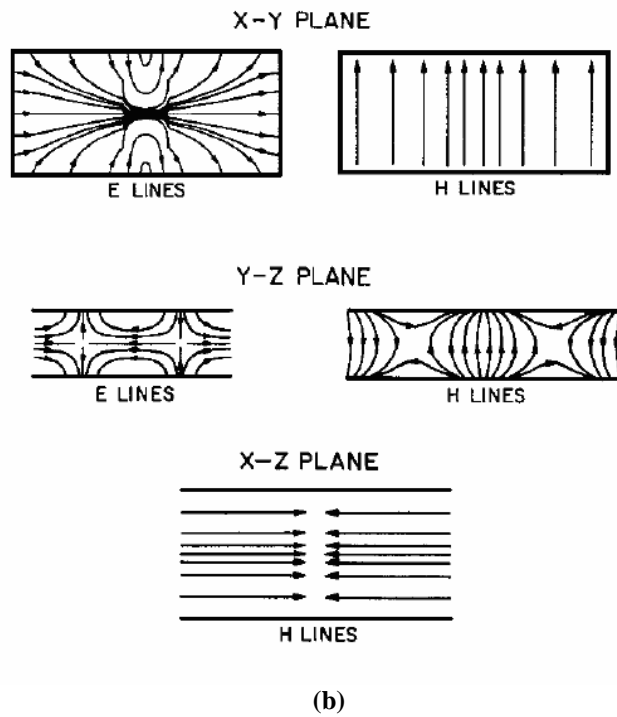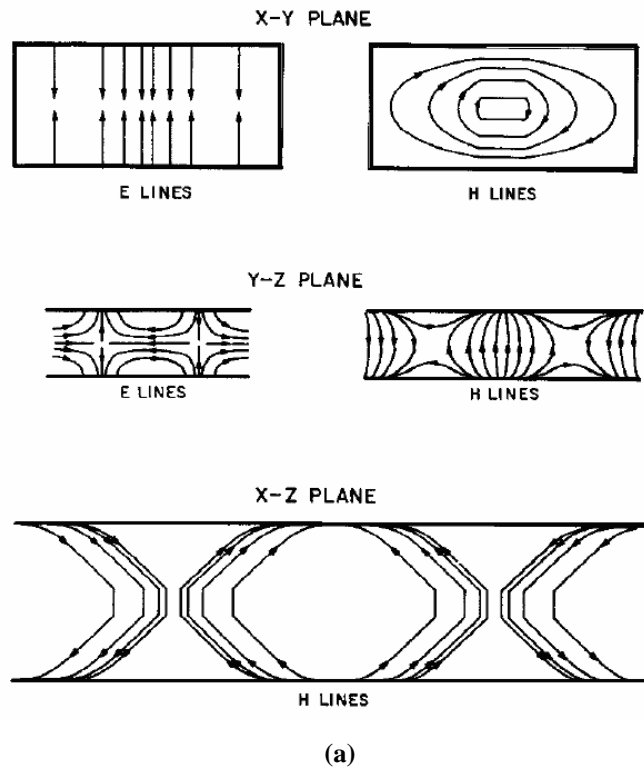
Figure 4.22 Field Lines for (a) LSE$_{11}$ Mode (b) LSM$_{11}$ Mode [37]

66
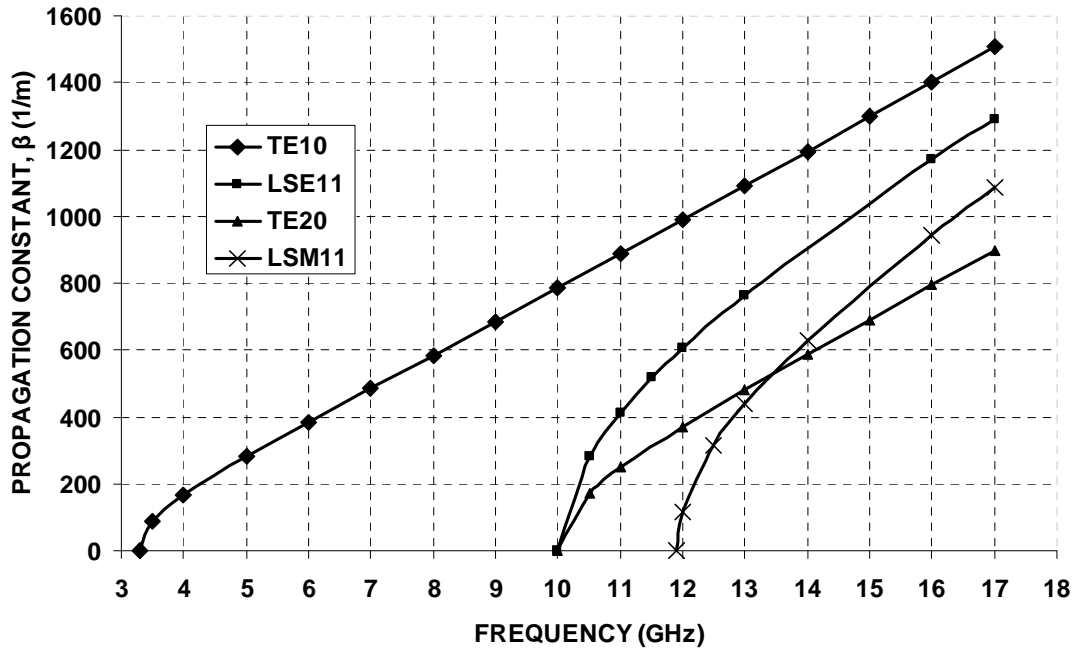
Figure 4.23 Propagation constants for the dominant mode and first three higher order modes

The effect of dielectric constant (ε_{rd}) and width of the dielectric slab (w_1) between the ferrite toroids on propagation of higher order modes is investigated and results are given in Figure 4.24-26. Generally, increase of ε_{rd} and w_1 lowers the cut-off frequencies for all the higher order modes showing the importance of the dielectric slab on propagation characteristics. The propagation of the first higher order mode limits the value of permittivity of the dielectric material used resulting in a decrease of the DPS as explained in Section 4.1.1.

Reduction of the waveguide height b increases the cut-off frequencies of LSE_{11} and LSM_{11} modes as shown in Figure 4.27. However this causes decrease of the cut-off frequency of TE_{20} mode. Also power handling capacity of the device decreases since H field magnitude in the ferrite material increases as height is reduced.
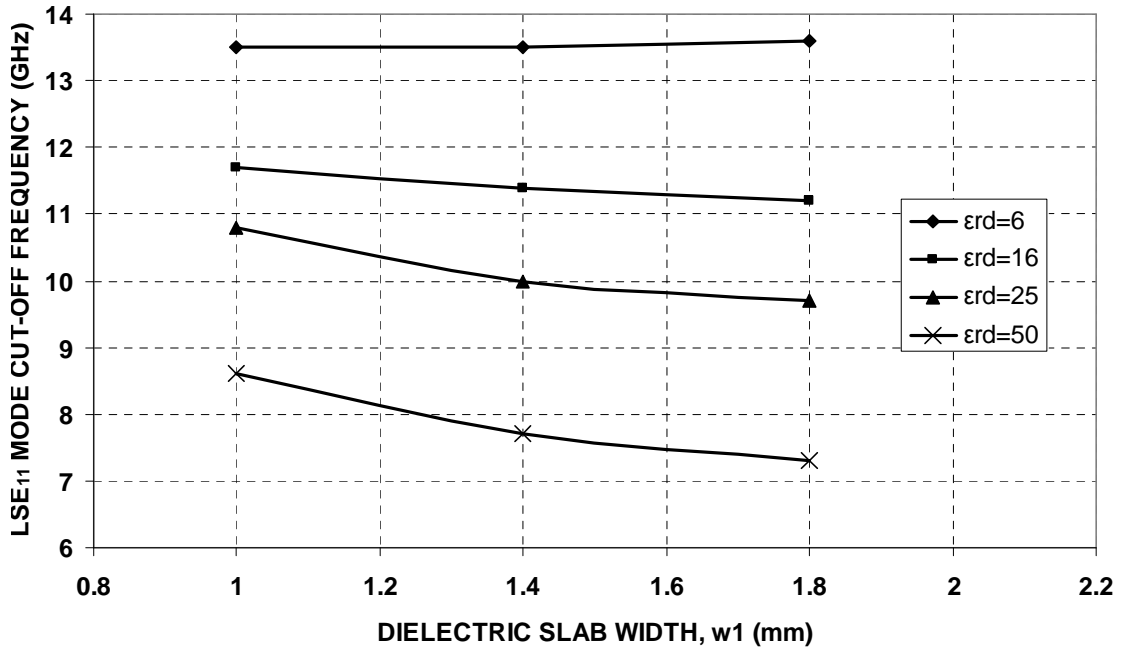
Figure 4.24 LSE$_{11}$ mode cut-off frequency versus dielectric slab thickness (w$_1$) for several dielectric slab permittivity (ε_{rd})
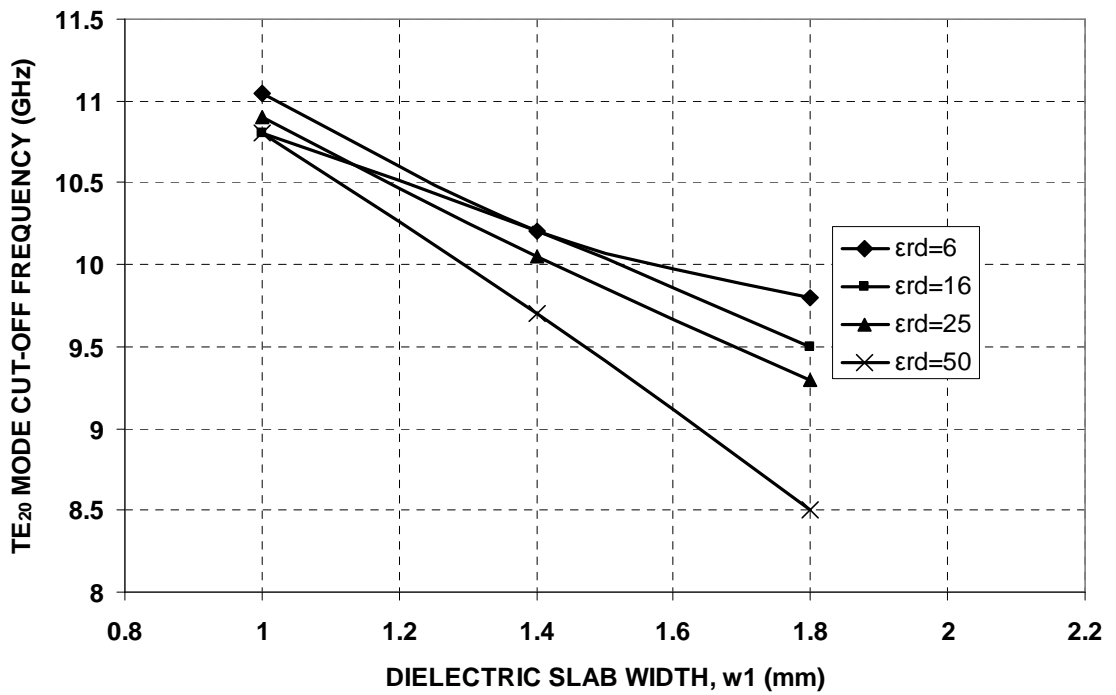
Figure 4.25 TE$_{20}$ mode cut-off frequency versus dielectric slab thickness (w$_1$) for several dielectric slab permittivity (ε_{rd})
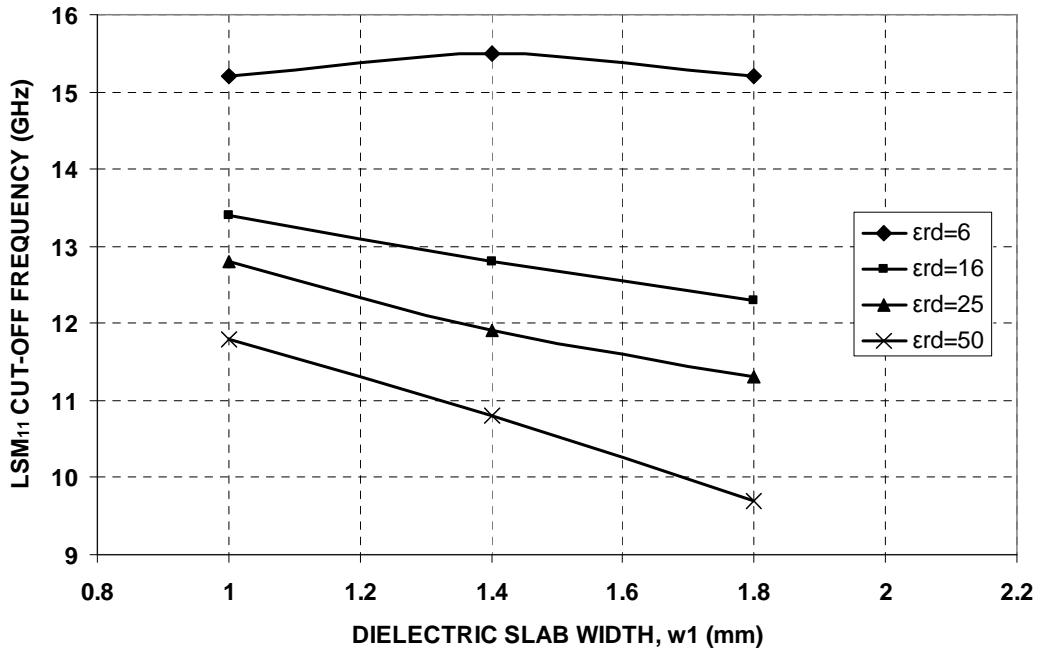
Figure 4.26 LSM$_{11}$ mode cut-off frequency versus dielectric slab thickness (w_1) for several dielectric slab permittivity (ε_{rd})
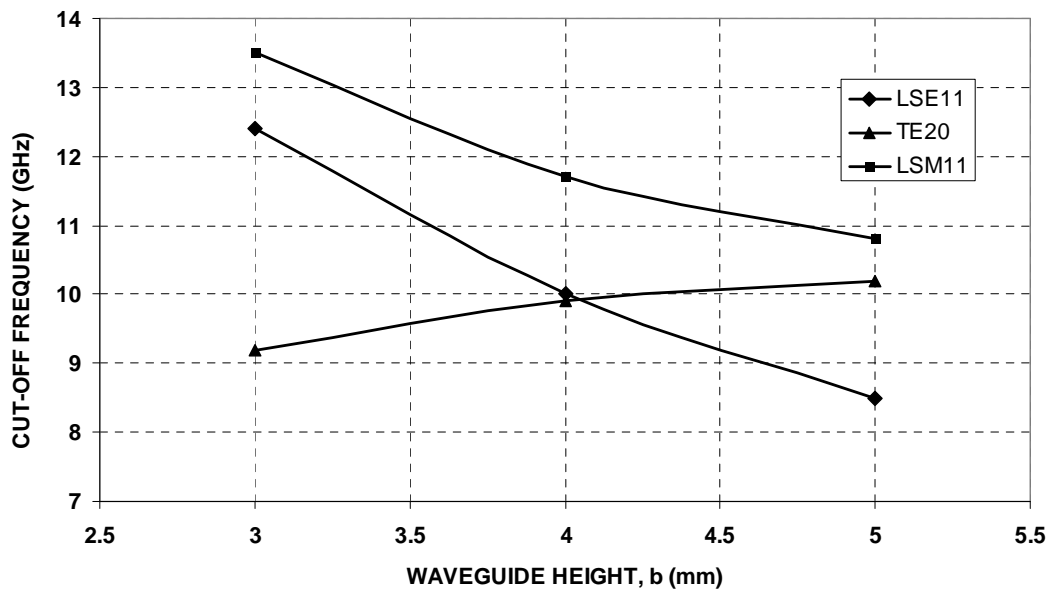
Figure 4.27 Cut-off frequencies of first three higher order modes versus waveguide height

CHAPTER 5

DESIGN AND MEASUREMENTS OF X-BAND TWIN-TOROID FERRITE PHASE SHIFTER

In Chapter 4, development of accurate EM simulation models for the twin-toroid FPS are presented. In this Chapter, using these models, design of an analog type X-band twin-toroid ferrite phase shifter is explained and trade-offs in terms of power handling capability, higher order mode propagation and DPS characteristics are discussed. Measurements of the fabricated prototype twin-toroid FPS are presented. Measurements are compared with EM simulation results.

Twin-toroid ferrite phase shifter design procedure involves the consideration of following stages:

- Determining approximate material parameters
    - Ferrite material parameters : $4\pi M_s$, $4\pi M_r$, ε_{rf}
    - Dielectric slab permittivity (ε_{rd})

- Cross-section optimization
    - Consideration of differential phase shift
        - Obtaining high DPS per unit length (Figure of Merit, degree/cm) and high DPS per dB loss (Figure of Merit, degree/dB)
        - Obtaining flat differential phase shift in frequency band of operation
    - Consideration of higher order modes
        - Preventing higher order modes to propagate
        - Suppressing higher order modes

- o Consideration of power handling
    - Reducing peak magnetic field intensity magnitude in the structure to improve peak power handling capacity
    - Reducing insertion loss to improve average power handling capacity

- Material selection
    - o Suitable value of $4\pi M_s$, square ferrite material with high $4\pi M_r$
    - o Low dielectric and magnetic losses
    - o High power handling capacity
    - o Low temperature sensitivity
    - o Low magnetostriction effects

- Matching transformer design
    - o Obtaining good impedance match in the BW
    - o Preventing the excitation of higher order modes

- Analog design
    - o Phase accuracy
        - Phase resolution
        - Phase repeatability
        - Temperature and frequency compensation
    - o Switching time
    - o Switching power

5.1 Determining Approximate Material Parameters

The selection of the ferrite material involves a compromise between several performance parameters, such as phase shift, insertion loss, and power handling capability as shown in Figure 5.1. Sharp increase of magnetic losses for normalized saturation magnetization $\gamma 4\pi M_S / \omega > 0.7$ is because of the low field loss phenomenon which is explained in the Appendix A.3.1. If $\gamma 4\pi M_S / \omega$ is chosen to be low, ferrite phase shifter length to obtain 360° DPS increases too much and resulting conductive and dielectric losses dominates to total loss. Optimum range for the $\gamma 4\pi M_S / \omega$ providing low dielectric, conductor and magnetic losses is determined between 0.2 and 0.6 for ferrite phase shifters. While the increase of the $\gamma 4\pi M_S / \omega$ increases DPS per unit length, power handling capability of ferrite phase shifters decreases because of the decrease of H_{cr} which is explained in the Appendix A.5.
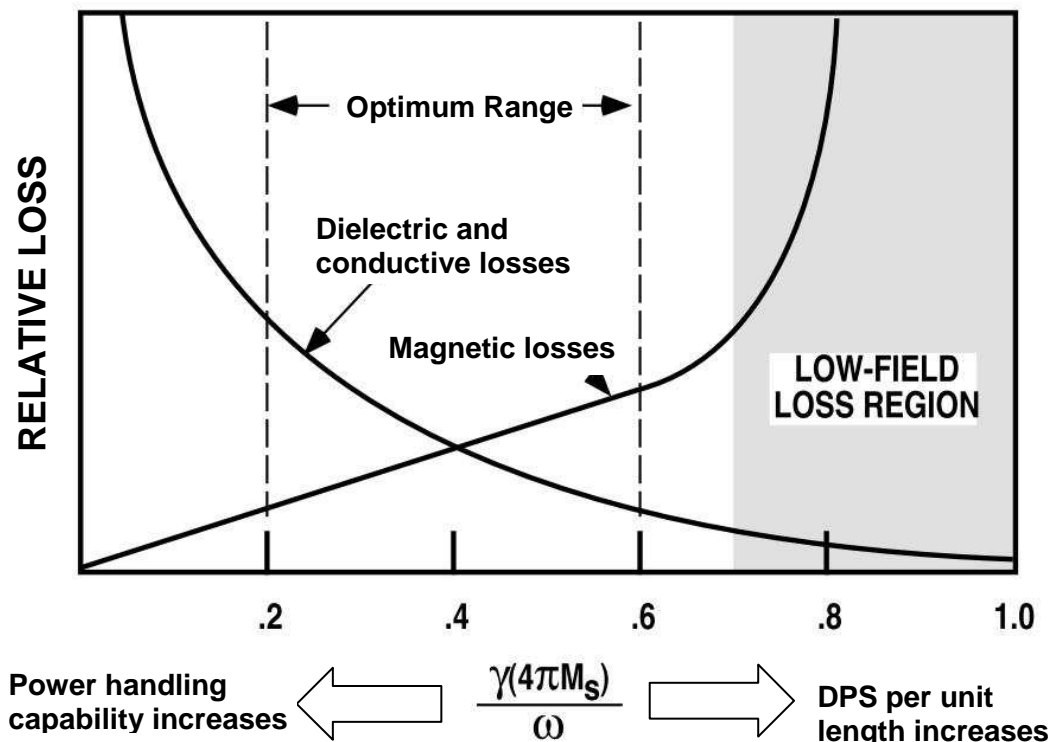
Figure 5.1 Loss components, power handling capability and DPS per unit length as a function of normalized saturation magnetization (Adapted from [65])

72

Phase shifting capacity of latching type ferrite phase shifters are directly proportional to the remanent magnetization, $4\pi M_R$ of the ferrite material used. Thus ferrite material should have square hysteresis characteristics, i.e, high $4\pi M_R$, to obtain high phase shifting capacity.

Permittivity of the dielectric slab (ε_{rd}) between the ferrite toroids is the other material parameter affecting the phase shifter performance. As shown in Chapter 4, as the value of the permittivity increases, phase shifting capacity increases. However the propagation of the higher order LSE and LSM modes limits the value of the dielectric slab permittivity. When determining the dielectric slab permittivity, DPS characteristics, higher order mode propagation and power handling characteristic should be taken into account. Optimum value of the dielectric slab permittivity is around 30. Above that value, temperature sensitivities of the dielectric constant of the dielectric materials can degrade the performance of the phase shifter [58].

5.2 Cross-Section Optimization

Cross-sectional parameters and material parameters of the twin-toroid ferrite phase shifter are given in Figure 5.1. Optimization of the structure cross-section constitutes the most important part of the design of nonreciprocal ferrite phase shifters. The main purpose of the cross-section optimization is to increase the DPS per unit length and obtain phase flatness while considering higher order mode propagation and power handling characteristics of the phase shifter. Total DPS of the phase shifter is directly proportional to the length of the structure. Thus by increasing the DPS per unit length, lower insertion loss can be obtained since the required length to obtain 360° of DPS will be shorter.
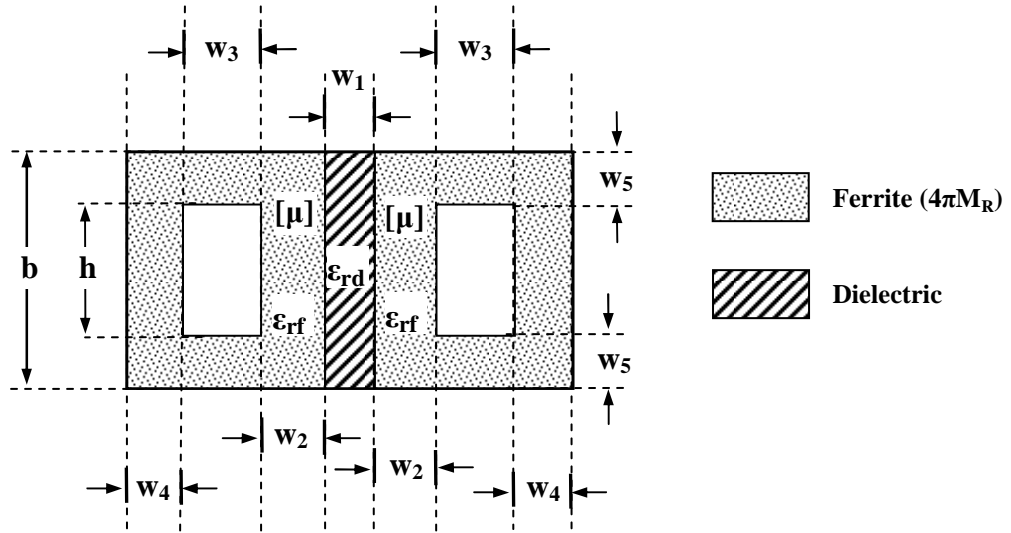
Figure 5.2 Structural parameters of twin-toroid structure

Table 5.1 Parametric EM simulation results of the twin-toroid ferrite phase shifter

Swept Parameter (Constant Parameters)	Parameter Value	DPS / cm at f=f₀	LSE₁₁ Cut-Off Frequency	LSM₁₁ Cut-Off Frequency	Relative Peak Power Handling Capability
		(degree/cm)	(Normalized wrt f₀)	(Normalized wrt f₀)	
ε_{rd} (b=0.127 λ_0, ε_{rf}=15 w1=0.044 λ_0, w2=w4=w5=0.032λ_0)	18	41.6	1.17	1.28	1.656
	25	53.5	**1.06**	1.23	1.460
	36	68.7	**0.94**	1.16	1.274
	50	81.5	**0.82**	1.11	1.079
b (ε_{rd}=36, ε_{rf}=15, w1= 0.044 λ_0, w2=w4=w5=0.032λ_0)	0.095 λ_0	60.4	1.15	1.32	1.000
	0.107 λ_0	64.3	**1.05**	1.24	1.084
	0.127 λ_0	68.7	**0.94**	1.16	1.274
	0.158 λ_0	73.7	**0.80**	1.07	1.600
w₁ (ε_{rd}=36, ε_{rf}=15, b=0.127 λ_0, w2=w4=w5=0.032λ_0)	0.025 λ_0	70.8	**1.04**	1.31	1.084
	0.032 λ_0	72.4	**1.00**	1.25	1.121
	0.038 λ_0	71.4	**0.96**	1.21	1.222
	0.044 λ_0	68.7	**0.94**	1.16	1.274
	0.050 λ_0	65.0	**0.91**	1.12	1.357

Dielectric slab permittivity ε_{rd}, dielectric slab thickness w_1, and waveguide height b are found to be the most critical cross-sectional parameters of the twin-toroid ferrite phase shifter considering DPS, power handling and higher order mode propagation characteristics. In Table 5.1 parametric EM simulation results of the twin-toroid ferrite phase shifter for $f=f_0$ are given. The widths of the toroid arms (w_2, w_4 and w_5) should be equal for both mechanical and magnetic reasons and optimum value of $0.032\lambda_0$ is used in all simulations. Also remanent magnetization is taken to be 1250 Gauss for all cases. Cut-off frequencies for two higher order LSE_{11} and LSM_{11} modes are investigated and the cases in which these modes start to propagate near or below the highest operating frequency $1.05f_0$ are written in bold letter.

Relative peak power handling values are calculated by normalizing the magnitude of the RF H fields in the ferrite material with the one having highest magnitude among all cases and squaring the inverse of the results.

Increase of the dielectric slab permittivity, ε_{rd} increases DPS per unit length remarkably as expected. However both power handling capability and cut-off frequencies of higher order modes decrease as ε_{rd} is increased. By reduction of the waveguide height b, cut-off frequencies of higher order modes can be translated to higher frequencies at the expense of a reduction in power handling capability and DPS per unit length. However, as far as the power handling is not a major concern, about 17% increase of DPS per unit length can be obtained with an increase of dielectric slab permittivity from 25 to 36 and a decrease of waveguide height from $0.127 \lambda_0$ to $0.107 \lambda_0$ with similar higher order mode propagation characteristics.

The decrease of the dielectric slab width w_1 also increases the cut-off frequencies of higher order modes. However as will be explained in the next section, w_1 has an optimum value providing maximum DPS per unit length and also around that optimum value flat DPS in the operation BW can be obtained. Because of these reasons, arrangement of the cut-off frequencies of higher order modes with reduction in the width, w_1 is limited.

75

DPS characteristics of twin-toroid ferrite phase shifter are generally a monotonic function of frequency. In Figure 5.3, EM simulation results of DPS characteristics of a twin-toroid ferrite phase shifter is given. Material and structural parameters are given in the inset of the figure. Reference phase state is chosen to be the negative remanent magnetization operating point ($4\pi M_R$ = -1250Gauss). Slope of the DPS in BW increases as operating point in the hysteresis loop moves away from the reference state. Maximum slope of DPS is obtained at the positive remanent magnetization operating point ($4\pi M_R$ = +1250Gauss).
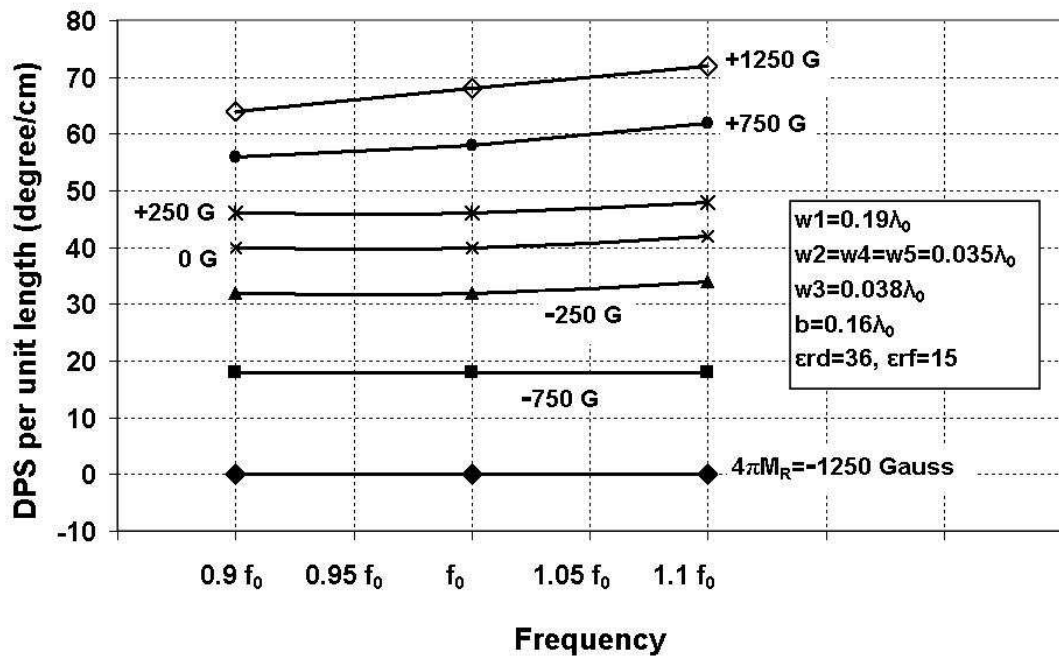
Figure 5.3 Frequency dependence of DPS for several phase states

In Table 5.2 the effect of the dielectric slab width on the DPS characteristics is given. DPS per unit length shows a pronounced maxima at $w_2=0.032\lambda_0$. Minimum frequency dependence of DPS in 10% BW is obtained for $w_1=0.038\lambda_0$.

Table 5.2 Effect of dielectric slab width, w_1 on DPS characteristics

w_1	DPS / cm at $f=f_0$	Peak to Peak Variation of DPS / cm in 10% BW
(Normalized with respect to λ_0)	(°/cm)	(°/cm)
0.0125	58.5	3.8
0.019	67.4	3.3
0.025	72.2	2.7
0.032	73.7	1.2
0.038	72.7	0.4
0.044	70.1	1.2
0.05	66.3	2.8

Another parameter affecting the frequency dependence of DPS is the width w_3. As shown in Figure 5.4, decrease of the parameter w_3, decreases the variation of the DPS in the BW for the twin-toroid structure. However DPS per unit length also decreases, since toroid arms close to the waveguide side walls having negative effect on phase shift interact with more microwave fields as they are moved towards the center. Also as w_3 is reduced, switching wire is positioned close to the center of the waveguide. This will cause higher losses and increase the possibility of excitation of higher order modes.
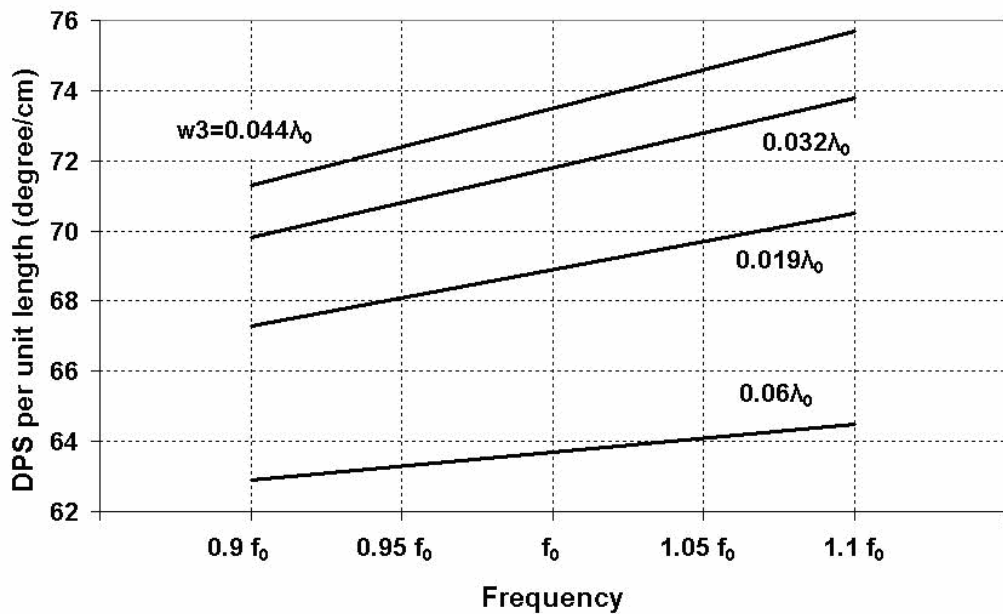
Figure 5.4 Effect of the parameter w_3 on DPS characteristics

5.3 Material Selection

In Section 6.1 some important points for determining material parameters are explained. Also in the Appendix A.5 comparison of materials in terms of microwave power handling is given. After determining the approximate value of $4\pi M_S$, material is chosen according to the power handling and temperature requirements. Choosing a high power material in low power application may bring extra average insertion loss. On the other hand, choosing a low power material in a high power application may cause the insertion to increase sharply after the critical power level.

Magnetostriction effects explained in the Appendix A.2.3 should also be considered when choosing ferrite material for twin-toroid ferrite phase shifter. MgMn ferrites are stress insensitive; however their low power handling capability and high temperature sensitivity makes them difficult to be used in high power and high temperature applications. By small addition of Mn^{+3} in YIG, ferrite materials having both high power handling capabilities and small stress sensitivities can be produced [66].

Lithium ferrites can be used in low and medium power ferrite phase shifters. Low temperature sensitivities and high Curie temperatures of lithium ferrites enable them to be used in very high temperature applications and in applications where temperature compensation with electronic driver circuitry is not possible. At X-Band lithium ferrites have more loss than garnets. However in millimeter-wave frequencies they offer the lowest losses for phase shifter applications. Also low cost of lithium ferrites makes them ideal for high volume applications.

Important microwave parameters of the ferrite material chosen for the twin-toroid ferrite phase shifter are given in Table 5.3. Material is obtained from microwave ferrite manufacturer, AFT Microwave Gmbh. A photograph of the purchased twin-toroid structure is given in Figure 5.5. Length of the structure is 38mm. Ferrite toroids are formed with pressing method and they are brought to tight mechanical tolerances with precise diamond grinding. Toroids and dielectric slab are glued together with a strong, electrically insulating adhesive. Side, top and bottom surfaces

of the twin-toroid structure are metalized with gold of thickness at least 3um which is greater than four times the skin depth. Gold metallization act as a waveguide wall and provides intimate contact of the conducting layer with the ferrite structure. By this method, air gaps between the ferrite and waveguide wall is minimized and higher order mode propagation is prevented.

Table 5.3 RG-11 material parameters [45]

Saturation Magnetization	Remanent Magnetization	Dielectric Constant	Resonance linewidth	Spinwave linewidth	Curie Temperature
$4\pi M_S$ (Gauss)	$4\pi M_r$ (Gauss)	ε_{rf}	ΔH (Oe)	ΔH_k (Oe)	T_c (°C)
1850	1300	14.9	25	1.3	240
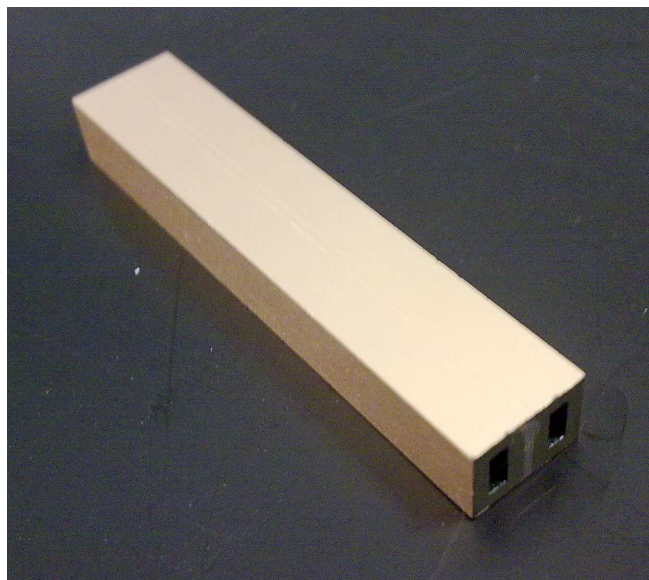
Figure 5.5 A photograph of the purchased twin-toroid structure with length 38mm

5.4 Matching Transformer Design

Impedance matching of the twin-toroid ferrite phase shifter is obtained by using multi-section or tapered dielectric sections and waveguide step transitions as shown in Figure 2.6. To obtain good impedance match in wide BW number of dielectric matching sections and waveguide step transition should be increased. Dielectric constant of the matching sections should be low and they must be machined precisely; otherwise higher order modes can be excited. Also dielectric material used in matching sections should have low dielectric loss tangent for low loss contribution.

Required return loss levels (<-15dB) in 10% BW is found to be possible with the dielectric matching transformer configurations shown in Figure 5.6. For the optimum performance, mechanical dimensions of the two-section asymmetric configuration turned out to be much easier to fabricate than for other configurations. In Figure 5.7 dimensions to be optimized in the EM solver for the two-section asymmetric configuration are given. After optimizing width transitions, height transitions are designed for standard WR-90 output. In Figure 5.8, return loss characteristic obtained by EM simulations is given.

(a)Two-section symmetric   **(b)Two-section asymmetric**   **(c) Tapered**
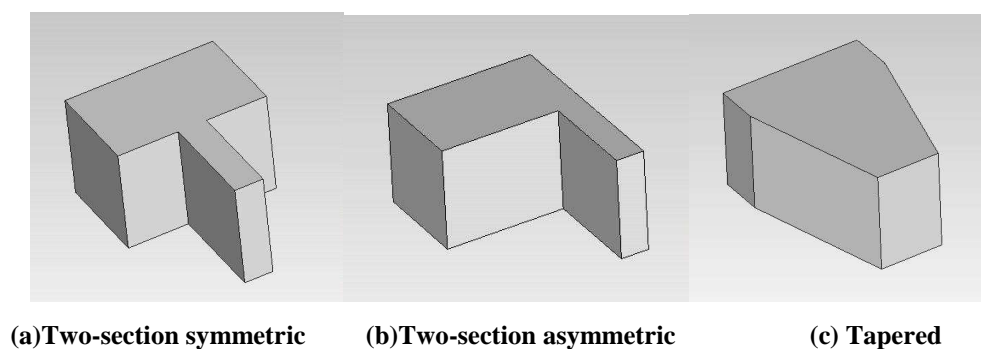
Figure 5.6 Several configurations for dielectric matching sections
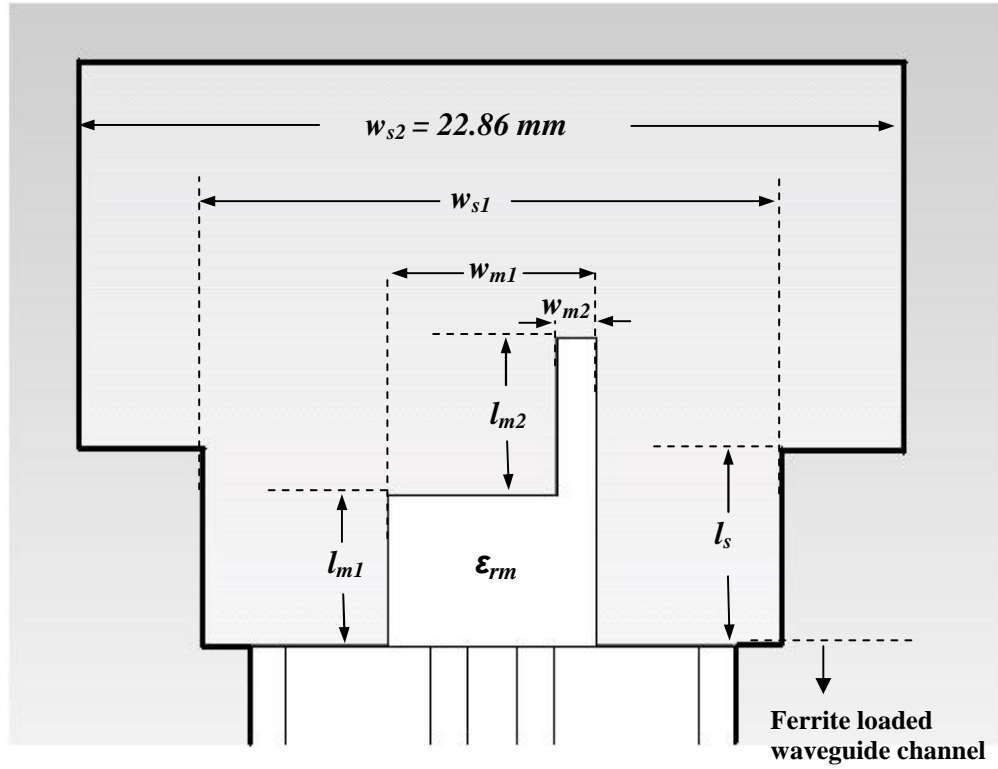
Figure 5.7 Top view of the structure showing dimensions of the dielectric matching sections and waveguide transitions
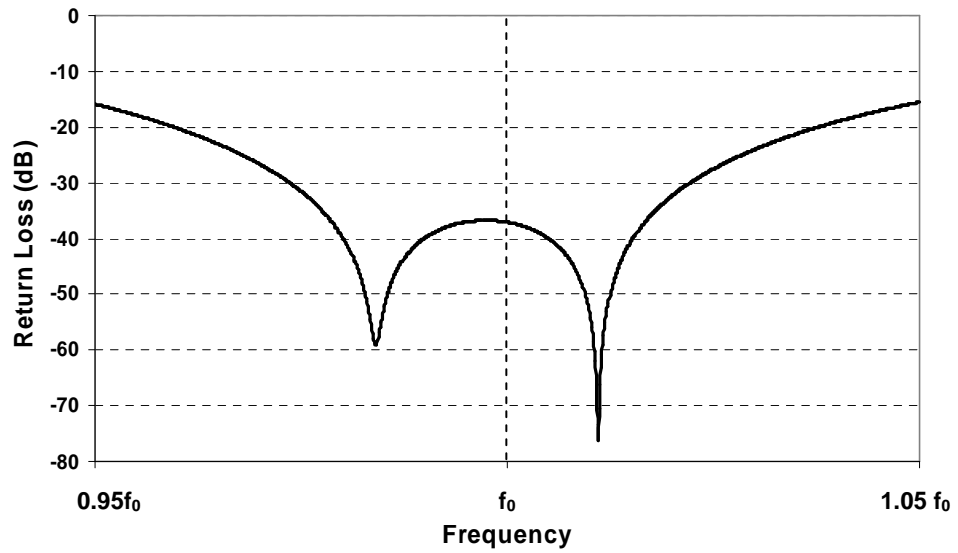
Figure 5.8 – EM simulation results of the S_{11} with two-section asymmetric matching

81

5.5 Analog and Digital Design

Ferrite phase shifters are current controlled devices and for the latching type ferrite phase shifters, analog driver circuitry should provide bidirectional current pulses having adjustable magnitudes. Since ferrite phase shifters are inductive loads to the driver circuitry, magnitude of the current can be adjusted by changing the pulse widths of the applied voltage pulses. Bidirectional current can be supplied either by a single-wire configuration or a two-wire configuration as shown in Figure 5.9.

(a) – Single-wire configuration

(b) – Two-wire configuration
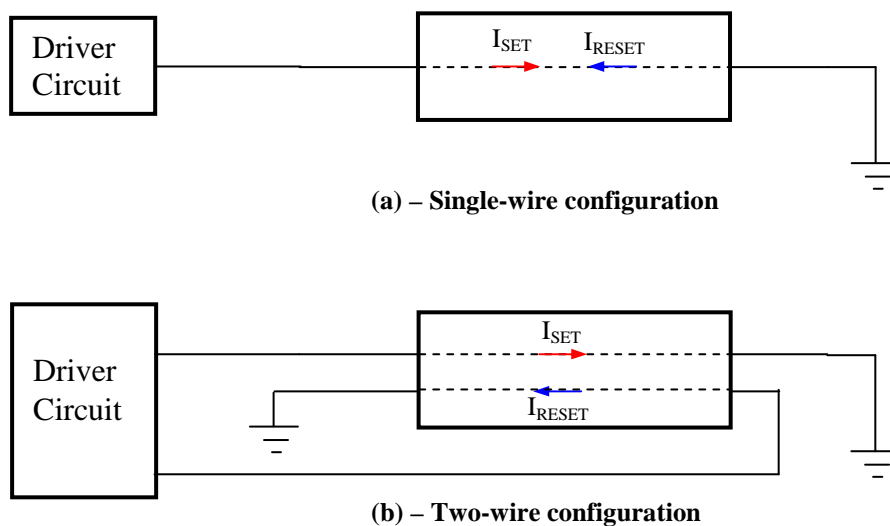
Figure 5.9 Single-wire and two-wire configurations for latching ferrite phase shifters

In the twin-toroid structure, conductive wires are directly exposed to EM fields. Thus they can cause an increase of the total insertion loss of the phase shifter. Also wires can excite higher order modes when there is an asymmetry in the placement, or even coaxial TEM modes can be excited. Since the amount of the conductor is less for single-wire configuration than two-wire configuration, the negative effects of the switching wires will be less. The placement of the switching wire and resulting magnetization in the twin-toroid ferrite phase shifter is shown in Figure 5.10.
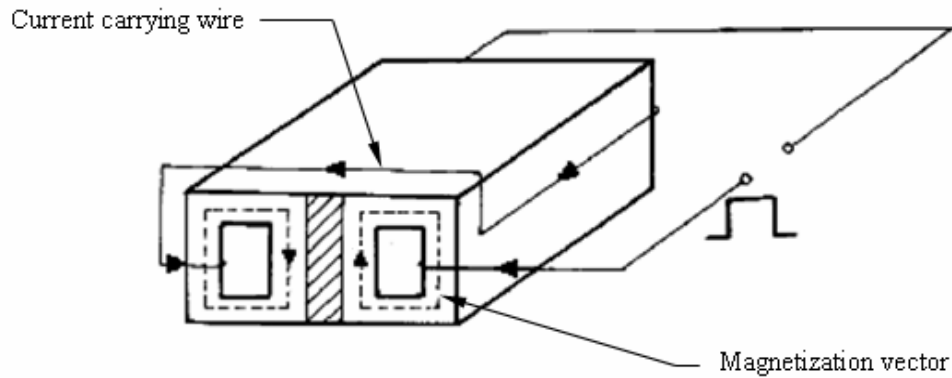
Figure 5.10 Placement of wires for single-wire configuration [1]

Digital control circuit for the twin-toroid ferrite phase shifter controls the phase shifter and holds phase characterization data. This data can be a 3 dimensional array including phase state information at different frequencies and at different temperatures.

5.5.1 Switching Methods with Single-Wire Configuration

Latching type ferrite phase shifters are operated at the operating points between $-4\pi M_r$ and $+4\pi M_r$ in the hysteresis loop. Before switching to the new phase state ferrite material is first reset to a reference phase state which is either $-4\pi M_r$ or $+4\pi M_r$ operating points. Resetting operation removes the flux of the previous phase state and provides repeatable operation. Then by applying an opposite direction current pulse, phase shifter is set to the desired phase state. This switching method is called RESET-SET switching and shown schematically for switching from phase state A to phase state E in Figure 5.11. Applied voltage waveform and resulting current in the switching wire are also shown. When resetting the phase shifter, current increases sharply at the knee of the hysteresis curve and applied voltage should be removed when it is assured that the material is in saturation. The length of the SET pulse depends on the desired phase state and should be determined for each phase state at several temperatures in the operating temperature range.

The dependence of RESET operation on the previous phase state is eliminated by FULL SET-RESET-SET switching method shown in Figure 5.12. More repeatable phase shift is obtained with this method than RESET-SET switching method [67].
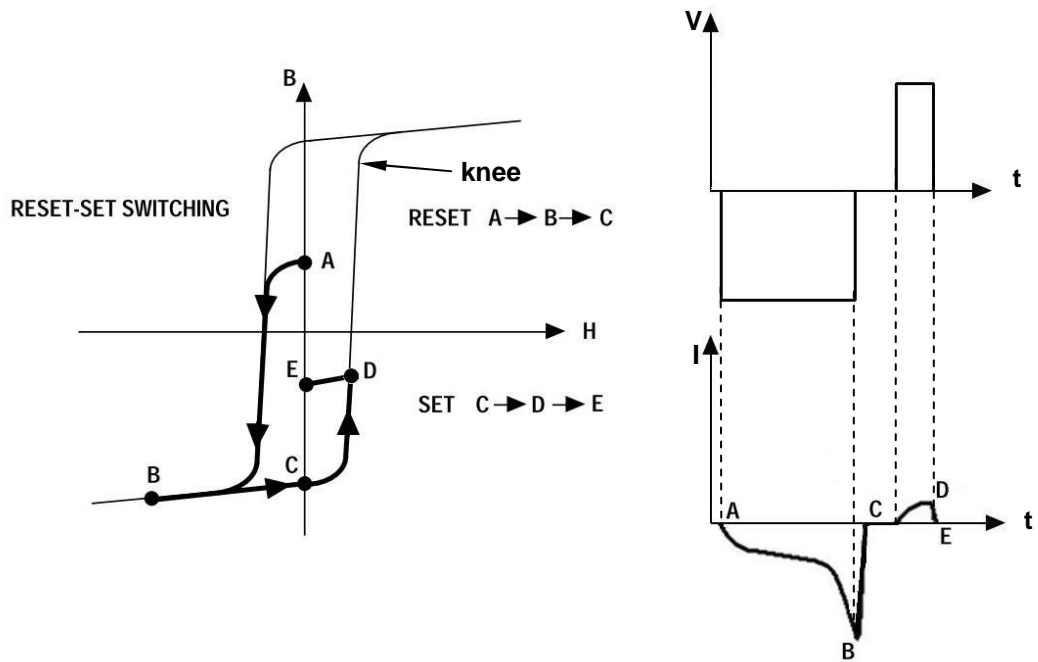
Figure 5.11 RESET-SET switching method
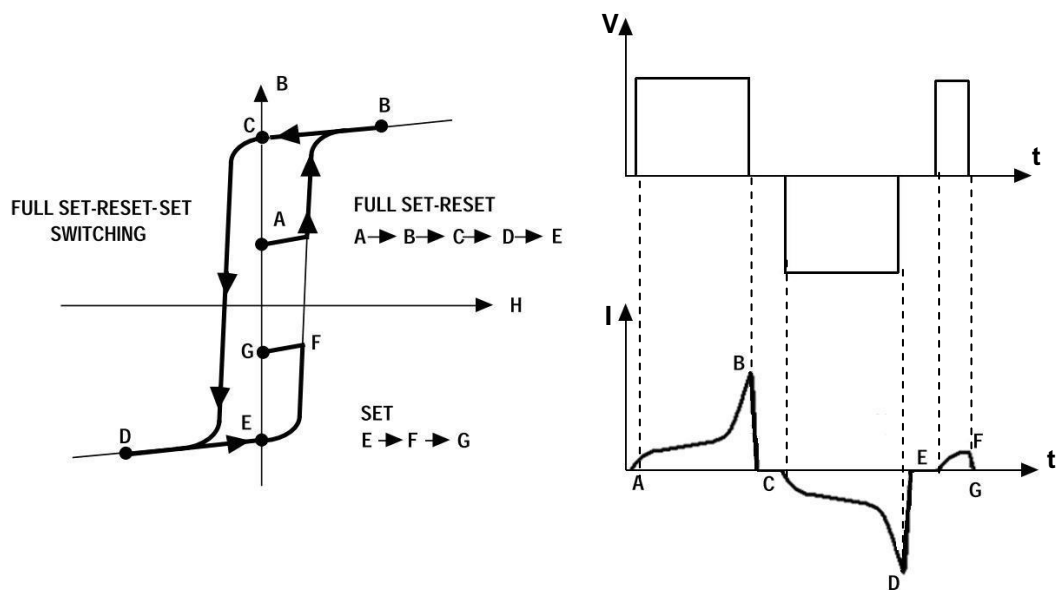
Figure 5.12 FULL SET-RESET-SET switching method

5.6 Measurement Results

Measurements of the designed prototype twin-toroid ferrite phase shifter are performed using the measurement setup given in Figure 5.13. Vector network analyzer (VNA) is used to characterize the microwave performance of the phase shifter. Calibrations are performed using several calibration kits including the standard WR-90 calibration kit, half-height WR-90 Thru-Reflect-Line (TRL) calibration kit, and 3.5mm SMA calibration kit. Measurements done with the calibration using 3.5mm SMA calibration kit differ from the measurements done with the calibration using the other calibration kits, since waveguide adapter is excluded from the calibration. Three versions of the mechanical waveguide structure are fabricated. One version is for a single twin-toroid structure having length of 38mm. Photograph of this structure is given in Figure 5.14. Tapered dielectric matching elements are placed at the front and back surfaces of the structure. The other two versions are produced for two cascaded twin-toroid structures having total length of 76mm. Waveguide height transitions for standard WR-90 waveguide is provided with external adapters for the earlier two versions. Photographs of the mechanical structure for the 76mm toroids are given in Figure 5.15 and Figure 5.16. In the last version, height transitions are integrated on the main structure and ferrite loaded waveguide channel is widened 0.2mm to incorporate indium foils to reduce mechanical stress on the ferrite.

Switching of the phase shifter is obtained with the designed analog driver circuits. Performance of analog circuits suitable for single-wire and two-wire configurations explained in Section 5.5 are compared. 0.1dB less average insertion loss is obtained with the former configuration. The effect of voltage switching time on DPS characteristics is investigated and its importance on the accuracy of phase shifting is seen. For 6-bit phase shifting operation SET pulses with pulsewidths being multiples of 10ns is needed. For repeatable and accurate phase shifting especially for the low phase states, shorter rise time (t_{rise}) and fall time (t_{fall}) is needed and <50ns t_{rise} and t_{fall} is obtained with an improved driver circuit. In the early stages, digital controls of the analog driver circuit are provided with function generators. A specific digital control program is written on an FPGA based test board. Voltage pulses for FULL

SET-RESET-SET switching method are generated in this board. Digital test board is controlled serially with a desktop computer. For phase repeatability measurements, automated measurement control program in Agilent VEE is written.
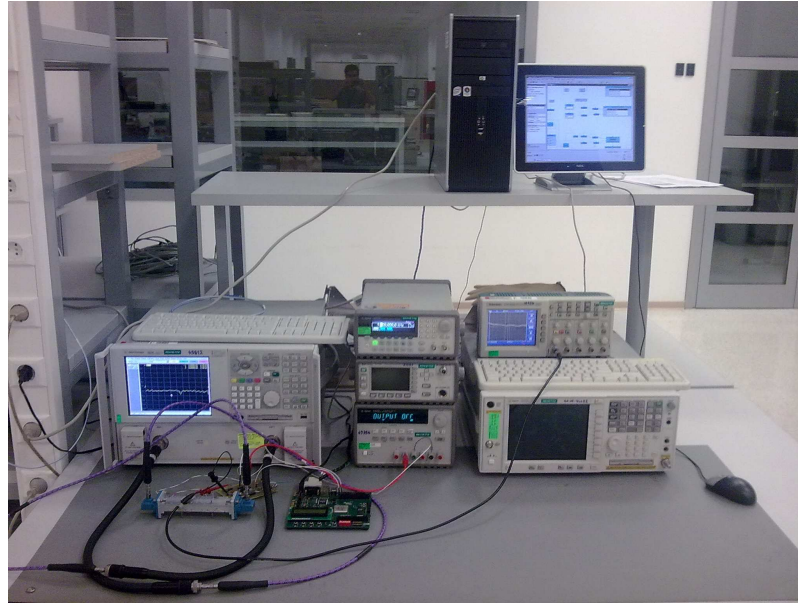
Figure 5.13 A photograph of the measurement setup for twin-toroid ferrite phase shifter
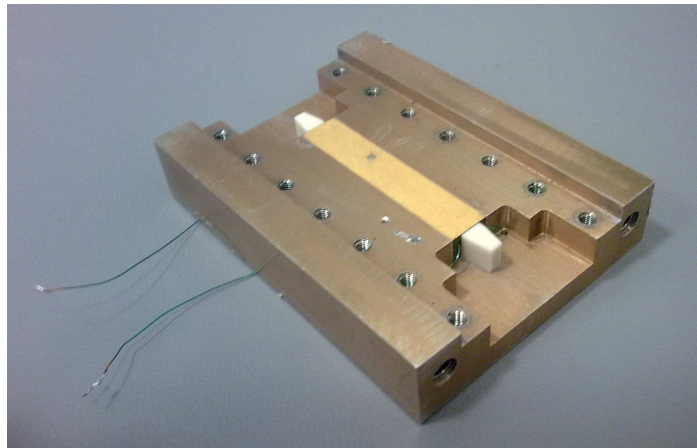
Figure 5.14 A photograph of the designed 38mm twin-toroid structure with dielectric matching elements
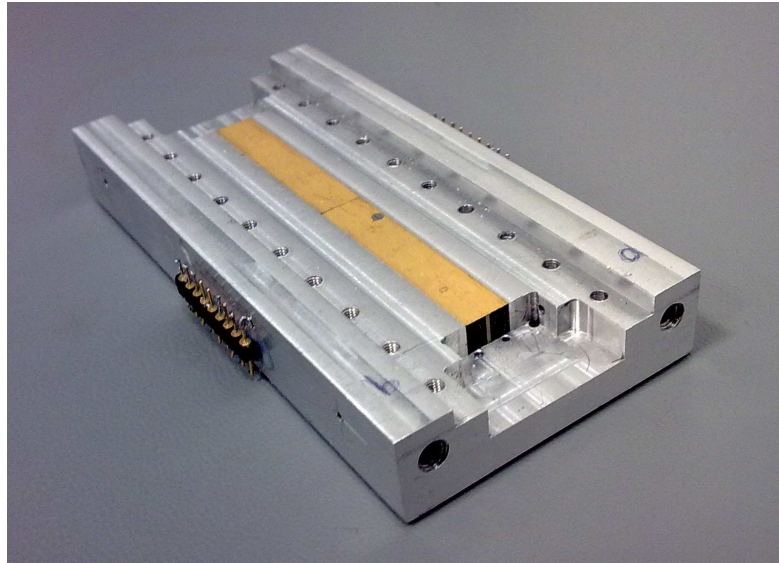
Figure 5.15 A photograph of the first version of designed 76mm twin-toroid structure
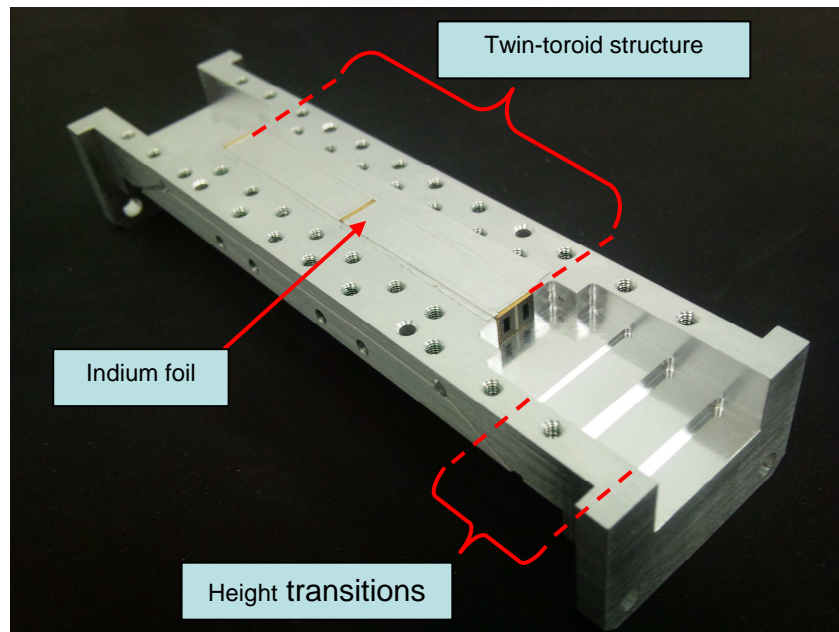
Figure 5.16 A photograph of the second version of designed 76mm twin-toroid structure

Although high power measurements couldn't be performed, minimum 500W of peak power handling capability is estimated from the results obtained from EM simulations and expression given in (A.11). Average power handling capability depends on the thermal design and it is expected that 100W continuous power do not degrade the performance significantly.

5.6.1 Insertion Loss and Return Loss Measurements

In Figure 5.17, comparison of the measurement results and EM simulation results of the insertion loss and the return loss for the 38mm structure with tapered dielectric matching is given. Dielectric constant of the matching element is 6. The results of the measurements are in good agreement with the results of EM simulations. Average insertion loss is measured as 0.3dB and return loss better than -27dB is obtained in 8% BW around f_0. Switching wire inside the twin-toroid structure bring 0.1dB extra insertion loss. Worst return loss value in 10% BW is measured as -14dB. In the measurements, insertion loss spikes are observed around three frequencies which are not seen on EM simulations. Peak value of the insertion loss is measured 0.44dB at $f=0.97f_0$. The reason of these insertion loss spikes is found to be because of the propagation of higher order LSE_{11} mode. Discontinuities and asymmetry in the twin-toroid structure causes coupling of the dominant TE_{10} mode and LSE_{11} mode.
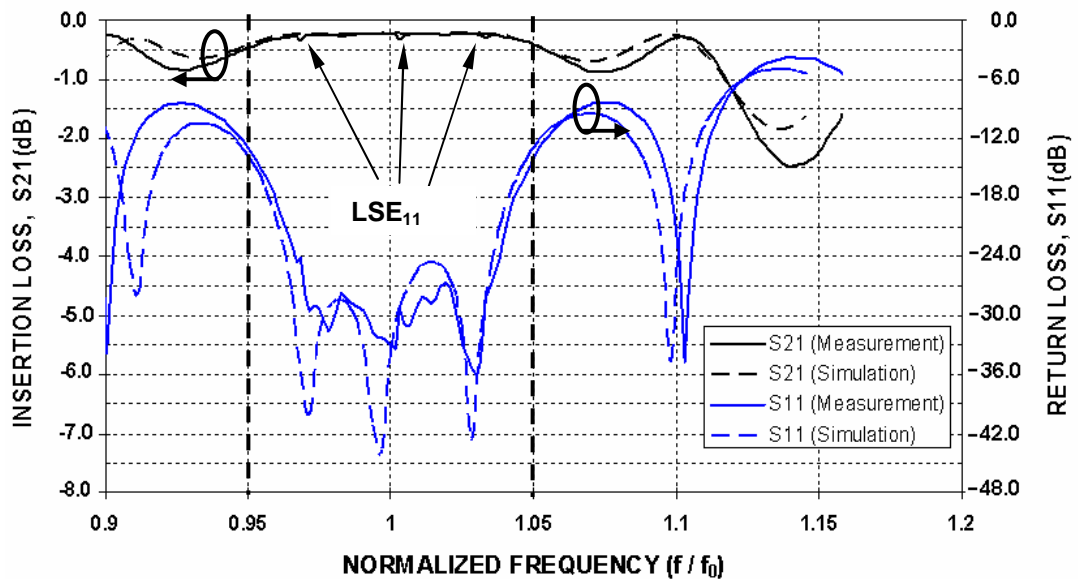
Figure 5.17 Comparison of measurement results and EM simulation results for 38mm structure with tapered dielectric matching

Magnitudes of these notches are highly sensitive to the placement of switching wires and dielectric matching sections, and also dielectric constant of the dielectric matching element used. In the experiments with high dielectric constant ($\varepsilon_r =16, 25$) matching elements, deep insertion loss notches approaching 3dB are observed. Since field intensity is higher in high dielectric constant materials, higher mechanical precision is needed to produce these elements.

In Figure 5.18; for several phase states, measurement results of the 76mm structure with the tapered dielectric matching element optimized for the 38mm structure is given. Average insertion loss is 0.75dB and maximum return loss is 12 dB in 10% BW.
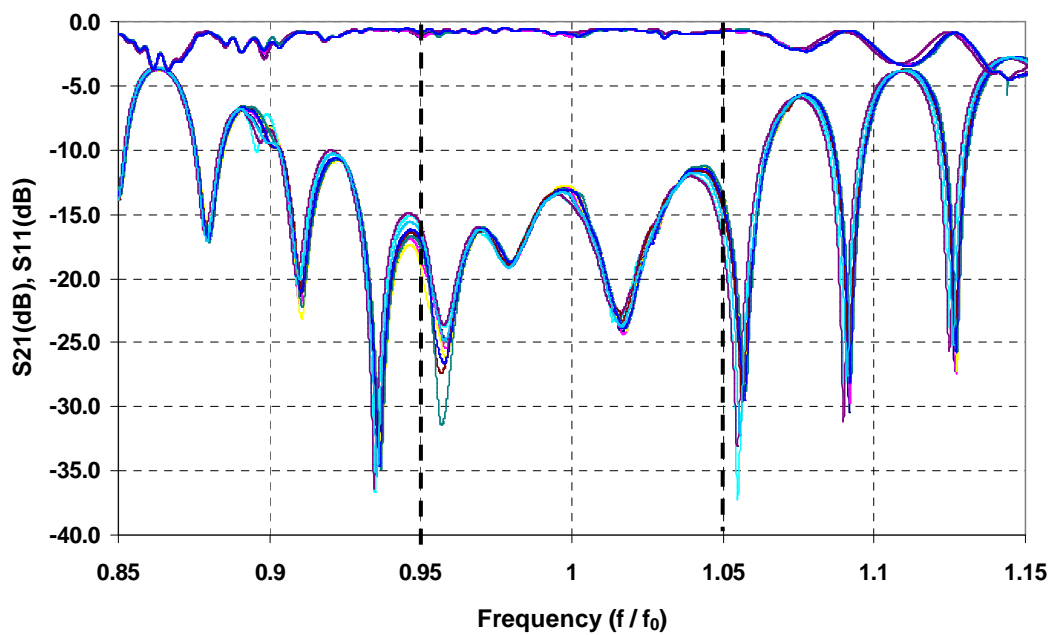
Figure 5.18 Insertion loss and return loss measurement results for different phase states for 76mm structure

In Figure 5.19, insertion loss measurements for the same structure are given in detail. Three insertion loss spikes are observed around $f=0.95f_0$, $f=f_0$ and $f=1.03f_0$. Peak value of the insertion loss is 1.25dB and insertion loss modulation is 0.4dB.
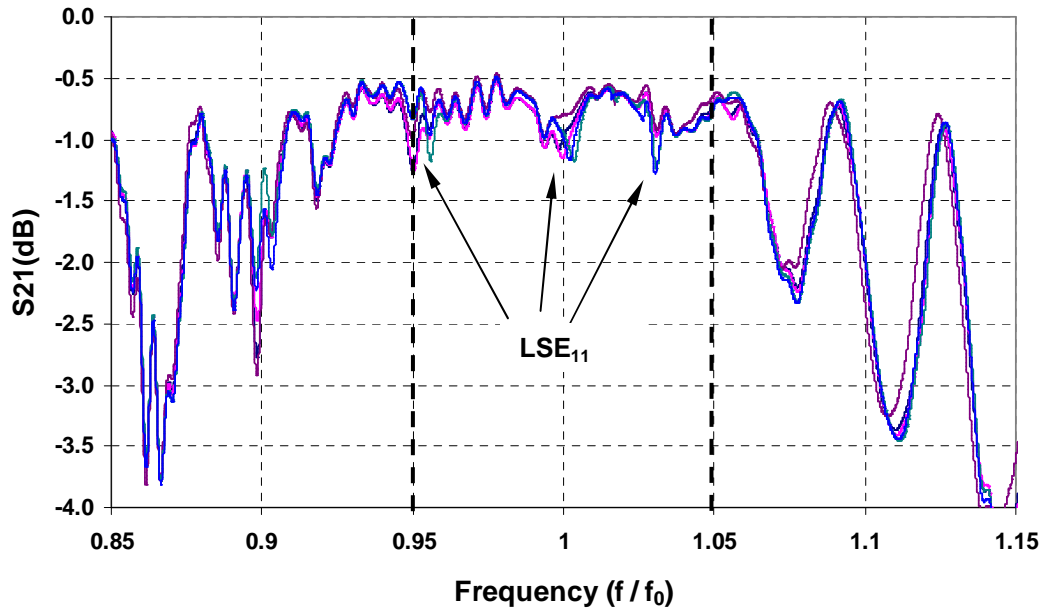
Figure 5.19 Detail of insertion loss measurement results for different phase states

In the insertion loss measurements, it is observed that the hole in the waveguide structure for the switching wires to enter and exit had an important effect on the magnitudes of insertion loss spikes. Filling of the hole with conductive epoxy and absorber material reduced the magnitudes of the spikes about 0.2dB. Also placement of DC feedthru in the holes improved the performance, however didn't solve the problem completely.

90

5.6.2 DPS Measurements

In Figure 5.20, comparison of the results of DPS per unit length between measurements and EM simulations is given. 4% discrepancy is obtained in 10% BW. The difference between the slopes of measurement result and EM simulation result is 0.8°/cm in 10% BW. These small differences may occur because of the dimensional tolerance of the twin-toroid structure or errors in the EM simulation models.
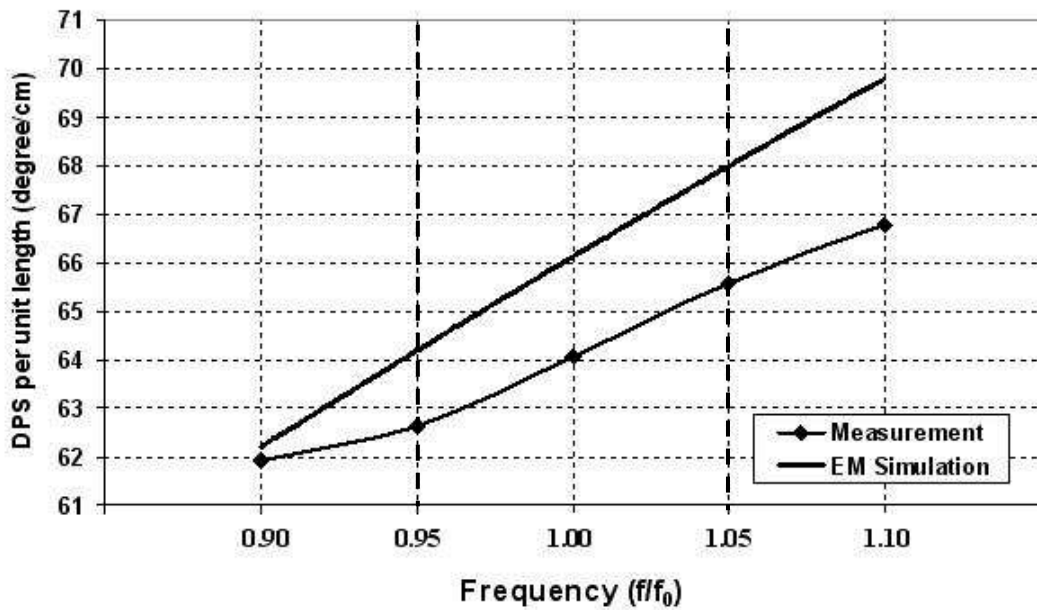
Figure 5.20 Measurement and EM simulation results of DPS per unit length

In Figure 5.21 measurement results of DPS of all phase states for 6-bit operation in 0-360° phase coverage at 25°C is given. As explained in Section 5.2 the slope of the DPS in the BW increases as DPS is increased. In Figure 5.22 and 5.23 group delay measurements for the reference phase state and maximum phase state are given respectively. Average value the group delay is 2.3ns for both states and maximum 1ns peak to peak variation is observed in 10% BW.

Pulse widths of the applied voltages are optimized for the best phase accuracy at the center frequency. Peak to peak phase error is measured as 13.2° and calculated RMS phase error in 10% BW is given in Figure 5.24. The details in the calculation of RMS

phase errors are given in Section 2.3.2. Phase errors occurred at the center frequency result from quantization errors in the driver circuitry and repeatability errors because of the hysteresis. Phase errors increase as frequency is moved away from center frequency because of the slope of the DPS. With RESET-SET switching method <1.2° and with FULL SET-RESET-SET switching method <0.5° phase repeatability is obtained with an automated measurement program developed in Agilent VEE. The program takes measurements by switching to random phase states and calculating maximum phase deviation with the desired phase state. The disadvantage of the FULL SET-RESET-SET switching method is the increase of the switching time by approximately 5 us.
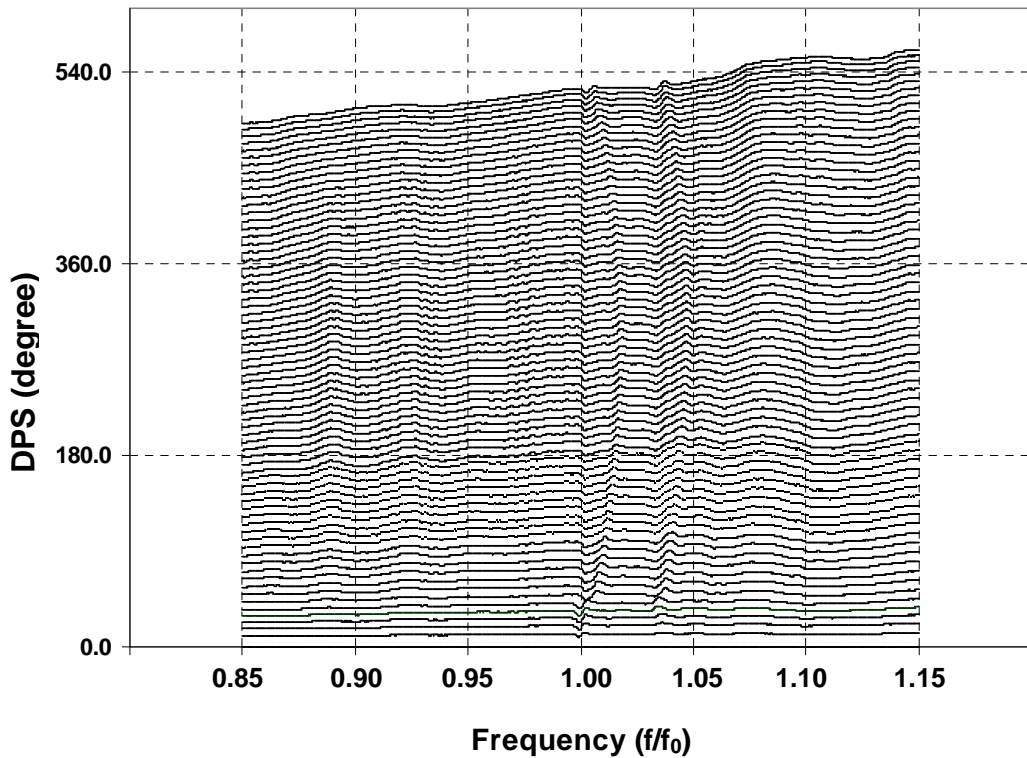
Figure 5.21 All phase states for 6-bit operation in 0-360° phase coverage at T=25°C
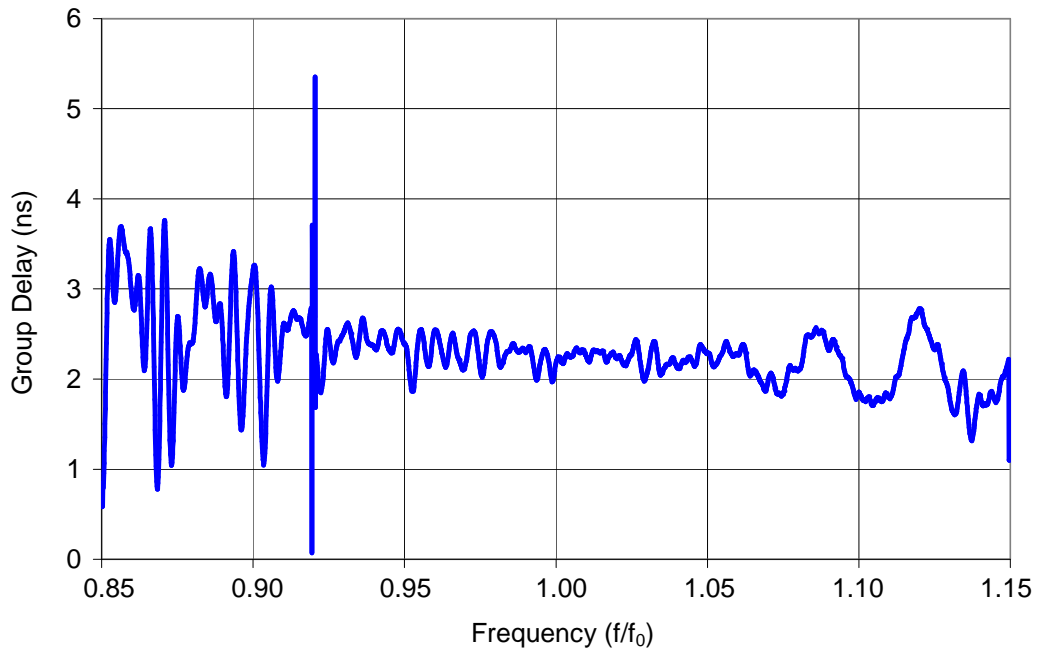
Figure 5.22 Group delay for the reference phase state
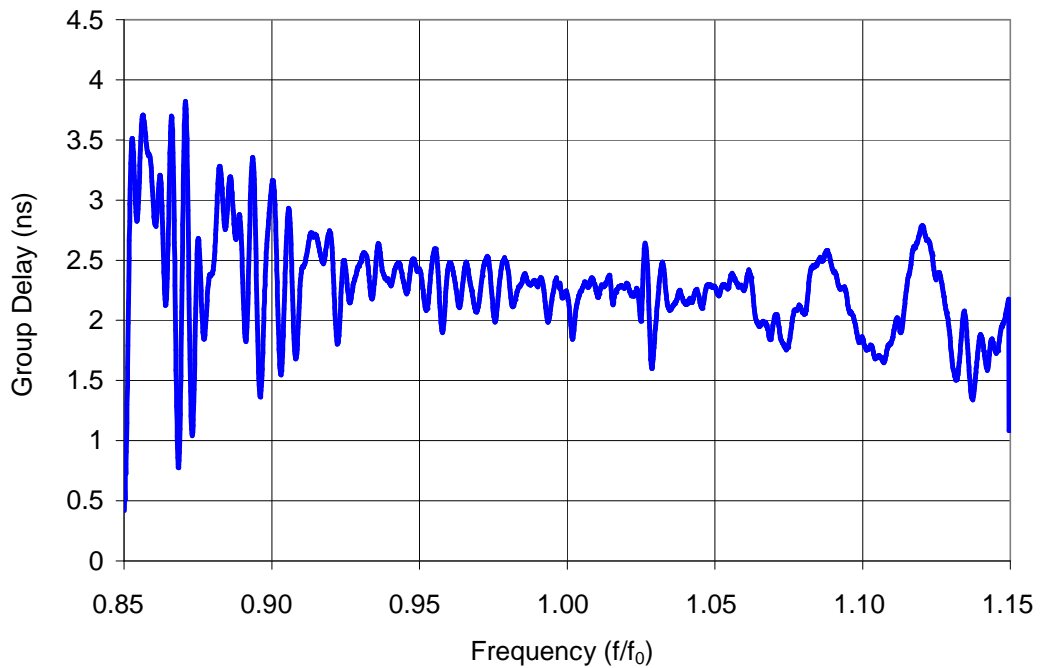
Figure 5.23 Group delay for the maximum phase state

In Figure 5.25, measurement results of DPS versus switching time are given at 4 different operating temperatures. The measurements at these temperatures are

performed on an adjustable hot/cold plate device. DPS increases slowly for pulse widths between 0 - 0.7 μs. There is a linear increase of DPS with pulse width is observed for 0.7 - 4 μs. After 4 us, the increase of DPS slows down as a result of the operation near saturation of the ferrite and at pulse width of 5 μs, 98% of maximum DPS is obtained.
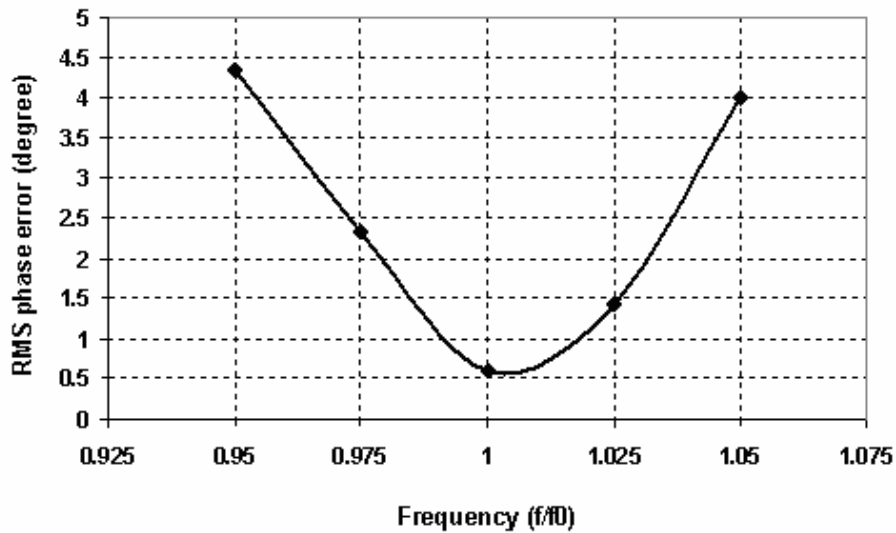
Figure 5.24 RMS phase error for 6-bit operation at T=25°C
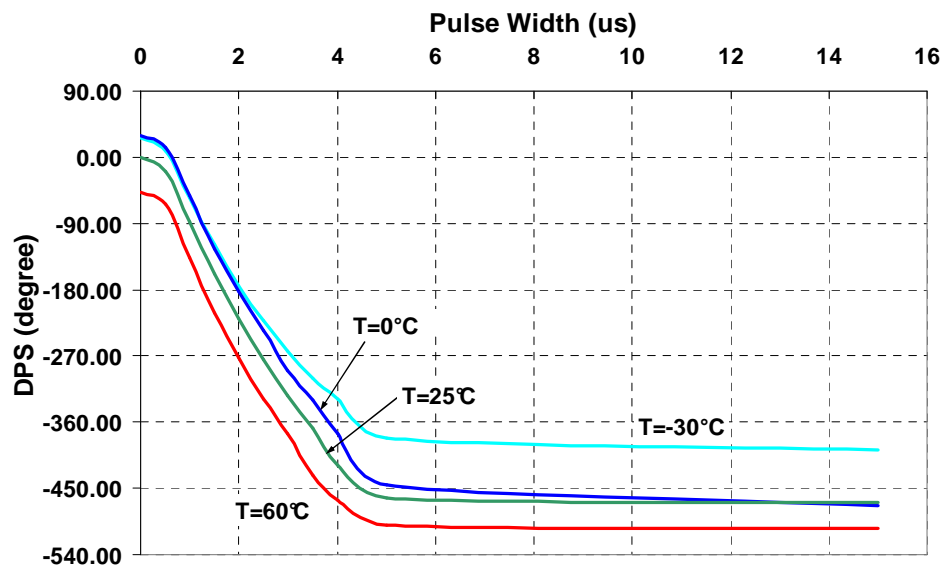
Figure 5.25 DPS measurements at several temperatures in operating temperature range

In Table 5.4, results of measurements given in Figure 5.25 are summarized. DPS results are normalized with respect to the results at room temperature (T=25°C). Total DPS reduced 43° at T=-30°C which is an unexpected result. However after some investigation, it is found that the mechanical stress on the ferrite can cause decrease of DPS via magnetostriction phenomenon explained in the Appendix A.2.3.

Table 5.4 Summary of the DPS measurements at different temperatures

Temperature (°C)	Reference Phase State Drift (degree) (w.r.t T@25°C)	Maximum Phase State Drift (degree) (w.r.t T@25°C)	Change of DPS (degree) (w.r.t T@25°C)
+60	-47	-36	-11
+25	0	0	0
0	+30	-5	+35
-30	+27	+70	-43

5.6.3 Summary of Electrical Performance

In Table 5.5, summary of the electrical performance of the fabricated 76mm twin-toroid ferrite phase shifter is given. Datasheets for a commercial twin-toroid ferrite phase shifter and a rotary-field ferrite phase shifter both operating at X-Band are given in Appendix B for comparison.

Table 5.5 Summary of electrical performance of produced twin-toroid ferrite phase shifter

Parameter	Specification
Bandwidth	10% at X-Band
Peak Power	500W
Average Power	100W
Phase Coverage	Min. 360 °
Phase Resolution	Min. 6 bit (5.6°)
Insertion Loss	1.25 dB max. 0.75 dB avg.
Insertion Loss Modulation	0.5 dB
Return Loss	12.0 dB min. 16.0 dB avg.
Phase Accuracy	< ±6.6° peak, <4.4° RMS
Phase Repeatability	< 0.5°
Operating Temperature Range	-30°C to +60°C
Output Flange	Standard WR-90
Switching Time	≤ 15μs
Switching Energy	<150μJ
Power Supply	+15V, +5V
Driver Control	3 TTL signals
Dimensions	15 X 4.1 X 4.1cm
Other Microwave Characteristics	Nonreciprocal, Latching

5.7 Practical Improvements

5.7.1 Temperature Compensation

The dependence of DPS on temperature is investigated for the designed twin-toroid FPS. Without any temperature compensation techniques, operating at a temperature different than the phase characterization temperature will cause phase errors to increase. Thus the characterization of the phase shifter should be done for several temperature points in the operating temperature range. Digital phase data to be written in the memory will be multiplied with the number of characterization temperatures. The temperature of the FPS can be measured by a temperature sensor sending information to the digital control circuit.

5.7.2 Frequency Compensation

DPS measurement results given in Figure 5.21 show the deterministic behavior of DPS with frequency. DPS is generally a monotonic function of frequency. Also radar systems generally operate in narrow instantaneous operating BW. This allows the division of the main BW to sub-BWs and operating the phase shifter in these sub-BWs. In Figure 5.26, operation in two sub-BWs is shown schematically. In this method, phase shifter is two sub-BWs each operating at different phase states.
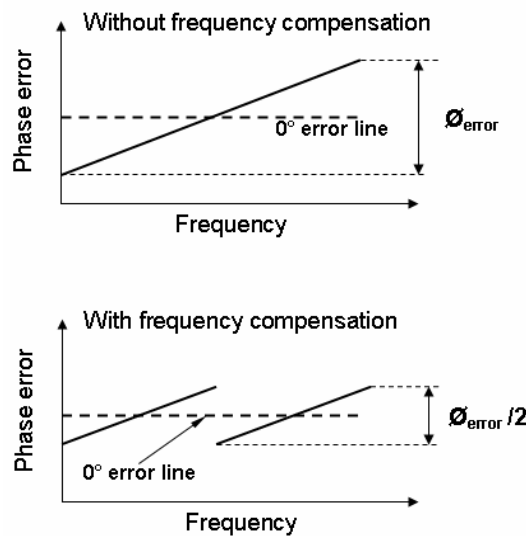
Figure 5.26 DPS measurements at several temperatures in operating temperature range

Theoretically, peak to peak phase error and RMS phase errors will be halved with operation in two sub-BWs. The improvement in phase accuracy increases as the number of sub-BWs is increased. However, digital phase data to be written in the memory will be multiplied with the number of sub-BWs used.

5.8 Future Works

5.8.1 Resistive Suppression

With the improvement of design capability and better understanding of the microwave behavior of the twin-toroid ferrite phase shifter, microwave performance can be improved with new designs. The difficulty of eliminating insertion loss spikes in the BW resulting from propagation of higher order modes is discussed in Section 5.2.

As explained in Section 2.4.4, for the the single-toroid type ferrite phase shifter, higher order modes can be suppressed by placing longitudinal resistive sheet between dielectric materials. The possibility of same approach for the twin-toroid geometry is investigated. In Figure 5.27 two different possible configurations are schematically shown. Since TE_{10} mode do not have an E field component parallel to the resistive material, it will not be affected. However LSE_{11} and LSM_{11} modes will be attenuated in the structure. This attenuation will decrease the magnitudes of insertion loss spikes in BW.
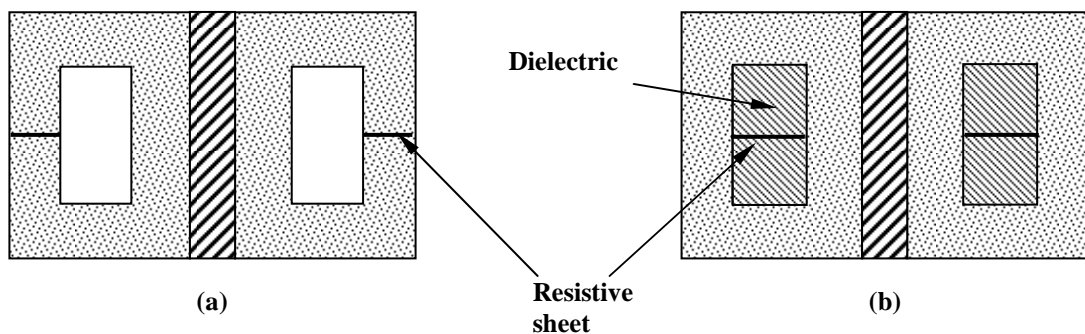
Figure 5.27 Possible configurations for resistive sheet placement

98

In 5.25.a, ferrite toroids are produced in separate pieces and resistive material is placed longitudinally on the side arms of the toroids. Since the continuity of magnetic path is broken, remanent magnetization level in the toroids will decrease which causes decrease of total DPS. In 5.25.b, toroidal hole will be filled with dielectric material which has longitudinally placed resistive material inside. The difficulty of that solution is the placement of dielectric in toroidal holes. The possibility of the production of these two configurations will be discussed with microwave ferrite manufactures.

5.8.2 Using a High Power Ferrite Material

The other approach to eliminate the insertion loss spikes is to prevent the propagation of higher order modes with reduction of waveguide height. However as explained in Section 5.2, with this method power handling capability decreases substantially. In order to accommodate the reduction of power handling, a higher power ferrite material with higher ΔH_k should be used.

In Table 5.5 important microwave characteristics of the material GD-1600-35 of TCI ceramics is given. This material is a Gd doped YIG material with power handling capability at around 10 times higher than for the RG-11 material used in the prototype design.

Table 5.6 GD-1600-35 material parameters [49]

Saturation Magnetization	Remanent Magnetization	Dielectric Constant	Resonance linewidth	Spinwave linewidth	Curie Temperature
$4\pi M_S$ (Gauss)	$4\pi M_r$ (Gauss)	ε_{rf}	ΔH (Oe)	ΔH_k (Oe)	T_c (°C)
1600	1100	15.1	35	4	280

The effect of switching wire on microwave performance will be reduced by placing the wire away from the center with the increase of the dimensional parameter, w_3. Also slope of DPS in frequency is reduced with the increase of w_1.

EM simulation results of the DPS per unit length for the designed structure is given in Figure 5.28. Total phase shifter length will be about 8.4 cm to obtain 360° DPS for -30/+60° operating temperature range.
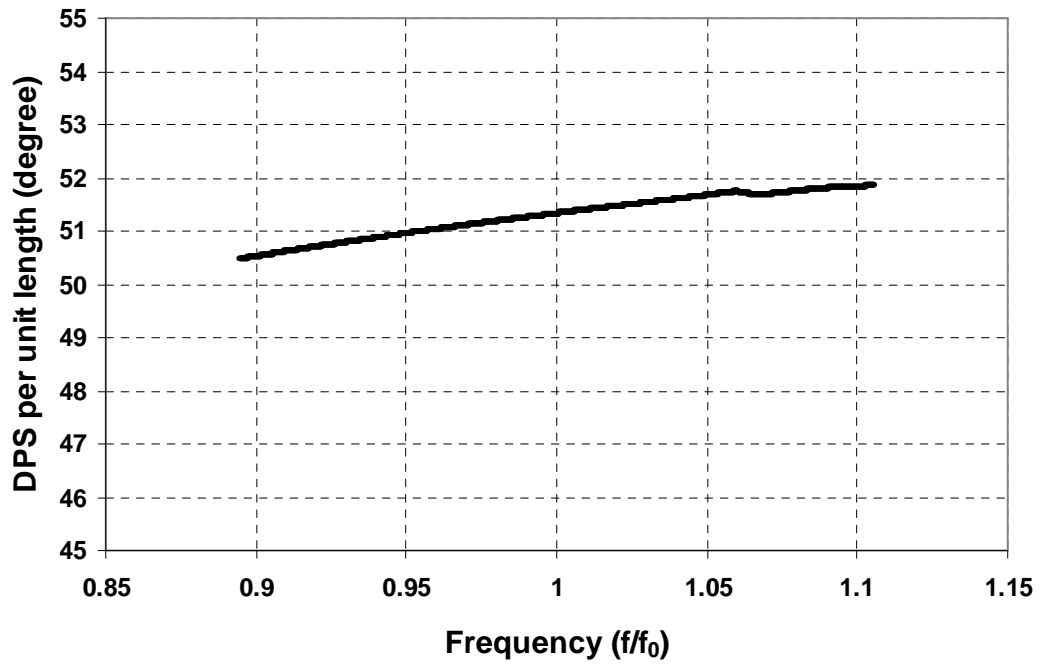
Figure 5.28 EM simulation results of the structure with no higher order mode propagation with material GD-1600-35

CHAPTER 6

CONCLUSION

Ferrite phase shifters are critical components for radar systems. Their electrical performance such as power handling capability, phase resolution and insertion loss determines accuracy and range of a system.

In this thesis, a reciprocal Reggia-Spencer type ferrite phase shifter and a nonreciprocal twin-toroid type ferrite phase shifter both working at X-band are designed, fabricated and measured. In the design of these phase shifters, EM simulation tools are effectively used. Accurate simulation models are developed for determining DPS, transmission, power handling and higher order mode propagation characteristics. These models are verified with measurement results.

Material selection is one of the most critical parts of ferrite phase shifter design. Thus, extensive study on microwave ferrite materials is carried out for this work. Nonlinear high power characteristics, magnetostriction effects and temperature dependencies of different material groups are investigated.

The importance of the exactness in the production of ferrite materials, mechanical structures and dielectric matching elements is seen. For the Reggia-Spencer type ferrite phase shifter, substantial improvement of transmission characteristics with tuning elements is observed. For the twin-toroid geometry, asymmetric placement of the switching wires and dielectric matching elements resulted in an increase of the insertion loss.

The effect of analog and digital control circuits on phase accuracy and switching time is investigated. Hysteresis effects on phase repeatability are reduced by using suitable switching configurations. For the twin-toroid phase shifter, depending on the

monotonic increase of DPS with frequency, phase errors can be reduced with the analog driver circuitry by operating the device in sub-BWs. Temperature dependence of ferrite materials also necessitates compensation with analog driver circuitry.

Although high power measurements couldn't be performed, peak power handling of the designed Reggia-Spencer phase shifter and twin-toroid phase shifter is found at least 500 W with the results of EM simulations and analytical expression given in literature. As explained in Chapter 5, by using a different ferrite material, peak power handling of at least 3kW can be obtained for twin-toroid geometry with possibly a small increase of insertion loss. Average power handling capability of the twin-toroid phase shifter is estimated 100W without significant degradation in the performance.

Because of the resonances in transmission characteristics, operation BW of the designed Reggia-Spencer ferrite phase shifter is limited to 5%. High temperature and high frequency sensitivity of DPS and low switching speed limits the practical usage of Reggia-Spencer type ferrite phase shifter in a phased array system. However, the information obtained in the design and fabrication processes of Reggia-Spencer type ferrite phase shifter has been a basis for the design of twin-toroid ferrite phase shifter.

Successful operation in 10% BW is obtained for the twin-toroid ferrite phase shifter. Moreover, using dielectric matching elements with more sections, BW of twin-toroid ferrite phase shifter can be broaden up to 25%. With the electrical performance given, the designed twin-toroid ferrite phase shifter can be used in a practical phased array antenna system.

REFERENCES

[1] S. Koul and B. Bhat, "Microwave and Millimeter Wave Phase Shifters," Volume I, Boston, MA: Artech House, 1991.

[2] J. L. Snoek, "Magnetic and electrical properties of the binary System MO Fe,O,," Physics, vol. 3, pp. 463-483, June 1936.

[3] J. L. Snoek, "Non-metallic magnetic materials for high frequencies," Philips Tech. Rev., vol. 8, pp. 353-360, Dec. 1946.

[4] J. L. Snoek, New Developments in Ferromagnetic Materials. New York, NY: Elsevier, 1947.

[5] L. Neel, "Proprietes rnagnetiques des ferrites, ferrimagnetisms et antiferromagnetisome," Ann. Phys., vol. 3, pp. 137-198, Mar. 1948.

[6] D. Polder, "On the theory of ferromagnetic resonance," Phil. Mag., vol. 40, pp. 99-115, Jan. 1949

[7] A. G. Fox, "An adjustable wave-guide phase changer," Proc. IRE, pp. 1489–1498, Dec. 1947.

[8] L. Stark, "A Helical Line Scanner for Beam Steering a Linear Array", IRE Trans. On Antennas and Propagation, vol. AP-15, pp.211-216, April 1957.

[9] H. Scharfman, "Three new ferrite phase shifters," Proc. IRE, vol. 44, pp. 1456-1459, Oct. 1956.

[10] D. J. Angelakos and M. M. Korman, "Radiation from ferrite filled apertures," Proc. IRE, vol. 44, pp. 1463-1468, Oct. 1956.

[11] F. Reggia and E. G. Spencer, "A new technique in ferrite phase shifting for beam steering in microwave antennas," Proc. IRE, vol. 45, pp. 1510–1517, Nov. 1957.

[12] F. Reggia and T. Mak, "Reciprocal latching phase modulator for microwave frequencies," IEEE Trans. Magn., vol. MAG-2, pp. 269–273, Sept. 1966.

[13] A. Clavin, "Reciprocal ferrite phase shifters in rectangular waveguide," IEEE Trans. Microwave Theory Tech., vol. MTT-6, p. 334, July 1958.

[14] M. A. Treuhaft and L. M. Silber, "Use of microwave ferrite toroids to eliminate external magnets and reduce switching power," Proc. IRE, vol. 46, pp. 1538, Aug. 1958.

[15] W. J. Ince and E. Stern, "Nonreciprocal remanence phase shifters in rectangular waveguide," IEEE Trans. Microwave Theory Tech., vol. MTT-15, pp. 87–95, Feb. 1967.

[16] G. F. Rodrigue, "A Generation of Microwave Ferrite Devices," Proc. IEEE, vol. 76, pp. 121-137, February 1988.

[17] C. R. Boyd, Jr., "A dual-mode latching reciprocal ferrite phase shifter," IEEE Trans. Microwave Theory Tech., vol. MTT-18, pp. 1119-1124, Dec. 1970.

[18] L. R. Whicker and C. R. Boyd, "A new reciprocal phaser for use at millimeter wavelengths," IEEE Trans. Microwave Theory Tech., vol. MTr-19, pp. 944-945, Dec. 1971.

[20] C. R. Boyd and G. Klein, "A precision analog duplexing phase shifter," in IEEE MTT-S Int. Microwave Symp. Dig., pp. 248–250, 1972.

[21] C. R. Boyd, Jr. "A Latching Ferrite Rotary-Field Phase Shifter", 1995 IEEE MTT-S International Microwave Symposium Digest, pp. 103-106, May, 1995

[22] R. R. Jones, "A slow wave digital ferrite stripline phase shifter," IEEE Trans. Microwave Theory Tech., vol. MTT-14, pp. 684–688, Dec. 1966.

[23] W. M. Libby, "Microstrip two-meander line on ferrite substrate," IEEE Trans. Microwave Theory Tech., vol. MTT-21.

[24] R. R. Romanofsky, "Array Phase Shifters: Theory and Technology," NASA Technical Memorandum TM—2007-214906, Oct. 2007.

[25] G. F. Dionne et al., "Superconductivity for Improved Ferrite Devices," Lincoln Laboratory Journal, vol. 9, no. 1, pp. 19–31, 1996.

[26] W.J. Ince, E. Stern, "Nonreciprocal remanence phase shifters in rectangular waveguide", IEEE Trans. Microwave Theory Tech., vol.15, pp. 87-95, 1967.

[27] J. Svedin, B. Carlegrim, S. Hagelin, " Accurate Design of Ferrite Toroid Phase Shifters - Theoretical and Experimental Results" 18th European Microwave Conference, pp. 391 – 396, 1988

[28] J. Braj and L. Roy, "Ferrite-filled, antisymmetrically-biased rectangular waveguide phase shifter." U.S. Patent 6 867 664, Mar. 15, 2005

[29] F. Reggia, E.G. Spencer, "A New Technique in Ferrite Phase Shifting for Beam Scanning of Microwave Antennas", Proc. IRE, vol. 45, pp. 1510-1517, November 1957.

[30] K. J. Button, B. Lax, "Perturbation Theory of the Reciprocal Ferrite Phase Shifter" Proc. IEE, vol. 109.B, .Supplement 21, 1962.

[31] P. A. Rizzi, B. Gatlin, "Rectangular Guide Ferrite Phase Shifters Employing Longitudinal magnetic Fields" Proc. IRE, vol. 47, pp. 1130-1137, June 1957.

[32] A. Clavin, "Reciprocal Ferrite Phase Shifters in Rectangular Waveguide" IRE Trans. Microwave Theory Tech., vol. MMT-6 , pp. 334, July 1958.

[33] W.E. Hord, F.J. Rosenbaum, C. R. Boyd, Jr., "Theory of the Suppressed-Rotation Reciprocal Ferrite Phase Shifter" IEEE Trans. Microwave Theory Tech., vol. 16, pp. 902-910, 1968.

[34] J.A. Weiss, "A Phenomenological Theory of the Reggia-Spencer Phase Shifter" Proc. IRE, vol.47, pp. 1130-1137, June 1959.

[35] D. M. Pozar, "Microwave Engineering", Second Edition, John Wiley & Sons, NY., 1998

[36] N. R. Landry et al., "Practical Aspects of Phase Shifter and Driver Design for a Tactical Multifunctional Phased Array Radar System", IEEE Trans. Microw. Theory Tech, vol. MMT-22, pp. 617-624, June 1974.

[37] G.N. Tsandoulas, D.H. Temme, F.G. Willwerth, "Longitudinal section mode analysis of dielectrically loaded rectangular waveguides with application to phase shifter design", IEEE Trans. Microw. Theory Tech., vol.18, pp. 88–95, 1970.

[38] W. J. Ince, D.H. Temme, F.G. Willwerth, "Toroid Corner Chamfering as a Method of Improving the Figure of Merit of Latching Ferrite Phasers", IEEE Trans. Microw. Theory Tech., vol. MMT-19, pp. 563-564, June 1971.

[39] C. R. Boyd, "Selected topics on reciprocal ferrite phase shifter design", IEEE S-MTT Workshop, June 2000

[40] W. Zieniutez, "Modes of Propagation in Slot Line with Layered Substrate Containing Magnetized Ferrite", Electronics Letters, vol. 19, pp. 135-136, 1983.

[41] W.E. Hord, F.J. Rosenbaum, C. R. Boyd, Jr., "Theory of the Suppressed-Rotation Reciprocal Ferrite Phase Shifter" IEEE Trans. Microwave Theory Tech., vol. 16, pp. 902-910, 1968.

[42] W.P. Clark, "A High Power Phase Shifter for Phased-Array Systems" IEEE Trans. Microwave Theory Tech., vol. 13, pp. 785 – 788, 1965.

[43] A. Clavin, "Reciprocal Ferrite Phase Shifters in Rectangular Waveguide" IRE Trans. Microwave Theory Tech., vol. MMT-6 , pp. 334, July 1958.

[44] R. Kasevich, E. Wantuch, P. Mahalic, R. Moore, "High-performance high-power analog phase shifter " Proc. IEEE, vol. 57, pp. 1427 – 1429, 1969.

[45] AFT Ferrite Material Catalog, Revised: 2006

[46] E. Schloemann, "Theoretical analysis of twin-slab phase shifters in rectangular waveguide ", IEEE Trans. Microw. Theory Tech., vol. 14, pp. 15–23, 1967.

[47] W.P. Clark, K.H. Hering, A. Charlton, "TE-mode solutions for partially ferrite filled rectangular waveguide using ABCD matrices", IEEE Int. Convention Record, vol. 14, (5), pp. 39–48, March 1966.

[48] G. Klein, "Transient thermal behavior of latching ferrite phase shifters" , IEEE Trans. Microw. Theory Tech., vol.15, pp. 429–430, 1967.

[49] TCI Ferrite Material Catalog, Revised: 2007

[50] J.J. Green, H.J. Van Hook, "Microwave Properties of Lithium Ferrites (Short Papers) ", IEEE Trans. Microw. Theory Tech., vol.25, pp. 155-159, 1977.

[51] W. Hauth, "Accurate analysis of latching phase shifters", IET Microwaves, Antennas &Propagation, vol. 133, pp. 165-168, 1986

[52] G. Skutt, F.C. Lee, "Use of computer visualization tools for examining flux distributions in magnetic structures", APEC '95. Tenth Annual , vol.2, pp.567-573, 1995.

[53] J. M. Park; D.C. Park; "X-band ferrite phase shifter in waveguide geometry" TENCON '93 , vol.3, pp. 464 – 467, 1993.

[54] W.D. Callister, "Fundamntals of Materials Science and Engineering", Fifth Edition, John Wiley & Sons, NY., 2001

[55] E. Stern, W.J. Ince, "Design of Composite Magnetic Circuits for Temperature Stabilization of Microwave Ferrite Devices " IEEE Trans. Microwave Theory Tech., vol. 15, pp. 295-300, 1967.

[56] G. Dionne, "Temperature and stress sensitivities of microwave ferrites" IEEE Trans. on Magnetics, vol. 8, pp. 439-443, 1972.

[57] G. Rodrigue, L. Lavedan, L Hodges, G. Harrison, "Magnetostrictive effects on latching Ferrite devices " IEEE Trans. Magnetics, vol. 4, pp. 609-610, 1968.

[58] W.J. Ince, D.H. Temme, F.G. Willwerth, R.L. Huntt, "The Use of Manganese-Doped Iron Garnets and High Dielectric Constant Loading for Microwave Latching Ferrite Phasers " G-MTT Int. Microwave Symp. Dig., pp. 327-331, 1970.

[59] Trans-Tech, RF/Microwave Products Catolag, Revised: 2005

[60] J.J. Green, F. Sandy, "Microwave Characterization of Partially Magnetized Ferrites" IEEE Trans. Microwave Theory Tech., vol. 22, pp. 641-645, 1974.

[61] A. Abuelma'atti, J. Zafar, I. Khairuddin, A.A.P. Gibson, A. Haigh, I. Morgan, "Variable toroidal ferrite phase shifter " IET Microwaves, Antennas & Propagation, vol. 3, pp. 242-249, 2009.

[62] J.J. Green, F. Sandy, "A Catalog of Low Power Loss Parameters and High Power Thresholds for Partially Magnetized Ferrites " IEEE Trans. Microwave Theory Tech., vol. 22, pp. 645-651, 1974.

[63] E. Schloemann, "Theory of low-field loss in partially magnetized ferrites " IEEE Transactions on Magnetics, vol. 28, pp. 3300-3302, 1992.

[64] F.P. Wohlfarh (ed.), Ferromagnetic Materials, vol. 2, North-Holland, 1980.

[65] C. R. Boyd, Jr., "Design Considerations For Rotary-Field Ferrite Phase Shifters," Microwave J., vol. 31, pp. 105-115, November 1988.

[66] Vaughn, J.T., Cox, P.R., Rodrigue, G.P., Harrison, G.R., "Ferrite phase shifters using stress insensitive garnet materials," IEEE Trans. Microwave Theory Tech., vol. 43, pp. 1017 – 1022, 1995.

[67] Stoker, J.; Nisbet, W.T., "Hysteresis effects in non-reciprocal and rotary field ferrite phase shifters," IEE Colloquium on Ferrite Materials, Devices and Applications, pp. 8/1 - 8/7, 1989.

APPENDIX A

GENERAL PROPERTIES AND MICROWAVE CHARACTERISTICS OF FERRITE MATERIALS

Ferrite materials played an important role in microwave community for above 60 years because of their irreplaceable microwave characteristics. Material technology evolved in years to respond the needs of the microwave industry as new devices are invented. In this Chapter general properties of microwave ferrites are explained and important microwave characteristics of ferrite materials are discussed in detail.

A.1 General Properties

Ferrites are mixed oxide, ceramic-like materials having ferrimagnetic properties. High resistivity (on the order of 10^{13} Ω.m) of ferrite materials allows them to be used in high frequency applications without eddy currents. Microwave ferrites are special class of ferrite materials having dielectric constants in the range 10 to 20 and specially designed for the microwave applications. They can be classified in 3 groups in terms of their crystal structure: spinel ferrites, garnet ferrites and hexagonal ferrites. Spinel ferrites are manufactured by sintering a mixture of ferric oxide Fe_2O_3 and metal oxide MO where M is any divalent metal. In particular lithium ferrites $(LiFe)_{1/2}Fe_2O_4$, magnesium-manganese ferrite $MgMnFe_2O_4$, and nickel ferrite $NiFe_2O_4$ are commonly used in microwave devices. Garnets have a general composition $R_3Fe_5O_{12}$ where R is a rare- earth element. The most important garnet materials are yttrium iron garnet (YIG) and gadolinium iron garnet (GdIG). Hexagonal ferrite materials are used in development of circulators, isolators and phase shifters at millimeter wave frequencies [1].

A.2 Magnetic Hysteresis

As in ferromagnetic and other ferrimagnetic materials magnetic flux density in microwave ferrites do not change linearly with the applied magnetic field. This is because of the complex interactions of magnetic domains. Figure A.1 shows magnetic flux density variation of initially demagnetized magnetic material with applied magnetic field. For a demagnetized ferrite material domains are aligned such that their cumulative magnetic moments are zero. As magnetic field applied domain walls start to move increasing the size of the domains having a component of the applied magnetic field. This process is called *domain wall movement*. At the knee of the hysteresis curve there is a single domain and further increase of the magnetic field causes to the *domain wall rotation* process. When all domains are aligned in the direction of H field, material cannot hold more magnetic flux and B field converges to a point called *saturation magnetization*; B_s or $4\pi M_s$ in units of Gauss. Initial relative permeability, μ_i is the slope of the magnetization curve at origin and it determines the ease of magnetization of the material.
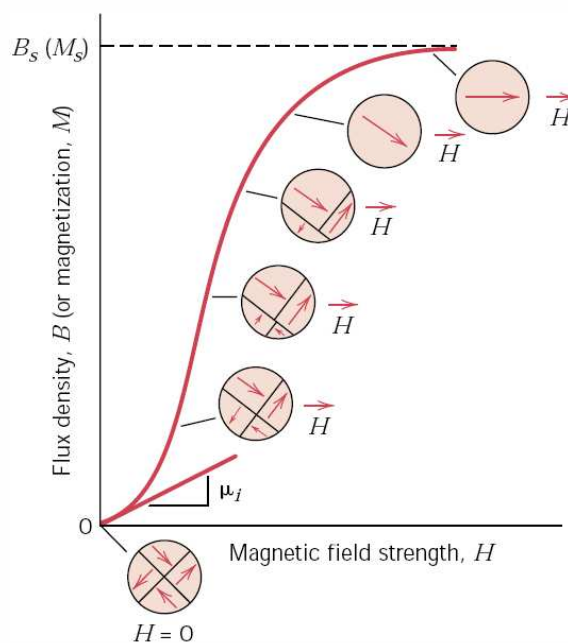

Figure A.1 B-versus-H behavior for initially demagnetized magnetic materials [54]

Figure A.2 shows a complete magnetization curve of ferromagnetic and ferrimagnetic materials known as *hysteresis curve*. At saturation, if the applied field is removed, B field does not retrace its original path, curve 1; instead it reduces along curve 2 and reaches a value known as *remanent magnetization, B_r* or $4\pi M_r$ in units of Gauss. The ratio B_r/B_s is called *squareness ratio* or *remanence ratio* and generally high squareness ratio is wanted especially in magnetic recording and microwave applications.
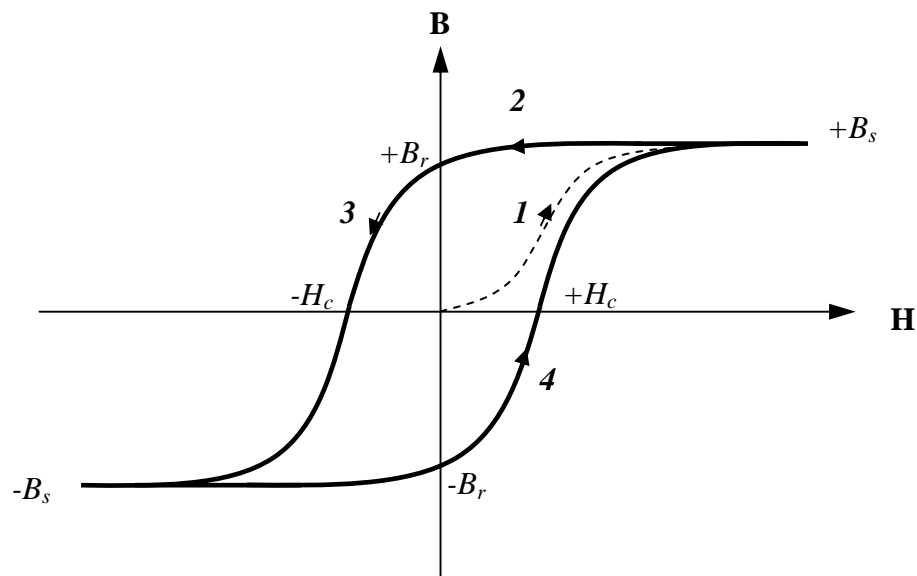
Figure A.2 Hysteresis Curve

When magnetic field is reversed magnetic flux density reduces along curve 3 and at *coercive force H_c*, its value is zero. H_c generally determines the ease of magnetization of the material. Materals with low H_c are called soft materials and they are used in AC applications because of their low magnetic field needs. However in DC applications such as permanent magnets, hard materials with high H_c values are needed to make the demagnetization difficult. Further increase of the H field in reverse direction brings the material at negative saturation magnetization point, *-B_s* or $-4\pi M_s$. As H field again is reduced to zero and increased in forward direction, magnetic flux density increases along curve 4 and hysteresis loop is completed.

A.2.1 Minor Hysteresis Loops

Hysteresis curve drawn in Figure A.2 is the major hysteresis loop obtained by magnetizing the material to the negative and positive saturation points. Actually there are infinite numbers of minor hysteresis loops which can be obtained by applying smaller H fields. In Figure A.3 a major loop and several minor hysteresis loops inside the major loop for YIG are shown. By applying proper H fields, ferrite materials can be operated in any point inside the major hysteresis loop.
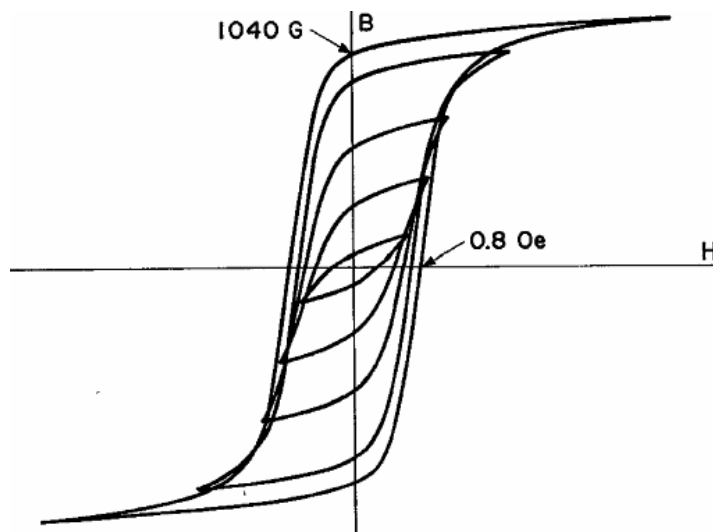
Figure A.3 Major and minor hysteresis curves for YIG [55]

A.2.2 Effect of Temperature on Magnetization

Characteristics of magnetic materials are also influenced by the temperature. As temperature is increased, the magnitude of thermal vibration of the atoms increases causing the atomic moments to rotate in random directions. This results in a decrease of coupling forces between adjacent atoms in a magnetic domain and thus a decrease of saturation magnetization. At the critical temperature called *Curie Temperature T_c*, saturation magnetization value drops to zero. The value of T_c only depends on composition of the material. In Figure A.4 hysteresis curves for YIG at several temperatures are shown. As temperature is increased, both width and height of the hysteresis curve decreases showing the reduction of magnetic activity.

113
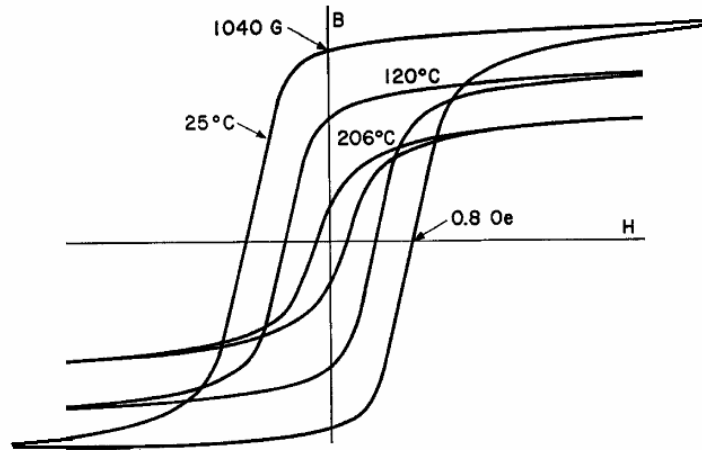
Figure A.4 Major hysteresis loop for YIG at several temperatures [55]

In Figure A.5 saturation magnetization for several room temperature 1000G materials are sketched for purposes of comparison. MnMgAl ferrite is most severely degraded in this respect. LiTiZn is the most temperature stable material having the highest T_c value. It is seen that Gd addition to YAlFe garnet greatly improved the temperature stability.
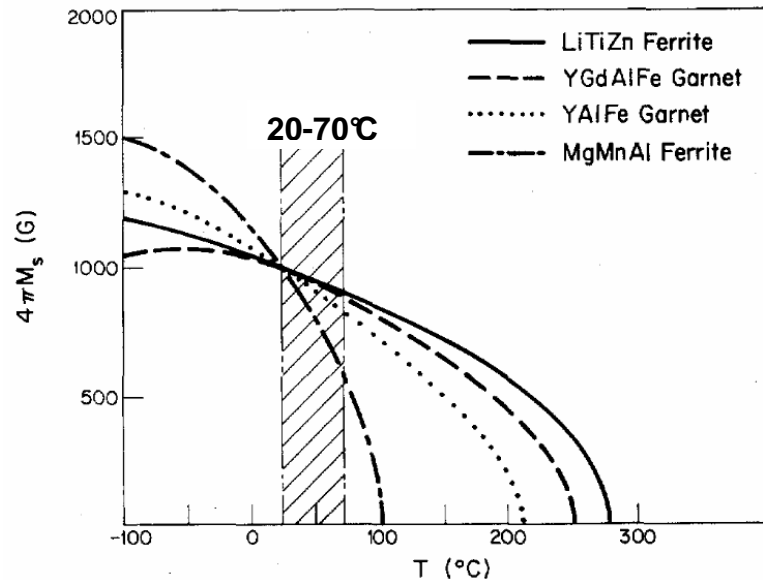
Figure A.5 Saturation magnetization versus temperature characteristics of room temperature 1000G microwave ferrites [56]

114

A.2.3 Effect of Stress on Magnetization

Mechanical stress is another factor influencing the hysteresis characteristics. Ferrite materials are magnetostrictive, i.e. their shape and size changes when subjected to a magnetic field as illustrated in Figure A.6. Mechanical stress changes the direction of magnetization via magnetostriction. As a result the remanent magnetization level of the ferrite material decreases [57].

The sources of the mechanical stress in ferrite phase shifters are the inexact mechanical fitting between ferrite material and waveguide housing or internal stress caused by nonuniform RF heating in high average power devices. The former source of stress can be reduced to acceptable levels by proper mechanical design. However the latter source of stress can severely affect remanent magnetization level regardless of the precautions taken in the mechanical design.

In Figure A.7 change in hysteresis characteristics for the circular toroid given in inset of the figure is shown for a thermal gradient of 20°C between the inner and outer walls.
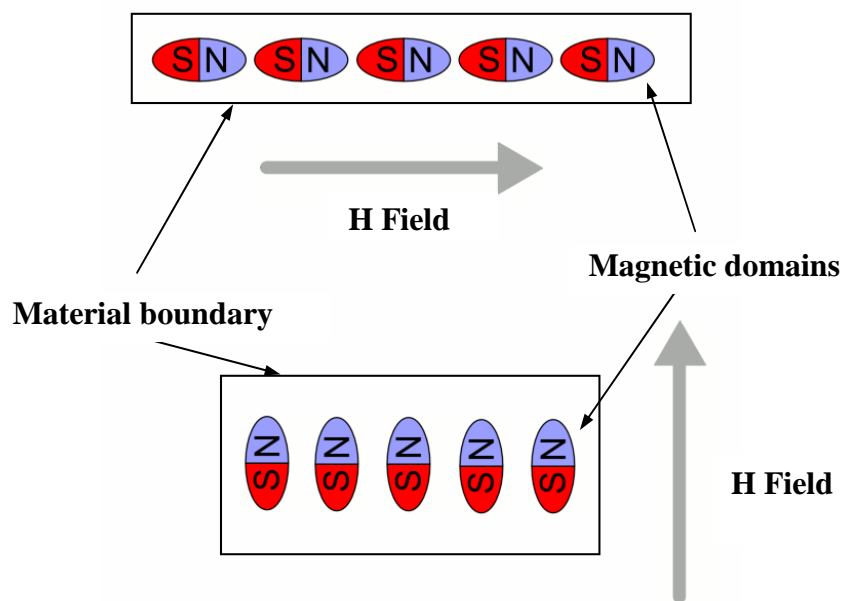

**Figure A.6 Schematic description of the effect of magnetostriction**
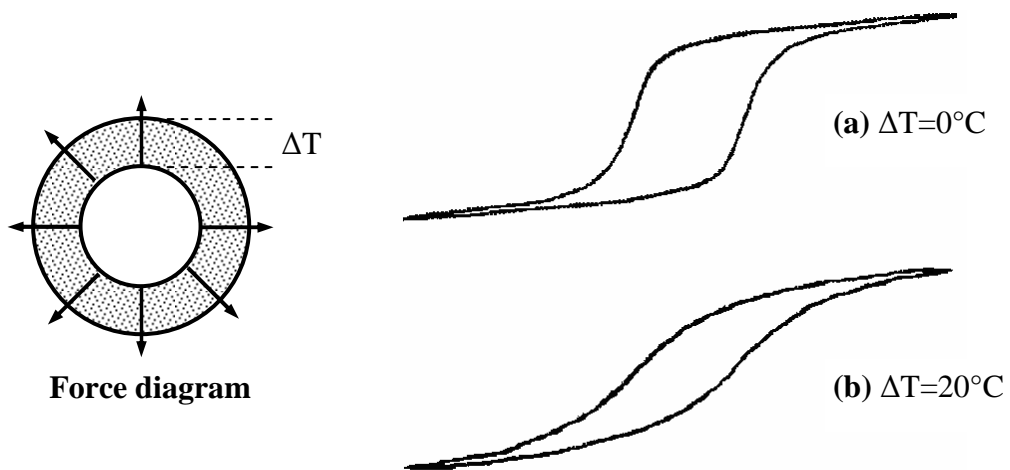
Figure A.7 Effect of a 20°C temperature gradient between inner and outer walls of the toroid to hysteresis characteristics [58]

The effect of applied stress on the remanant magnetization of a number of ferromagnetic toroids is given in Table A.1. Notice that MgMn spinel ferrites are not affected from stress whereas garnet type ferrites and Ni-Co ferrites exhibit greater magnetostrictive properties.

Table A.7 Effect of mechanical stress on remanent magnetization for ferrite materials [59]

Material Group	$4\pi M_S$	$B_r/B_{r(0)}$ *at 3000 psi*
MgMn Spinel	680	1
	1250	1
	2150	1
Ni-Co Spinels	1400	1.55
	3000	0.93
	3150	0.84
Garnets	1000	0.84
	1200	0.88
	1780	0.95

Thermal annealing of machined ferrite parts relieves the stress occurred when mechanical finishing and improves hysteresis characteristics as in Figure A.8.

AS MACHINED		THERMAL ANNEAL 1200°C—1 hr.	
REMANENT INDUCTION = 285 gauss	COERCIVE FORCE = 0.96 oerstads	REMANENT INDUCTION = 651 gauss	COERCIVE FORCE ≈ 0.77 oerstads
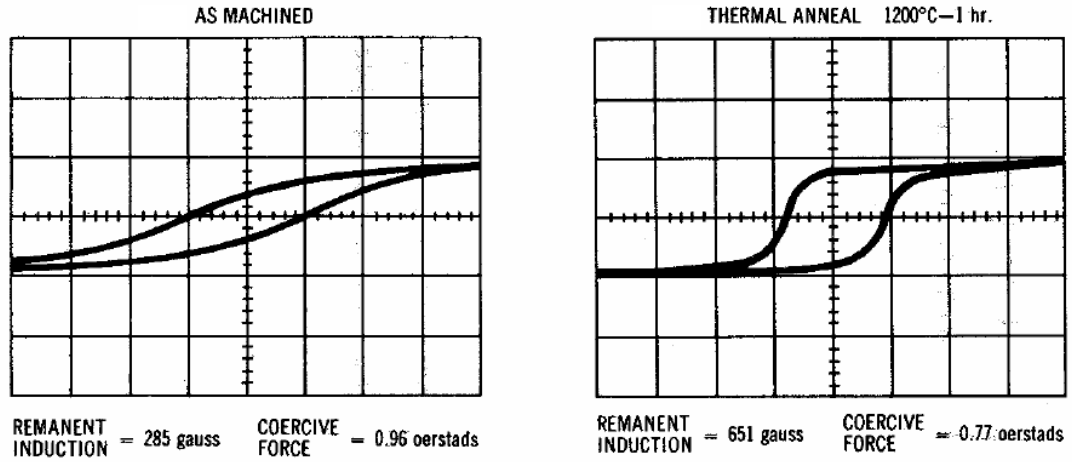
Figure A.8 Effect of thermal annealing on machined ferrite parts [59]

A.3 The Permeability Tensor

The permeability tensor of a ferrite material magnetized to saturation in +z direction is represented as

$$[\mu] = \begin{bmatrix} \mu & j\kappa & 0 \\ -j\kappa & \mu & 0 \\ 0 & 0 & \mu_0 \end{bmatrix} \quad \text{(z bias)} \tag{A.1}$$

The elements of the permeability tensor are given as

$$\mu = \mu_0 \left(1 + \frac{\omega_0 \omega_m}{\omega_0^2 - \omega^2} \right) \tag{A.2}$$

$$\kappa = \mu_0 \frac{\omega \omega_m}{\omega_0^2 - \omega^2} \tag{A.3}$$

117

where $\omega_0 = \gamma H_0$, $\omega_m = \gamma 4\pi M_s$ and ω is the angular frequency of the applied signal.

For partially magnetized ferrites, i.e. for ferrite materials magnetized bellow saturation, the permeability tensor is similar and it is represented as [60]

$$[\mu] = \begin{bmatrix} \mu & j\kappa & 0 \\ -j\kappa & \mu & 0 \\ 0 & 0 & \mu_P \end{bmatrix} \quad \text{(z bias)} \tag{A.4}$$

Using coordinate transformation permeability tensor for ferrite material magnetized in +x and +y directions is represented as

$$[\mu] = \begin{bmatrix} \mu_P & 0 & 0 \\ 0 & \mu & j\kappa \\ 0 & -j\kappa & \mu \end{bmatrix} \quad \text{(x bias)} \tag{A.5}$$

$$[\mu] = \begin{bmatrix} \mu & 0 & -j\kappa \\ 0 & \mu_P & 0 \\ j\kappa & 0 & \mu \end{bmatrix} \quad \text{(y bias)} \tag{A.6}$$

In the x-y plane if we define θ as being coincident with y-axis and positive direction towards x-axis then the permeability tensor can be derived for general x-y directions of magnetizations as [61].

$$[\mu] = \begin{bmatrix} \mu\cos^2\theta + \mu_P\sin^2\theta & (\mu-\mu_P)\cos\theta\sin\theta & -j\kappa\cos\theta \\ (\mu-\mu_P)\cos\theta\sin\theta & \mu\sin^2\theta + \mu_P\cos^2\theta & -j\kappa\sin\theta \\ j\kappa\cos\theta & j\kappa\sin\theta & \mu \end{bmatrix} \tag{A.7}$$

By assuming small magnetic losses in the ferrite material, the elements of the permeability tensor can be represented with real and imaginary parts as

$$\mu = \mu' - j\mu''$$
$$\kappa = \kappa' - j\kappa''$$
$$\mu_P = \mu_P' - j\mu_P''$$

(A.8)

The real parts of the elements of the permeability tensor for partially magnetized ferrite are used to calculate insertion phase and are given by

$$\mu' = \mu_d' + (1 - \mu_d')(\frac{M}{M_S})^{3/2}, \ \kappa' = \gamma 4\pi M / \omega$$

$$\mu_P' = \mu_d'(1 - \frac{M}{M_S})^{5/2}, \ \mu_d' = \frac{2}{3}\left[1 - \left(\frac{\gamma 4\pi M_S}{\omega}\right)^2\right]^{1/2} + \frac{1}{3}$$

(A.9)

where μ_d' is the permeability of ferrite for the completely demagnetized state ($4\pi M = 0$) and is plotted as a function of $\gamma 4\pi M_S / \omega$ in Figure A.9.

Note that the equations in (A.9) depend only on two parameters, the normalized saturation magnetization $\gamma 4\pi M_S / \omega$ and the normalized average magnetization $\gamma 4\pi M / \omega$. In Figures A.10 and A.11 measured values of the real parts of the elements of the permeability tensor are plotted as a function of $\gamma 4\pi M / \omega$ for several values of $\gamma 4\pi M_S / \omega$. The normalized saturation magnetization $\gamma 4\pi M_S / \omega$ is changed by altering the temperature of the ferrite material at a fixed frequency.

119
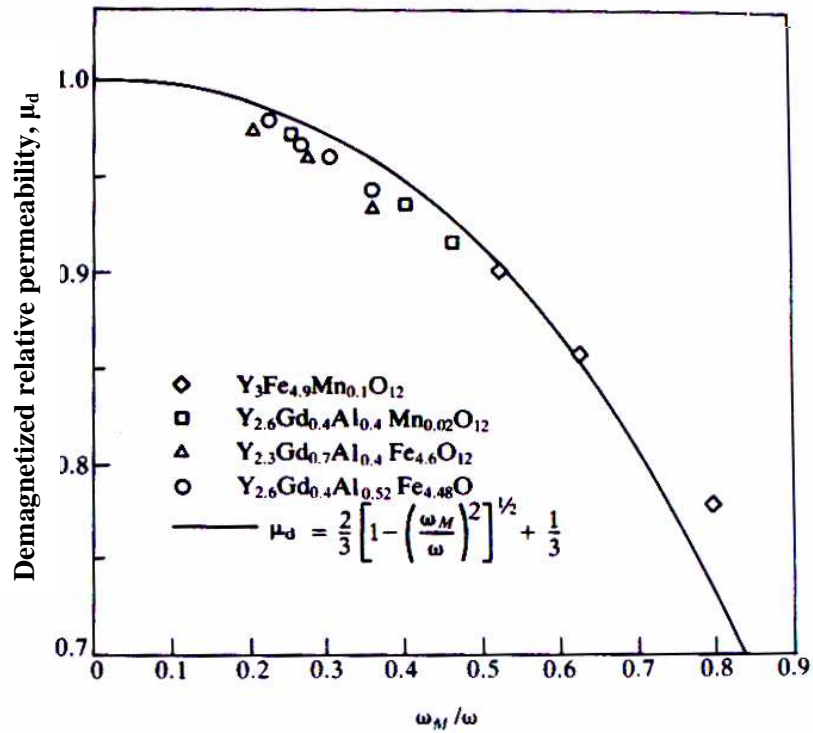
**Figure A.9 Demagnetized relative permeability for several ferrite materials [60]**
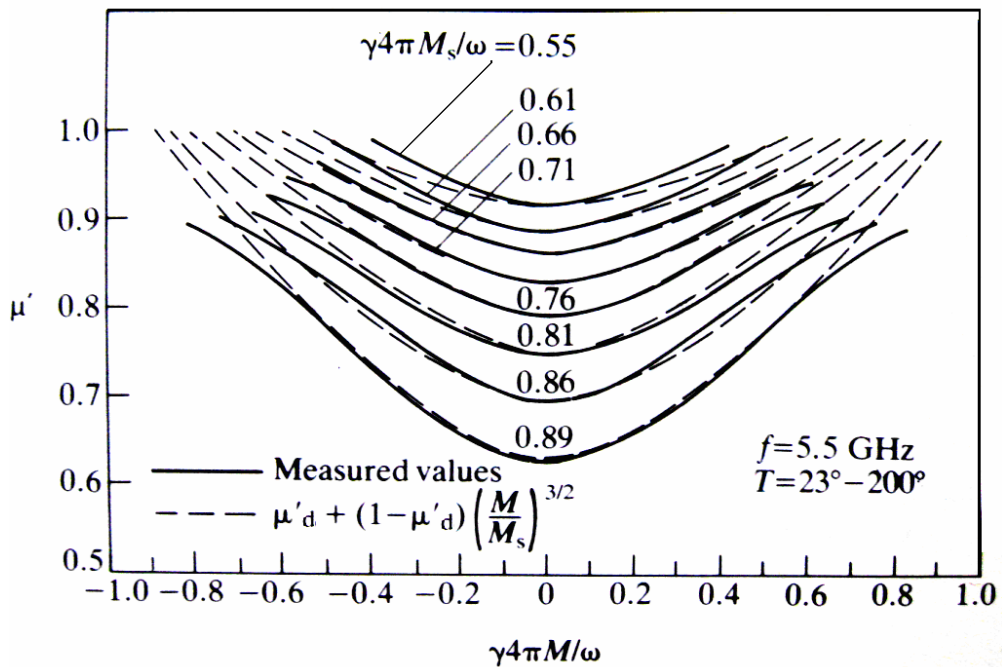
**Figure A.10 μ' versus $\gamma 4\pi M/\omega$ with $\gamma 4\pi M_S/\omega$ as parameter for pure YIG [60]**

120
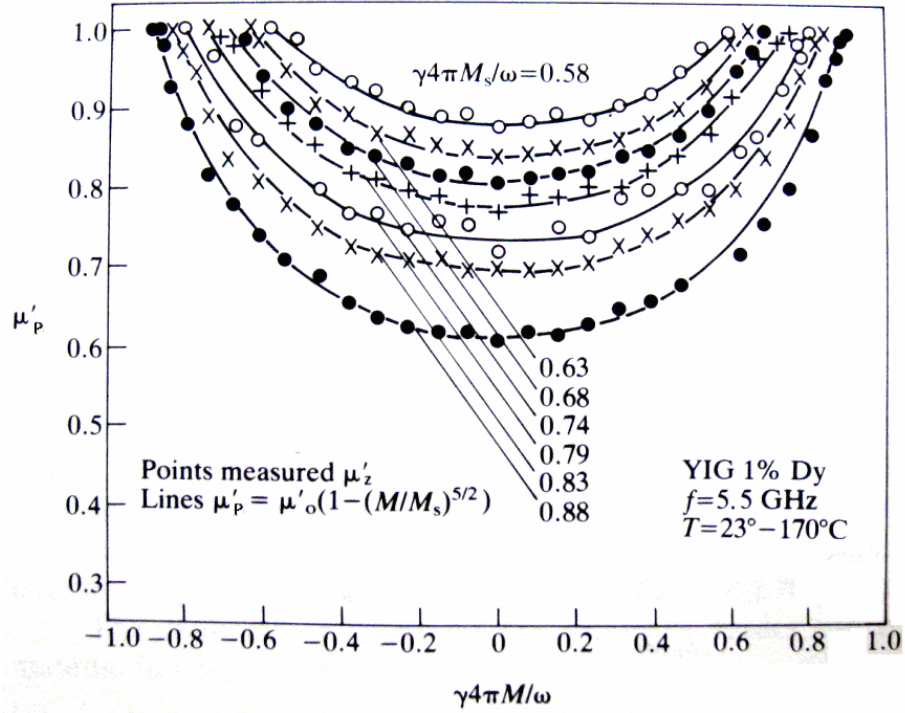
Figure A.11 $\mu_P{'}$ versus $\gamma 4\pi M/\omega$ with $\gamma 4\pi M_S/\omega$ as parameter for YIG doped with 1% Dy [60]

A.3.1 Magnetic Losses and Low-field Loss Phenomenon

The imaginary parts of the components of the permeability tensor are used in calculating the magnetic loss in the ferrite structure. In [62], it is shown that for $\gamma 4\pi M_S / \omega < 0.7$ the imaginary parts of the diagonal components of the permeability tensor follow a simple power law relationship

$$\mu{''} = \mu_P{''} = A\left(\frac{\gamma 4\pi M_S}{\omega}\right)^N \tag{5.10}$$

where A and N depend on the ferrite material composition and tabulated for several ferrite materials in Table 5.1

Table A.8 Measured values of loss parameters for several ferrite materials [62]

Material Composition	$4\pi M_S$ **(Gauss)**	$A\ (\times 10^4)$	N
YIG	1780	7.5	2.5
YIG+Al	1200	10	2.4
YIG+Al+Gd	1200	34	1.9
YIG+Gd	1200	50	1.8
MgMn	2150	16	2.2
MgMn+Al	1750	18	2
Ni+Al	2100	95	3

For $\gamma 4\pi M_S / \omega$ greater than 0.7, magnetic losses of the ferrite materials increases rapidly as *low field losses* (Polder-Smit losses) set in. Absorption in ferrite materials increases seriously when magnetization in the ferrite material is below saturation. The physical mechanism responsible for the low field loss is a gyromagnetic resonance in which the magnetization vectors of oppositely polarized magnetic domains precess around the directions of local DC magnetization. The precessional motion gives rise to a divergence of magnetization at the domain walls, and hence to a RF magnetic field. Since the field is proportional to the saturation magnetization, the resonant frequency is proportional to the saturation magnetization [63].

In Figure A.12 and Figure A.13 increase of the magnetic loss parameter μ'' is seen with the increase of $\gamma 4\pi M_S / \omega$ for YIG with 1% Dy doping and MgMn ferrite respectively. Because of the low field loss effects for $\gamma 4\pi M_S / \omega > 0.7$ μ'' increases at low magnetization levels. This can cause unacceptable insertion loss modulation for different phase states at different magnetization levels for a practical ferrite phase shifter.
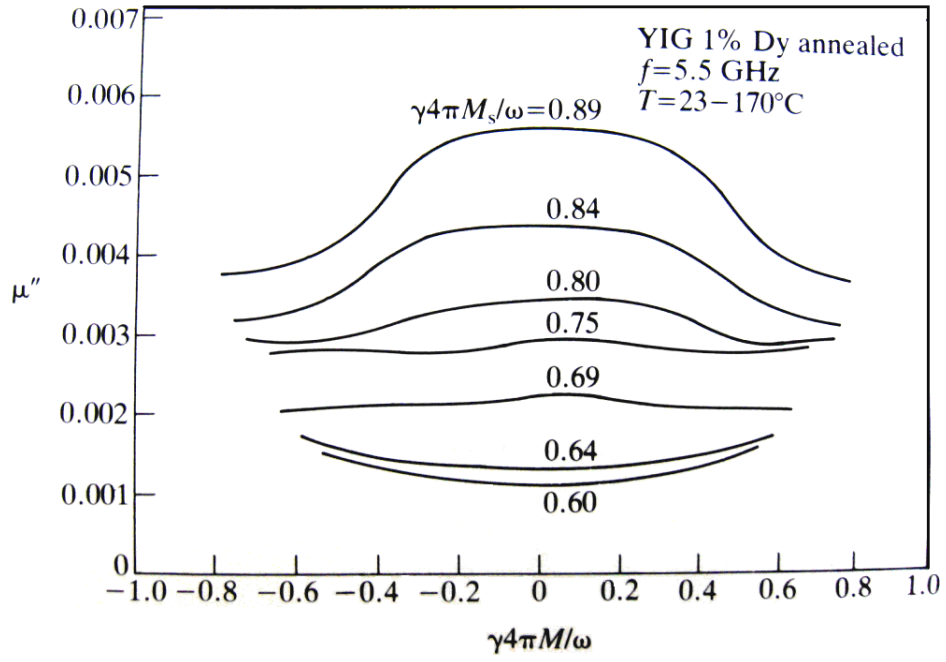
**Figure A.12** μ'' versus $\gamma 4\pi M/\omega$ with $\gamma 4\pi M_S/\omega$ as parameter for YIG doped with 1% Dy [60]
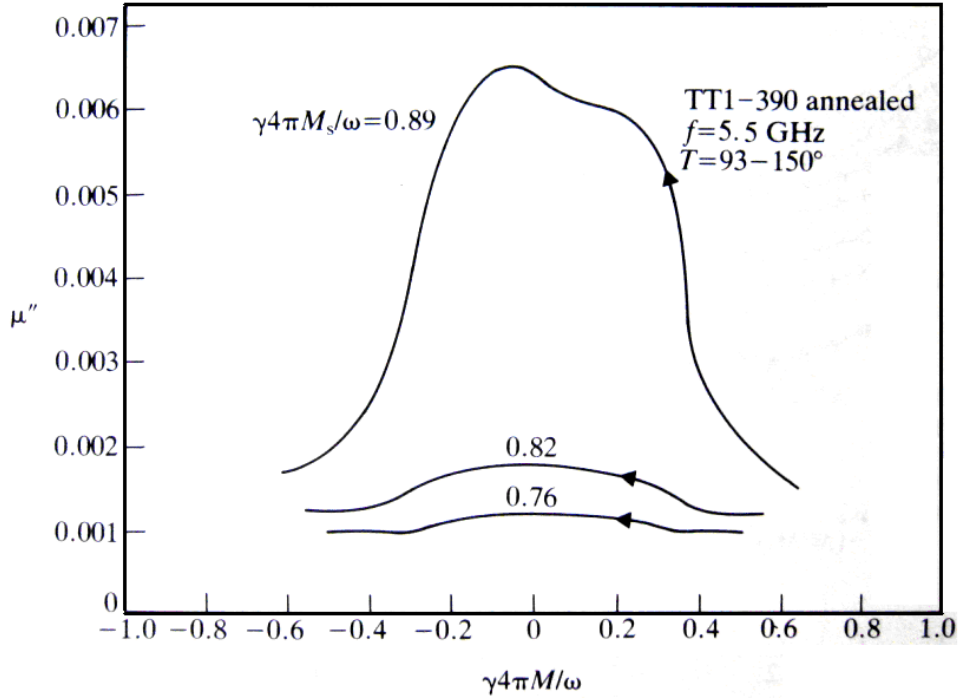
**Figure A.13** μ'' versus $\gamma 4\pi M/\omega$ with $\gamma 4\pi M_S/\omega$ as parameter for MgMn ferrite [60]

A.4 Resonance Linewidth

In (A.2) and (A.3) it can be observed that at $\omega = \omega_0$, the elements μ and κ become infinity, indicating resonance absorption in the material. In practice the absorption is broadened by the inhomogeneities in the ferrite structure and increase of RF power level. The resonance linewidth ΔH of the ferrite materials is defined as the difference between the magnetic field values at a constant frequency where κ'' (or χ'') falls to half of its maximum value as shown in Figure A.14. This phenomenon of resonance absorption is utilized in nonreciprocal devices such as isolators. Nonreciprocal action occurs because an incident circularly polarized RF wave having the same sense of rotation as that of an electron precession undergoes resonance absorption. On the other hand, for the circularly polarized wave having opposite sense of rotation to that of electron precession will not be attenuated as there is no coupling [1].

Resonance linewidth on the order of 0.3 Oe can be obtained for single crystals of YIG. Thus these high-Q (on the order of 3000) materials are used in YIG filters at microwave and millimeter-wave frequencies.
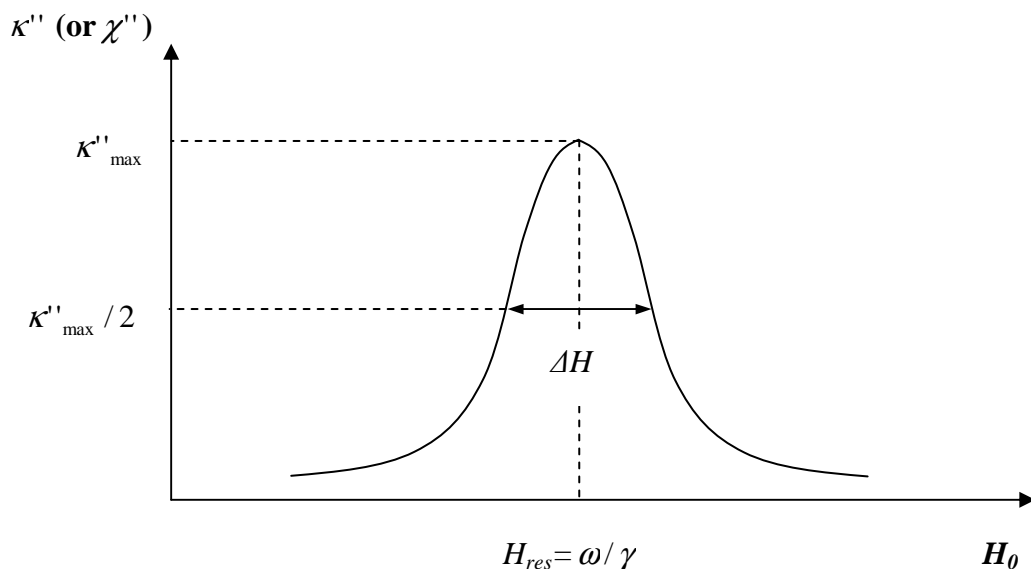

Figure A.14 Definition of resonance linewidth

Note that for ferrite phase shifter applications where the ferrite material is partially magnetized, resonance linewidth has small effect on magnetic loss since the operation is far below resonance.

A.5 Spin-wave Linewidth

The spin-wave linewidth ΔH_k is a measure of the peak power handling of the ferrite material. As RF power in the ferrite material is increased, the precession angle of the electrons increases to accommodate the incident power. Beyond some critical RF power P_c no further power can be absorbed via resonance mechanism and spin-waves having half the precession frequency are excited. As seen in Figure A.15 when spin-waves are excited, main resonance peak lowers and broadens. In addition, a subsidiary resonance occurs at a DC magnetic field below that required for main resonance [1].
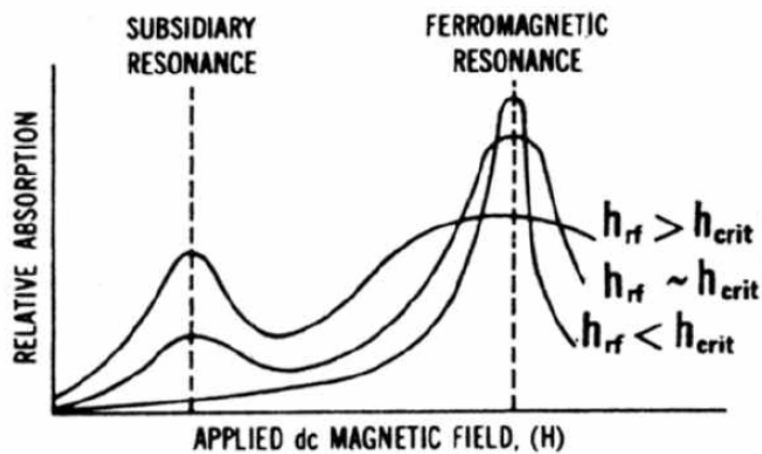

Figure A.15 Broadening of the main resonance and development of subsidiary resonance at high power levels [59]

The critical RF power level is related to the critical magnetic field strength H_{cr} which depends on spin-wave linewidth, saturation magnetization and signal frequency and is given by [64].

$$H_{cr} = \frac{2\Delta H_k \left(\dfrac{\omega}{\omega_m}\right)\left[1 - \left(\dfrac{\omega_0}{\omega}\right)\right]}{1 - \left(\dfrac{\omega_m}{2\omega}\right) + \left[1 + \left(\dfrac{\omega_m}{2\omega}\right)^2\right]^{\frac{1}{2}}}$$

(A.11)

It is observed from (A.11) that the value of H_{cr}, thus peak power handling can be increased by increasing ΔH_k or by lowering saturation magnetization. In Figure A.16 frequency dependence of H_{cr} for several commercial microwave ferrite materials are given. H_{cr} increases almost linearly with frequency for all materials as expected from (A.11).
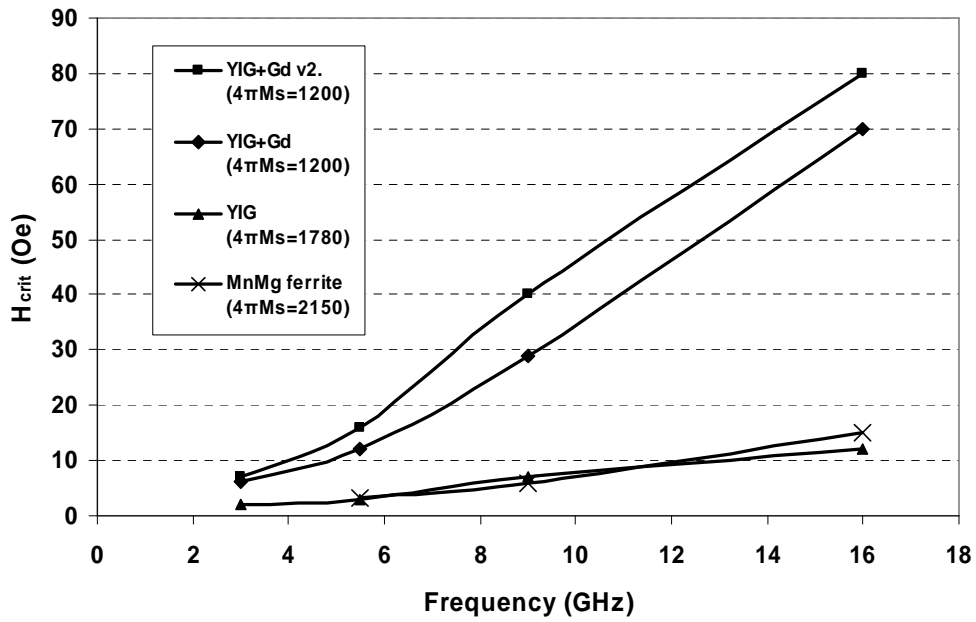

Figure A.16 Frequency dependence of critical RF H field level for several ferrite materials [59]

Addition of rare-earth metals such as Gd^{+3} and Ho^{+3} in the ferrite material increases ΔH_k and consequently H_{cr}, because of the fast relaxing nature of these ions However addition of these ions in the crystal structure causes the intrinsic linewidth

of the ferrite material to increase resulting in an increase of insertion loss at low RF power levels. This trade-off is given for a practical phase shifter using a garnet material doped with different levels of Ho^{+3} in Figure A.17. As RF power is increased beyond the critical level, insertion loss of the phase shifter starts to increase as the spin-waves are excited.
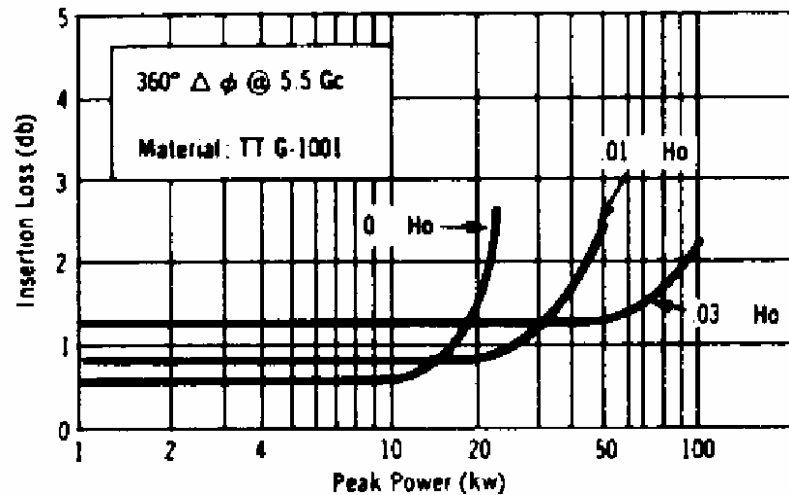

Figure A.17 Peak RF power dependence of insertion loss of a C-Band phase shifter for different levels of Ho substitution [59]

A.5.1 Polycrystalline Grain Size Effects on High Power Characteristics

Reduction of the polycrystalline grain size increases the critical power level of the ferrite material by providing sufficient discontinuity to break up spin waves [59].

In Figure A.18 measurement results of the insertion loss of a C-Band phase shifter shows the increase of the instability threshold as grain size is reduced. Note that insertion loss at low RF power levels remained same. However coercive force H_c of the ferrite increases due to domain wall involvement.

127
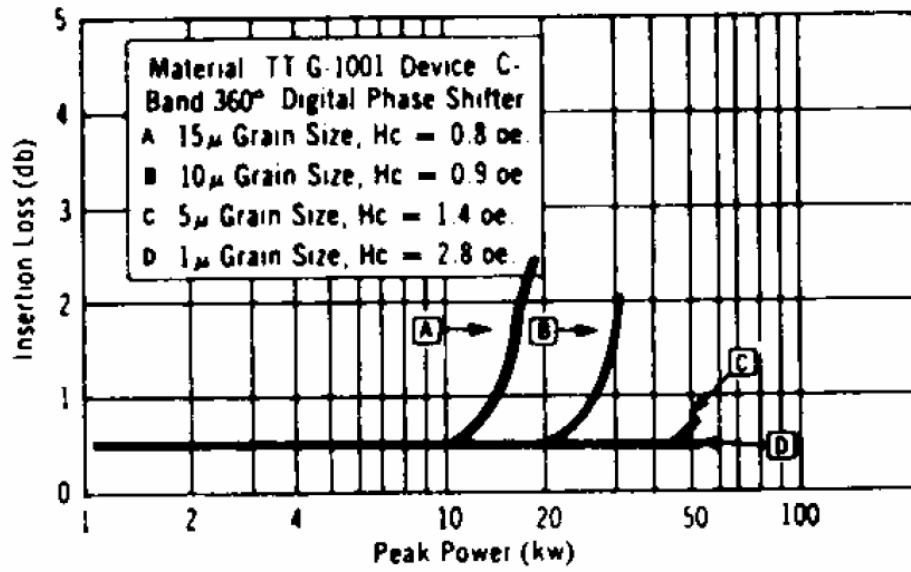
Figure A.18 Peak RF power dependence of insertion loss for different grain sizes [59]

APPENDIX B

DATASHEETS FOR COMMERCIAL FERRITE PHASE SHIFTERS

B.1 X-Band Twin-Toroid Ferrite Phase Shifter

Parameter	Specification
Bandwidth	10% at X-Band
Peak Power	1500W
Average Power	75W
Phase Coverage	Min. 360 °
Phase Resolution	6 bit (5.6°)
Insertion Loss	1.00 dB max.
Insertion Loss Modulation	±0.2 dB
Return Loss	20.0 dB min.
Phase Accuracy	$< 4°$ peak
Phase Repeatability	$< 1°$
Operating Temperature Range	-30°C to +60°C
Switching Time	$\leq 10\mu s$
Power Supply	±15V, +5V
Driver Control	4 LVDS lines
Other Microwave Characteristics	Nonreciprocal, Latching

B.2 X-Band Rotary-Field Ferrite Phase Shifter

Parameter	Specification
Bandwidth	10% at X-Band
Peak Power	1500W
Average Power	100W
Phase Coverage	Min. 360 °
Insertion Loss	1.2 dB max. 0.9 dB avg.
Return Loss	17.7 dB min.
Phase Accuracy	< 3.5° RMS
Operating Temperature Range	-30°C to +60°C
Other Microwave Characteristics	Reciprocal, Latching
Size (with analog driver circuit)	3.87 x 6.81 x 0.7 Inches
Weight	12.3 Ounces